10-2018

OSL Dating of the Tolleston Beach at Indiana Dunes National Lakeshore and its Implications for Interpreting the Archaeological Record

Malgorzata Mahoney
University of Nebraska-Lincoln, gosia_ida@yahoo.com

OSL Dating of the Tolleston Beach at Indiana Dunes National Lakeshore and its Implications for Interpreting the Archaeological Record

by

Malgorzata Mahoney

A THESIS

Presented to the Faculty of

The Graduate College at the University of Nebraska

In Partial Fulfillment of Requirements

For the Degree of Master of Science

Major: Earth and Atmospheric Sciences

Under the Supervision of Professors David B. Loope and Paul R. Hanson

Lincoln, Nebraska

October, 2018

OSL Dating of the Tolleston Beach at Indiana Dunes National Lakeshore and its Implications for Interpreting the Archaeological Record

Malgorzata Mahoney, M.S.

University of Nebraska, 2018

Advisors: David B. Loope and Paul R. Hanson

The puzzling scarcity of archaeological sites on the Tolleston Beach, the most lakeward shoreline complex at Indiana Dunes National Lakeshore, prompted an investigation into the development of these parabolic dunes in an attempt to determine whether the distribution of known archaeological sites is governed by ancient human behaviors, or influenced by its dune setting which can affect site preservation and discoverability. In order to accurately understand patterns of past human occupation, it is important to know the timing and extent of dune reactivation. Specifically, whether it was frequent enough to influence settlement patterns in the past, or if it was extensive enough to disturb archaeological deposits later on. Soil samples collected from shovel test pits and from vibracores on the crests of two compound parabolic dunes were dated using Optically Stimulated Luminescence to refine the chronology of the Tolleston, determine the age of near surface deposits (those accessible to archaeologists using standard field methods), and to evaluate the validity of applying those methods in this environment. An examination of sedimentary structures in the vibracores and the variability within the OSL data demonstrated that, even for the shallowest samples in this study, bioturbation was likely not significant enough to affect the reliability of the OSL

ages. The Tolleston dunes were shown to be active around 4 thousand years ago and possibly also around 2 thousand years ago. OSL ages from shovel test pits clustered around the timing of stabilization of the parabolic dunes on the Tolleston, while ages from the deeper vibracore samples represented the earliest stages of their formation. Subsequent dune reactivation appears to have not been substantial enough to place archaeological deposits outside of the reach of standard archaeological methods, essentially validating the use of these methods to inventory cultural resources in this environment. Since the geologic setting does not appear to preclude the archaeologists' access to potential archaeological resources, the sparse distribution pattern of human occupation on the Tolleston Beach might be better explained by exploring cultural habitation choices of past populations.

Table of Contents

1. Introduction

1.1 Purpose of Study

Stretching along the southern shore of Lake Michigan between Gary and Michigan City, Indiana, Indiana Dunes National Lakeshore (INDU) contains three relict shoreline complexes which preserve a record of fluctuating lake levels in the 14,500-year-long post glacial history of the Lake Michigan basin (Figure 1; Chrzastowski and Thompson 1992, 1994). It also preserves a 10,000-year-long history of human occupation in the area (Bringelson and Sturdevant 2007). While the robust archaeological record on two older shorelines within INDU attests to widespread human occupation in the past, the distribution of archeological sites on the youngest, most lakeward dune system – the Tolleston Beach – is sparse, especially at its westernmost extent which comprises the West Unit of the park. The lack of prehistoric sites could be explained in three possible ways: (1) prehistoric people chose not to occupy this area, or they did, but either (2) the nature of the geologic setting prevents us from reaching the depth necessary to recover that record using standard archaeological methods, or (3) the sites were eroded and thus not preserved. Recognizing the challenges associated with interpreting archeology in coastal sand dune environments (Lovis et al. 2009, 2012a, 2012b), this study addresses the question as to whether the distribution of archaeological sites at the park reflects cultural choices of past populations or the natural constraints of the environment.

Recent studies (Argyilan et al. 2014; Kilibarda et al. 2014) have shed light on the geologic history of the Tolleston dune field, its initial formation, stabilization and subsequent episodes of reactivation. But the extent and chronology of this reactivation, and especially its impact on shallow deposits is not well understood. This study uses Optically Stimulated Luminescence (OSL) dating to determine the age of near surface deposits in the older, more landward, part of the Tolleston, where remnants of the oldest human occupation may be preserved. In order to understand patterns of past human occupation, it is important to know the timing and extent of dune reactivation, whether it was frequent enough to influence settlement patterns, or if it was extensive enough to disturb archaeological deposits later on. Even if the episodes of eolian reactivation were localized events, they have the potential to affect both the preservation of archaeological sites and our chances of discovering them.

OSL dates obtained in previous studies on the Tolleston come almost exclusively from a depth beyond 1 m below the ground surface in an attempt to avoid dating potentially bioturbated sediments (Argyilan et al. 2014; Kilibarda et al. 2014; G.W. Monaghan, personal communication 2017). However, the purpose of this study is to determine the age of shallow deposits which are accessible to archaeologists using standard archaeological field methods (such as shovel testing) and to determine the validity of applying those methods in this environment. Most samples analyzed in this study were collected from dune crests at the depth of 0.7 m below ground surface. This sampling strategy placed them at a depth that is beyond the soil's A horizon, which is usually most affected by root growth and other

bioturbating agents, but still within the normal range of a standard shovel test. If the sediment found at this depth is heavily bioturbated, then this information can be used in deciding on a better, more suitable survey method in the future. Additional OSL samples were collected from vibracores. They extend the vertical column to almost 3 m depth and provide a comparative context for the shallower samples. They also facilitate an examination of sedimentary structures which can be used to evaluate the extent of bioturbation at different depths. Furthermore, a comparison with ages from deeper samples throughout the park will help archaeologists and geologists explore the question as to whether any significant sediment reactivation has happened since dunes were believed to have been stabilized last. Further, it will determine whether those shallow deposits, which archaeologists have been working within for decades, can be effectively dated using OSL.

Sampling from dune crests may be considered problematic and is often avoided because it is the part of the dune that is most sensitive to reactivation and related disturbance. Consequently, OSL ages obtained from crests may be indicative of those localized blowout events rather than the actual age of the landform (Argyilan et al. 2014; Muhs and Maat 1993). However, one of the purposes of this study is to evaluate the extent of potential post-stabilization disturbance, especially involving shallow, near surface deposits which are the target of archaeological studies. If post-stabilization blowout activity can be detected in the ages of those shallow deposits on crests, this information can be used in project planning as well as resource interpretation, as this is inevitably the depth to which archaeological surveys are typically constrained.

1.2 Regional setting

Indiana Dunes National Lakeshore lies within a region of humid continental climate with cold winters (average high/low temperature: 31º/15º F) and warm summers (average high/low temperature: 80º/63º F) and an average annual precipitation of 37 inches (Indiana State Climate Office, accessed August 2018). Prevalent winds are presently from the northerly direction in the winter and southwesterly in the summer, although shifts in wind direction have been recorded throughout the late Holocene (Thompson et al. 2004). The local surficial geology is dominated by dune and beach ridge complexes, with prevailing well drained sandy entisols (Oakville fine sand; USDA NRCS Web Soil Survey, accessed August 2018). They are interspaced with wetlands, and preserve the pro- and postglacial geomorphic evolution of the Lake Michigan shoreline.

After the Laurentide ice sheet had receded from the end moraines at the southern lake margin about 14,500 years ago, ancestral Lake Michigan experienced several major episodes of fluctuating water levels (Chrzastowski and Thompson 1992, 1994). For the following 4,500 years, these changes in lake level were controlled mainly by periodic re-advance and retreat of the ice sheet which, coupled with the effects of isostatic rebound, caused the opening and closing of northern and southern lake outlets and, consequently, the recurrent damming and draining of the ancestral lake (Baedke and Thompson 2000; Chrzastowski and Thompson 1992, 1994; Hansel et al. 1985). This “proglacial” phase ended with the final opening of

the North Bay outlet around 10 ka, after which the ice sheet was no longer marginal to the lake (Chrzastowski and Thompson 1994).

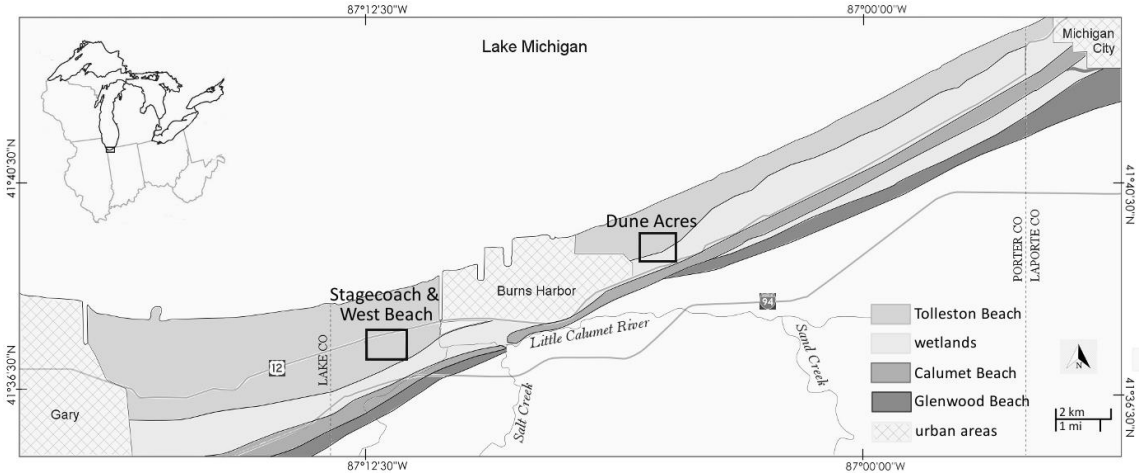

Figure 1. Lake Michigan shoreline in northern Indiana, indicating locations of the three relict shorelines, the wetlands (its eastern extent referred to as the Great Marsh) and study areas mentioned in the text.

As a result of these processes, three relict shoreline complexes are preserved in northern Indiana (Figure 1) which record three distinct transgressive episodes within a period of an overall lake level fall to its historical elevation of approximately 177m amsl. Both Glenwood Beach (~14.5 – 12.2 ka; ~195 – 190.5 m amsl) and Calumet Beach (~11.8 – 11.25 ka; ~189 – 187.5 m amsl) formed as mainland attached barrier beaches with bays behind them, terminated with westward growing spits. They are separated by the Two Creek phase of low lake level when the lacustrine plain and the Glenwood Beach were exposed and subject to subaerial erosion (Chrzastowski and Thompson 1992, 1994). The Algonquin phase (~10.6 – 10.3 ka; ~184 m amsl) shoreline, present in Lake Huron and in the northern part of Lake Michigan, is not well identified on the southern shore. However, Chrzastowski and Thompson (1992, 1994) interpret parts of the Calumet

as representing the short-lived Algonquin phase (also see Capps et al. 2007). Following the final retreat of the ice sheet and the opening of the North Bay outlet at around 10 ka, the lake entered the Chippewa phase – an over 4,000 year-long phase of extremely low lake level (perhaps as low as ~80 m amsl) and a long period of erosion to the lacustrine plain (Chrzastowski and Thompson 1994). From this time on the lake entered a "postglacial" phase as its level was no longer controlled by the re-advance and retreat of the ice sheet.

The youngest shoreline complex, which is the focus of this study, is the Tolleston Beach and it is associated with the Nipissing phase highstand. In its eastern part it is a complex network of parabolic dunes which widens to the West and terminates in a broad strandplain of more than 100 beach ridges near Gary, IN (Thompson 1992; Thompson and Baedke 1997). Continued isostatic uplift of the North Bay outlet throughout the Chippewa phase caused a gradual rise in lake level which eventually exceeded the present level at about 6.0 ka. This marks the beginning of the Nipissing phase which reached its peak of 184 m amsl at about 4.7 ka (Chrzastowski and Thompson 1994; Hansel et al. 1985). Initially, the Tolleston developed as a barrier beach that terminated at a westward prograding spit. At the peak of the Nipissing phase, the lake level was high enough that a lagoon formed between the new barrier beach and the relict Calumet shoreline (Thompson 1990, 1994; Chrzastowski and Thompson 1994). As the lake level began to fall, the lagoon gradually drained westward through the Sag channel to the Chicago outlet, and, by ~4.4 – 4.2 ka, it was a well-developed wetland, currently referred to as the Great Marsh (Argyilan et al. 2014; Thompson 1994). Continued sediment supply enabled

further westward extension of the Tolleston spit and caused shoreline progradation which is preserved in beach ridges west of Gary, IN. Meanwhile, east of Gary, steady westerly winds reworked the sand, causing the development of a network of transgressive parabolic dunes. Argyilan et al. (2014) found that those dunes were likely stabilized by ~3.5 ka. Kilibarda et al. (2014) extended the chronological framework for this process to ~3.0 ka, although they recognized two brief episodes of dune stabilization at ~4.0 ka and ~3.5 ka, as indicated by the presence of paleosols.

At the western end of the Tolleston shoreline, beach progradation with continued lake level fall restricted drainage through the Sag channel until it eventually stopped by ~2.5 ka (Chrzastowski and Thompson 1994). For the first time, sediment transported along the western shore was able to reach the southern lake shore. The convergence of littoral transport from both sides of the lake facilitated the joining of the western and eastern spits and the continued formation of beach ridges, which record 30- and 150-year fluctuations in an otherwise long-term falling lake level (Baedke et al. 2004; Chrzastowski and Thompson 1992, 1994; Thompson and Baedke 1997).

Figure 2. Tolleston Dunes in the vicinity of the Stagecoach study area. Photo by Gosia Mahoney.

The most common types of sand dunes found on the Tolleston Beach are various morphological variants of parabolic dunes, which are currently covered by an oak forest (see Figure 2). Parabolic dunes are characterized by a parabola-shaped form in plan, and trailing arms pointing upwind that are usually fixed by vegetation during dune growth (Pye 1983). They can develop from any type of existing dune with the presence of a sufficient supply of sand, unidirectional winds and a stabilized surface over which to migrate (Hesp 2011; Pye 1983). Vegetation plays an important role in the morphological development of parabolic dunes (Durán and Herrmann 2006; Pye 1982, 1983; Pye and Tsoar 1990). With increased moisture and decreased wind energy, vegetation typically stabilizes the upwind end of the arms where there is the least amount of sand erosion and deposition. It traps the sand in place so that it starts to accumulate mostly on the dune crest (Hesp 2011;

Pye 1983). As a result, the apex moves forward with the direction of the wind, leaving trailing ridges (arms) behind. The speed of dune migration depends on the variability of the terrain the dunes are moving across, as well as wind energy and wind direction variability (Hesp 2011; Pye 1982, 1983). A subtle interplay between the ratio of sand erosion rate and vegetation growth rate determines which morphological type the parabolic dune will evolve into, with a general increase in morphological complexity with an increase in sand erosion and a decline in vegetation cover (Durán and Herrmann 2006; Hesp 2011; Pye 1983).

Parabolic dunes may be completely fixed by vegetation but if that subtle balance is broken, reactivation and dune migration will occur. As the crest of a simple lobate parabolic dune starts migrating, the trailing arms lengthen and the dune may gradually evolve into a hairpin dune, characterized by an elongated U-shape and a length to width ratio higher than 3 (Hesp 2011; in this study area recognized by Kilibarda et al. 2014). Increased wind speed and erosion may breach the apex leaving behind a windrift dune, which consists of remnant arms of what once was a hairpin dune (Pye 1982, 1983). Finally, the most common type is the compound nested parabolic dune which evolves from several simple lobate and hairpin dunes amalgamating into one large dune (Hesp 2011).

After the initial stabilization, the Tolleston dune field would have been exposed to these processes of sediment reworking and they would have likely varied through time, depending especially on specific climatic conditions which influence the extent of vegetation cover. Reworked windrift and compound

parabolic dunes are very common on the Tolleston Beach (Argyilan et al. 2014; Chrzastowski and Thompson 1992, 1994; Kilibarda et al. 2014). Their axes indicate a consistent westerly wind direction until about 1.0 ka (Kilibarda et al. 2014) and their large numbers suggest that the processes of sediment reworking indeed have taken place. While the extent of the reactivation and reworking is not clear, Kilibarda et al. (2014) interpret the wide distribution of OSL ages throughout the dune field as evidence of at least localized and sporadic reworking of the dunes between 3.0 and 1.0 ka.

The final stage in the development of the Tolleston Beach is marked by an increase in blowout activity along the shoreline and a shift in prevailing wind direction. The beach and foredune erosion associated with a rise in lake level around 1.0 ka (Baedke and Thompson 2000) provided steady sand supply for coastal dune growth and, coupled with increased storminess, initiated the formation of blowouts with a distinctively different axis indicating a northwesterly and northerly wind direction, as opposed to the previously prevailing westerlies (Kilibarda et al. 2014; Thompson et al. 2004). Beach ridges in the Gary-Miller area of West Tolleston also indicate the same shift in paleowind direction (Thompson et al. 2004). Most of the blowouts cut through only the linear ridges and parabolic dunes closest to the coastline, although the Big Blowout at Indiana Dunes State Park extends over the entire Tolleston Beach all the way to the Great Marsh.

1.3 Archaeology at Indiana Dunes National Lakeshore

The archaeological record at Indiana Dunes National Lakeshore (INDU) documents more than 10,000 years of human occupation in the area. Close to five decades of archaeological research in the park (for overview see Bringelson and Sturdevant 2007) has led to the identification of more than 500 archaeological sites (Figure 3). They are distributed throughout the three relict shoreline complexes although they are significantly more sparse on the Tolleston Beach. Sites are found in different geomorphic contexts: from low areas on the edges of marshes to dune crests.

Prehistoric sites are generally small and unstratified, and consist mainly of scatters of artifacts: chipped stone tools and debris, fire-cracked rock, and sometimes ceramics. These artifact scatters are incorporated into dune sand, and usually concentrated within the upper 30–60 cm below the ground surface (Frost 2001; Lynott et al. 1998). Only a handful of more intensely investigated sites exceed 300m^2 (Bringelson and Sturdevant 2007), but even those do not contain any identifiable structures, long-term storage/refuse pits, or obvious cultural layers with buried occupation horizons or paleosols, all of which may reflect short-term occupations of the lakeshore by prehistoric groups (Lynott et al. 1993, 1998). Furthermore, most of the artifacts are not chronologically diagnostic (Lynott et al. 1998; Sturdevant and Bringelson 2003) and that, coupled with the lack of organic fragments in archaeological features available for ^{14}C dating, is one of the biggest

challenges in the interpretation of the chronology of prehistoric occupation at Indiana Dunes.

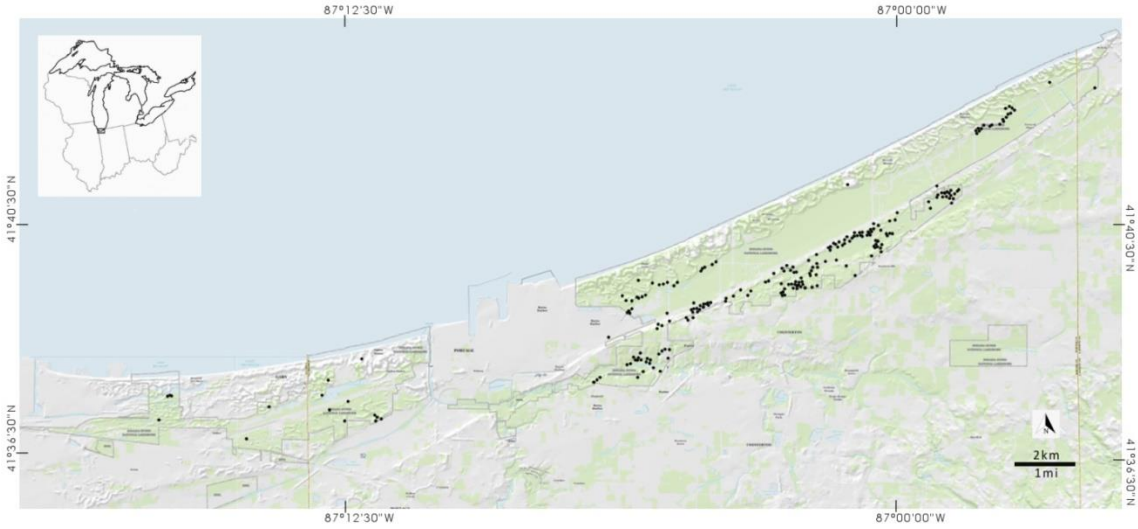

Figure 3. Distribution of archaeological sites (black dots) on the three beach complexes within Indiana Dunes National Lakeshore. Overlain on a topographic map obtained from USGS's The National Map (accessed August 2018).

Naturally, the oldest sites (Late Paleoindian through Early/Middle Archaic; see Figure 4) are on the Glenwood and Calumet beaches. The sites on the Tolleston are almost entirely devoid of chronologically diagnostic artifacts and, with the exception of a few sites which contain Woodland ceramics, can be only broadly attributed to the "precontact" period (Bringelson and Sturdevant 2007; also see Appendix 1).

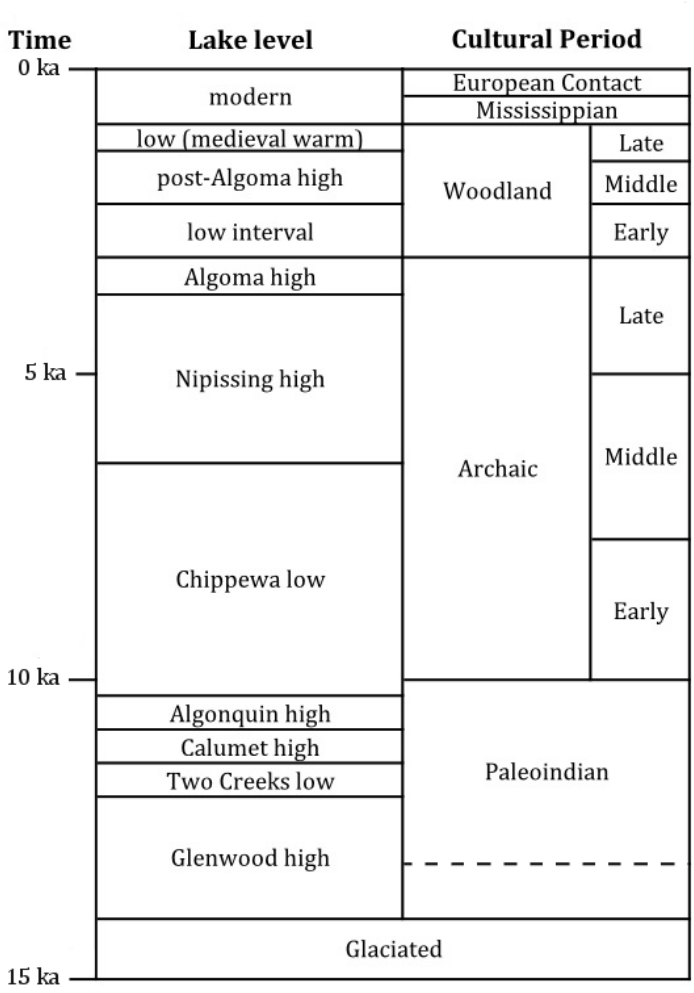

Figure 4. Lake level phases with corresponding cultural periods (after Chrzastowski and Thompson 1992; Lovis et al. 2012a). Ages are in thousands of years ago.

This sparse record has puzzled researchers for decades. Several models have been proposed to explain why there are no large-scale, at least semi-permanent, prehistoric settlements at INDU, unlike those found in other similar settings around Lake Michigan (Lovis et al. 2009, 2012a, 2012b; Richner 1973). These models range from interpreting the dunes as a "shared territory" at the convergence of transport routes, used by multiple diverse populations for their subsistence needs, to envisioning them as a "No-Man's land" – a kind of buffer zone between competing populations (Bringelson and Sturdevant 2007; Jeske 1990; Richards and Jeske 2002;

Schurr 2003; White 2000). These can be contemplated only if we assume that the known archaeology at INDU indeed reflects the total archaeological record. This dataset, however, may be incomplete because of the methods we apply to collect it.

Two methods are most commonly used in archaeological fieldwork: shovel test surveys and test excavations. While both have their applications, neither of them is free of problems. Shovel test surveys are generally used for the initial identification and recording of sites in an untested area while test excavations are usually designed to refine our understanding of already recorded archaeological sites. A shovel test is a shovel-dug circular test pit, small in size (usually less than 0.5 m diameter) and consequently quite shallow – usually well within 1 m below ground surface. Shovel tests are usually laid out as transects or in a grid (with a typical 10 m interval) and allow for a quick, though systematic, survey of relatively large areas. Excavation units are larger (usually 1x1 m or 2x1 m) square or rectangular holes, but they also rarely extend beyond the 1 m depth threshold, especially in unstable sandy soils. Being a more intensive type of survey, they obviously produce a more detailed and complete record of archaeology at a given site, but that fact is countered by the much slower pace of this type of testing. It inevitably limits the amount of space that can be covered in the same amount of time, a fact that is taken into account in project planning, and hence, test excavations are undertaken far less frequently than shovel test surveys when it comes to inventorying cultural resources in an area. This is true even though most of our data regarding the rare large sites comes from test excavations (Lynott et al. 1993, 1998; Frost 2001) – a clear methodological bias. Obviously, both survey methods have

their advantages and disadvantages but they are also essentially spatially limited – both horizontally and vertically. At the same time, the National Park Service requires park units to inventory their cultural resources and it is critical to know which type of survey would be the most informative in a given setting.

The survey methods used and the geomorphological context need to be taken into account when interpreting the nature and size of archaeological sites. Larger sites may be evidence of a more intensive past occupation but they may also be a record of several small-scale and short-term occupations that are overlapping spatially but are not chronologically contemporaneous; something that is hard to determine without the presence of chronologically diagnostic artifacts. Conversely, a number of small sites recorded through a less intensive shovel test survey may actually be a record of a more intensive contemporaneous occupation but, without the presence of chronologically diagnostic artifacts, that is impossible to determine because of the survey method applied.

Challenges associated with studying and interpreting the archaeological record in coastal sand dune environments have been noted in numerous studies in the Great Lakes, though most of this work has been focused on the northern part of the region (Brose 1970; Lovis 1990; Lovis et al. 1998, 2009, 2012b). In particular, eolian processes associated with the periodic reactivation and re-stabilization of coastal dune systems can cause differential preservation of archaeological deposits: from erosional processes that remove the record entirely, or alter its original context, to burial of cultural deposits deep within dunes, effectively placing them

outside of the range of discoverability with the use of traditional archaeological field techniques (Lovis et al. 2012b). A number of factors, including patterns of sediment supply, dune morphology, wind position, as well as the effects of isostatic rebound south of the "hinge line" (Baedke & Thompson 2000; Chrzastowski & Thompson 1992, 1994; Lovis et al. 2012a, 2012b; Thompson 1992) distinguish the southern shoreline from other areas around Lake Michigan, but the fact remains that its geologic and environmental setting is intricately linked to how the archaeological record is created, preserved, and how it is later discovered.

1.4 Shallow OSL sampling and bioturbation

Given the scarcity of other chronologically sensitive data, we turned to optically stimulated luminescence (OSL) dating to determine the age of dune deposits. During burial, quartz grains are exposed to naturally occurring radiation from radioactive elements (U, Th, K) present in the surrounding sediments (Huntley et al. 1985; Rhodes 2011). They absorb this radiation proportionately to the dose rate specific to that particular context. This process builds up the luminescence signal in the grains until the next exposure to sunlight (bleaching), which removes the signal, resets the clock, and the signal starts to build up again following redeposition and subsequent burial (Aitken 1998). By comparing the measured luminescence signal with the sediment's dose rate we can calculate the time elapsed since the quartz was last exposed to sunlight, or was last at the ground surface.

Two necessary conditions need to be met in order to ensure the reliability of an OSL date: 1. the quartz grains were fully bleached (i.e. exposed to sunlight) prior to deposition, and 2. there was no subsequent disturbance to the sediment or change in contributions to its dose rate. Eolian sediments are thought to be very well suited for OSL dating as they are usually well-bleached prior to burial because of the nature of sediment transportation by wind, which makes full exposure to sunlight highly likely (Bateman et al. 2007b; Clarke et al. 1999; Frederick et al. 2002; Murray and Olley 2002).

However, post-depositional disturbance (usually referred to as bioturbation since most of the processes at play involve living organisms) presents more of a challenge, especially in utilizing OSL dating in archaeology. Near surface (within 1 m depth), unconsolidated, sandy deposits which are most prone to bioturbation (Bateman et al. 2003, 2007a, 2007b; Forrest et al. 2003; Hanson et al. 2015), are usually best suited and most accessible for OSL dating (Bateman et al. 2007a) and are also of most interest to archaeologists, both because of the depth of cultural deposits that need to be dated and because of their accessibility for archaeological excavation methods.

Bioturbation can affect the sediment in various ways with grains potentially moving either upward or downward in the soil or sediment profile. Upward movement may potentially shift older grains higher in the profile and cause OSL age calculations to be older than the actual age of the sediment; that is usually caused by tree tips and by different types of rodents or insects which first burrow down and

then bring some of the sediment back up (Araujo 2013; Bateman et al. 2007b; Forrest et al. 2003; Rink et al. 2013). A potentially more common alternative, however, may shift younger, bleached or partially bleached, grains downwards as pedogenic processes, root growth, or animal burrowing create pathways for this downward movement of grains. This can result in OSL ages from deeper in the profile to be younger than their depositional age (Bateman et al. 2007a, 2007b; Forrest et al. 2003; Hanson et al. 2015). In archaeological applications, when dating cultural layers, we also must not discount the potential for sediment disturbance caused by humans themselves (Roberts et al. 2015). This could happen contemporaneously during the occupation or at a later time at multi-component sites.

There are a number of measures that can be taken to verify that the ages reflect depositional age and not the time of bioturbation or disturbance. This starts at the sampling stage while observing the sediment to avoid areas with obvious disturbance such as animal burrows, roots, and areas with active pedogenic processes taking place. That is the reason why most OSL samples are usually collected from the depth of 1 m or more below ground surface (for example Argyilan et al. 2014; Puta et al. 2013; Rawling and Hanson 2014). For the purposes of this study, however, and in archaeological contexts in general, it is most often those shallow deposits that need to be dated. The presence of preserved sedimentary structures could be an indicator of undisturbed deposits. However, Bateman et al. (2007b) have demonstrated that it is not always a reliable strategy. Their analysis of OSL ages in several case studies, where independent age controls (^{14}C and

archaeology) were used, revealed that the sites that exhibited a complete lack of bedding turned out not to be heavily bioturbated, while the sites with some of the bedding preserved showed very high degree of post-depositional bioturbation. Furthermore, in many sampling contexts (for example shovel test pits or augers) these visual characteristics might not be observable. If possible, collecting a longer stratigraphic profile in a core from the same area can help determine the level of preservation of sedimentary structures (Hanson et al. 2015), but to truly be able to determine the degree of bioturbation, these observations must best be combined with an analysis of the variability within the OSL data and equivalent dose and age distributions (Bateman et al. 2007a, 2007b; Bueno et al. 2013; Hanson et al. 2015).

2. Methods

2.1 Field sampling

Two compound parabolic dunes on the Tolleston Beach were selected for sampling in this study: one in the East Unit of the park (along Mineral Springs Rd, just south of the town of Dune Acres – referred to here as "Dune Acres") and one in the West Unit (just north of Stagecoach Rd, along the Tolleston Dunes trail – referred to here as "Stagecoach"). Two additional samples included in this analysis came from a simple lobate parabolic dune in the West Beach area in the West Unit, just north of Long Lake (referred to as "West Beach"), also on the Tolleston (see Figure 1 in chapter 1). The samples were collected along dune crests from fourteen shovel test pits and from four vibracores. Shovel test samples (UNL-3994, UNL-3995, UNL-4079 through UNL-4085, UNL-4090 through UNL-4092, and UNL-4301) were collected using light-proof aluminum tubes inserted horizontally into the walls of shovel test pits at the depth between 0.3 and 0.7 m below ground surface. Dose rate and moisture samples were collected from the sediment immediately adjacent to the OSL samples. The samples were transported to the Luminescence Laboratory at the University of Nebraska (UNL) in Lincoln and opened under amber and red lighting conditions. In addition, four vibracores were collected from the Dune Acres and Stagecoach locales: one in the middle of the arm and one closer to the apex of each dune. The cores were transported to the lab at UNL and opened under amber and red lighting conditions. They were inspected for the presence of bedding and

two OSL samples from each core were collected to be included in this analysis (UNL-4244 and UNL-4294 through UNL-4300): one from the shallowest depth where bedding was observed, and one from the deepest undisturbed section of the core. The OSL and dose rate samples were collected from the inner portions of vibracore tubes to avoid potentially contaminated grains that might be found on the edges of the tubes.

2.2 Laboratory preparation

All samples were wet-sieved to separate 90-150 μm grain size. Sample UNL-4244 did not yield sufficient amount of 90-150 μm grain size and 150-212 μm fraction was used. The 90-150 μm fraction was treated with hydrochloric acid to remove carbonates and floated in sodium polytungstate in order to remove heavy minerals. Following this, the samples were treated with 48% hydrofluoric acid for ~50 minutes. This treatment achieves two purposes: dissolving feldspars and etching quartz grains to remove the outer layer which stores the alpha radiation contribution to the luminescence signal (Aitken 1998). The samples were then treated with HCl again to remove any fluorides and then rinsed and dried again. The remaining quartz grains were dry-sieved to remove any grains outside of the 90-150μm fraction.

2.3 OSL measurement and data processing

Processed grains were mounted on aluminum disks with 5mm masks and analyzed on a Riso DA-20 luminescence reader using the single aliquot regenerative-dose (SAR) protocol (Murray and Wintle 2000a). Preheat plateau tests (Murray and Wintle 2000b) were run on sample UNL-3995 with the temperatures ranging from 180º C to 260º C at 20 degree increments. For this suite of samples, the temperature of 220º C was deemed the optimal preheat temperature. The OSL measurements were taken at 125º C.

The equivalent dose (D_e), which is the amount of radiation dose that is necessary to account for the measured luminescence signal, was calculated using the Central Age Model (Galbraith et al. 1999) and for each sample the age estimation was made based on a minimum of 40 accepted aliquots. Individual aliquots were rejected for three main reasons: if they showed measurable Infrared stimulated Luminescence (IRSL) values (indicating the presence of feldspars), if the recycling ratio (Regen1/Regen1' after correcting for quartz sensitivity change) was beyond ±10%, and if the equivalent dose was greater than Regen 3.

2.4 Dose rate estimation

The environmental dose rate is calculated by determining the concentration of radioactive materials (K, U, Th) in the sediment adjacent to the sample accounting

for the contributing cosmic irradiation, which varies slightly with latitude, elevation above sea level, and more significantly with burial depth (Prescott and Hutton 1994). Dose rate samples, collected from immediately above and below the OSL samples, were dried in the oven at ~50º C and pressed into nested petri dishes. The petri dishes were sealed with hot glue and analyzed in a gamma spectrometer at the UNL Luminescence Laboratory to calculate the concentrations of K, U, and Th. Taking into account the depth of each sample, the contribution of cosmic irradiation was estimated based on the equations from Prescott and Hutton (1994) and final dose rate values were calculated using the equations from Aitken (1998).

As water absorbs some of the radiation that would have otherwise reached the grains (Aitken 1998), a correction for water content needs to be made when calculating the dose rate and measuring the OSL to avoid age underestimation. For the samples from shovel tests, a separate sample was collected from the surrounding sediment and moisture content was calculated in the lab. This was not possible for the samples from vibracores as water is used to facilitate the extraction of the core and the sediment is thus completely saturated when collected. An estimate of 5% water content was used for these. For dose rate calculations, 50% variability of the measured values was added to account for changes in moisture content through time.

3. Results

3.1 Dune Acres results

A total of 10 OSL ages were obtained from the Dune Acres study area (Table 1 and Figures 5 and 6). They range from 1.4 to 5.2 ka and come from depths ranging from 0.3 to 2.8 m below ground surface. Sample UNL-3994 was collected from 0.3 m depth and dates to 1.4 ± 0.1 ka. It came from a layer which contained cultural material. Samples UNL-4301 and UNL-4079 through UNL-4082 were collected at 0.6 and 0.7 m depth and most of these ages cluster between 3.3 and 3.7 ka. However, two fall outside this range: UNL-4081 dates to 5.2 ± 0.4 ka and UNL-4301 (which comes from the same shovel test pit as UNL-3994, though at deeper depth) produced an OSL age of 1.4 ± 0.1 ka.

Samples UNL-4244 and UNL-4294 through UNL-4296 were extracted from vibracores. VC1 (see Appendix 2) was collected from the middle portion of the dune's arm, near sample UNL-4082. Surface soil consists of 10 cm of dark grayish brown fine sand with coarse roots throughout, followed by a horizon of brown to yellowish brown fine sand (with some roots present as far down as 50 cm below surface), which grades into light yellowish brown fine sand. Traces of horizontal parallel laminations are visible at 1.2-1.5 m depth and low angle parallel laminations are preserved at approximately 3m depth. OSL samples were collected from the depth of 0.8 m and 2.8 m (UNL-4294 and UNL-4244) and produced age estimates of 4.6 ± 0.4 ka and 4.0 ± 0.3 ka, respectively. VC2 (Figure 7), collected

closer to the apex of the dune, has a somewhat thicker A horizon consisting of approx. 20 cm of very dark grayish brown fine sand with some roots. The B horizon extends to about 80 cm below ground surface and consists of dark brown to yellowish brown fine sand with minimal presence of roots. Horizontal parallel laminations are clearly visible at 0.7 m depth. The remainder of the core consists of light yellowish brown fine sand with traces of low angle and horizontal laminations preserved throughout. OSL samples were collected at 1.0 and 2.8 m depth (UNL-4295 and UNL-4296) and yielded age estimates of 4.2 ± 0.3 ka and 4.5 ± 0.4 ka, respectively.

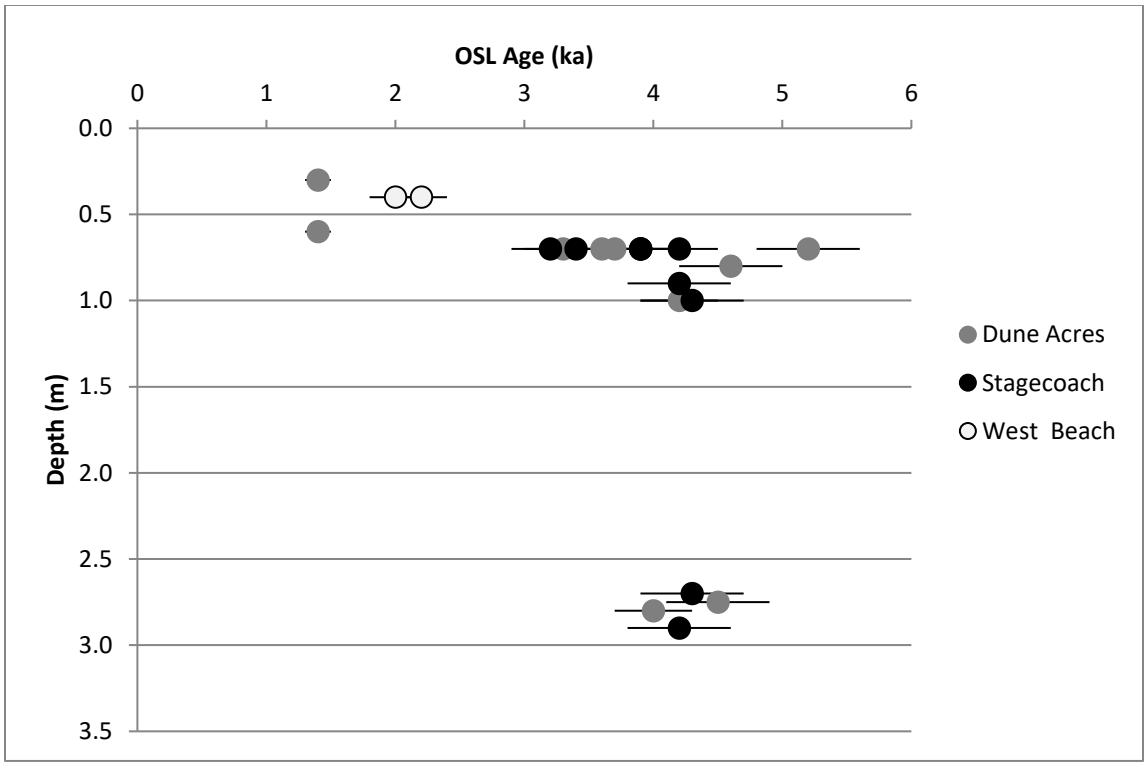

Figure 5. OSL ages with 1 σ errors vs. depth for samples collected at Dune Acres, Stagecoach and West Beach sites.

Dune Acres

UNL Lab #	Field #	Depth (m)	U (ppm)	Th (ppm)	K_20 (wt %)	In Situ H_20 (%)[a]	Dose Rate (Gy/ka)	CAM[b] D_e (Gy) ± 1 Std. Err.	Aliquots (n)[c]	Skewness	O.D.[d] %	OSL Age ka ± 1 σ
UNL-3994	2014-7	0.3	0.5	1.9	1.6	1.0	1.68 ± 0.10	2.3 ± 0.1	42/48	0.58	16.3	1.4 ± 0.1
UNL-4301	2014-8	0.6	0.4	1.5	1.5	0.1	1.62 ± 0.10	2.2 ± 0.1	42/63	0.58	12.1	1.4 ± 0.1
UNL-4082	2015-4	0.7	0.4	1.3	1.4	4.0	1.44 ± 0.09	5.2 ± 0.4	49/62	-0.42	46.4	3.6 ± 0.4
UNL-4080	2015-2	0.7	0.4	1.3	1.6	4.2	1.60 ± 0.10	5.9 ± 0.2	40/48	0.09	25.0	3.7 ± 0.3
UNL-4081	2015-3	0.7	0.5	1.6	1.4	3.8	1.51 ± 0.09	7.8 ± 0.2	44/55	1.19	19.5	5.2 ± 0.4
UNL-4079	2015-1	0.7	0.4	1.4	1.5	4.4	1.53 ± 0.10	5.0 ± 0.1	59/73	1.72	21.4	3.3 ± 0.3
UNL-4294	VC1-1	0.8	0.5	1.4	1.6	5.0	1.57 ± 0.10	7.3 ± 0.2	41/63	0.26	17.4	4.6 ± 0.4
UNL-4244	VC1-5	2.8	0.6	1.5	1.6	5.0	1.54 ± 0.10	6.1 ± 0.2	42/62	-0.02	23.0	4.0 ± 0.3
UNL-4295	VC2-1	1.0	0.5	1.5	1.7	5.0	1.64 ± 0.10	6.9 ± 0.2	45/58	0.49	17.5	4.2 ± 0.3
UNL-4296	Vc2-4	2.8	0.5	1.5	1.5	5.0	1.50 ± 0.10	6.8 ± 0.2	44/62	0.38	18.9	4.5 ± 0.4

Stagecoach

UNL Lab #		Depth (m)	U (ppm)	Th (ppm)	K_20 (wt %)	In Situ H_20 (%)[a]	Dose Rate (Gy/ka)	CAM[b] D_e (Gy) ± 1 Std. Err.	Aliquots (n)[c]	Skewness	O.D.[d] %	OSL Age ka ± 1 σ
UNL-4083	2015-5	0.7	0.4	1.3	1.6	4.1	1.58 ± 0.10	5.4 ± 0.1	58/68	0.22	16.1	3.4 ± 0.3
UNL-4084	2015-6	0.7	0.4	1.4	1.7	3.4	1.71 ± 0.11	6.7 ± 0.1	65/93	-0.19	18.0	3.9 ± 0.3
UNL-4085	2015-7	0.7	0.4	1.8	1.8	2.3	1.80 ± 0.11	5.7 ± 0.1	71/78	-0.08	19.4	3.2 ± 0.3
UNL-4092	2015-14	0.7	0.4	1.6	1.8	2.4	1.82 ± 0.12	7.0 ± 0.2	50/64	0.9	23.9	3.9 ± 0.3
UNL-4091	2015-13	0.7	0.5	1.4	1.9	2.2	1.89 ± 0.12	7.4 ± 0.2	47/60	0.63	18.7	3.9 ± 0.3
UNL-4090	2015-12	0.7	0.5	1.4	1.7	2.0	1.75 ± 0.11	7.3 ± 0.2	65/81	0.39	17.2	4.2 ± 0.3
UNL-4297	VC3-4	1.0	0.4	1.4	1.7	5.0	1.61 ± 0.11	6.9 ± 0.2	42/57	0.08	21.4	4.3 ± 0.4
UNL-4298	VC3-5	2.7	0.4	1.4	1.7	5.0	1.59 ± 0.11	6.8 ± 0.2	41/57	0.23	14.5	4.3 ± 0.4
UNL-4299	VC4-1	0.9	0.4	1.5	1.8	5.0	1.74 ± 0.12	7.4 ± 0.2	46/58	0.63	19.2	4.2 ± 0.4
UNL-4300	VC4-4	2.9	0.4	1.3	1.8	5.0	1.69 ± 0.11	7.1 ± 0.2	45/53	0.27	21.2	4.2 ± 0.4

West Beach

UNL Lab #		Depth (m)	U (ppm)	Th (ppm)	K_20 (wt %)	In Situ H_20 (%)[a]	Dose Rate (Gy/ka)	CAM[b] D_e (Gy) ± 1 Std. Err.	Aliquots (n)[c]	Skewness	O.D.[d] %	OSL Age ka ± 1 σ
UNL-3995	2014-9	0.4	0.4	1.4	1.6	2.2	1.65 ± 0.10	3.6 ± 0.1	28/36	0.02	19.4	2.1 ± 0.2
UNL-3996	2014-10	0.4	0.5	1.5	1.5	1.0	1.59 ± 0.10	3.2 ± 0.1	49/69	-0.17	25.2	2.0 ± 0.2

[a]Assumes 50% variability in estimated moisture content

[b]Central Age Model (Galbraith et al. 1999)

[c]Accepted disks/all disks

[d]Overdispersion

Table 1. Equivalent dose, dose rate data, skewness, overdispersion (O.D.), and OSL age estimates for Dune Acres, Stagecoach and West Beach study areas. Samples from vibracores are shaded out.

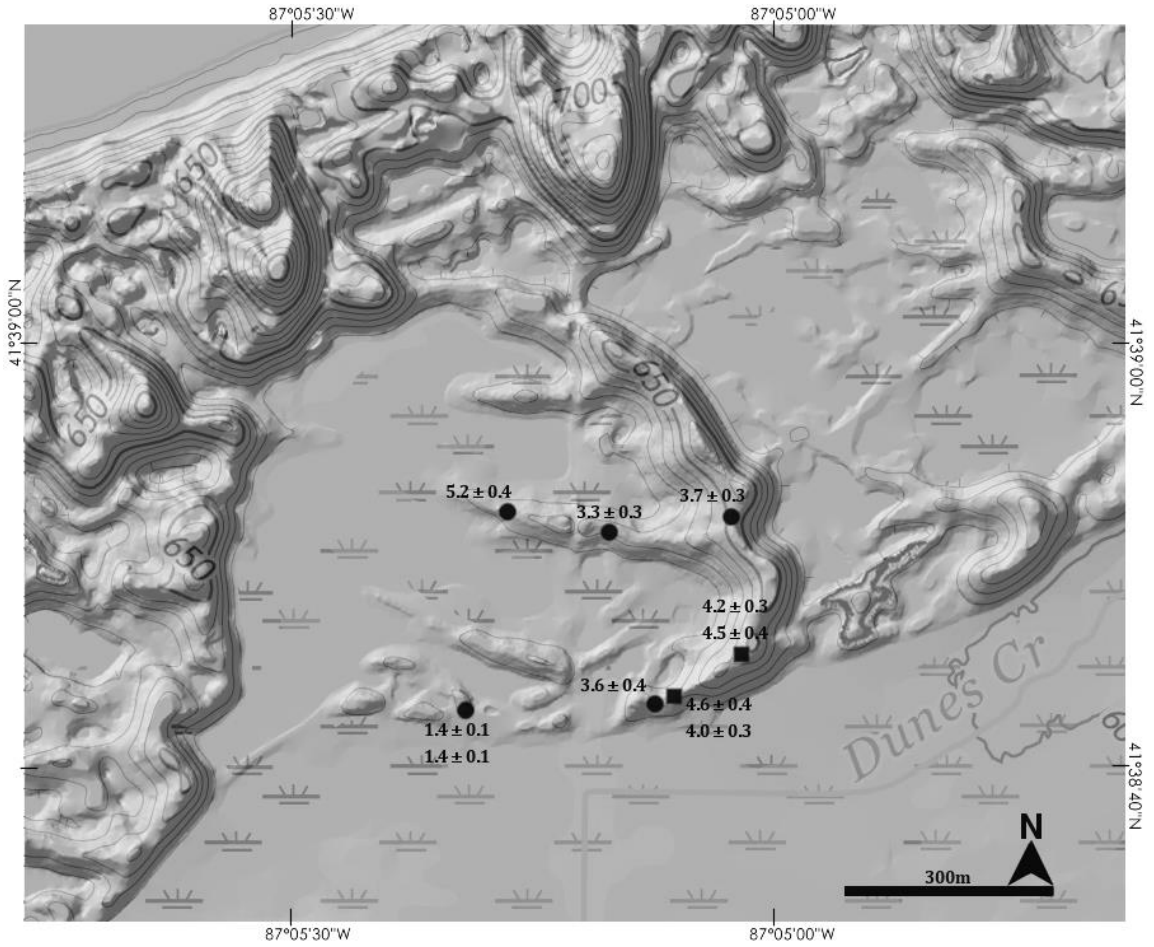

Figure 6. Sample locations with OSL ages at Dune Acres, overlain on a 1 m resolution LiDAR derived hillshade and a topographic map obtained from USGS's The National Map. Elevation is in feet, contour interval is 10 feet. Circles are shovel test and squares are vibracore locations. Lake Michigan is in the NW corner of the image. OSL ages are in thousands of years ago.

Figure 7. Photograph of vibracore VC 2, collected from Dune Acres. Depths are in meters below surface. The arrows indicate prominent laminations. OSL ages are in thousands of years ago.

To assess the potential for post-depositional mixing of grains in a sample, two measures in the OSL data, both of which examine the departures from normal equivalent dose (D_e) distribution, are particularly useful. Skewness is a measure of the asymmetry of a statistical distribution. Positive skewness (skewed to the right – high D_e tail) might indicate a poorly bleached sample that contains grains still carrying a residual older signal from previous burial, but can also indicate the presence of older grains added via bioturbation. Negative skewness (skewed to the left – low D_e tail), on the other hand, might indicate the inmixing of younger grains with a lower OSL signal (Bateman et al. 2007b). Assuming that grains from an eolian sample would likely have been fully reset prior to burial, any significant departure of skewness values from zero could potentially indicate post-depositional disturbance and the mixing of grains of different ages (Bateman et al. 2007a; Hanson et al. 2015). Skewness values at Dune Acres range from -0.42 to 1.72 (Figure 8). While the range for vibracore samples falls between -0.02 and 0.49, the samples from shovel tests are more skewed with the values ranging from -0.42 to 1.72.

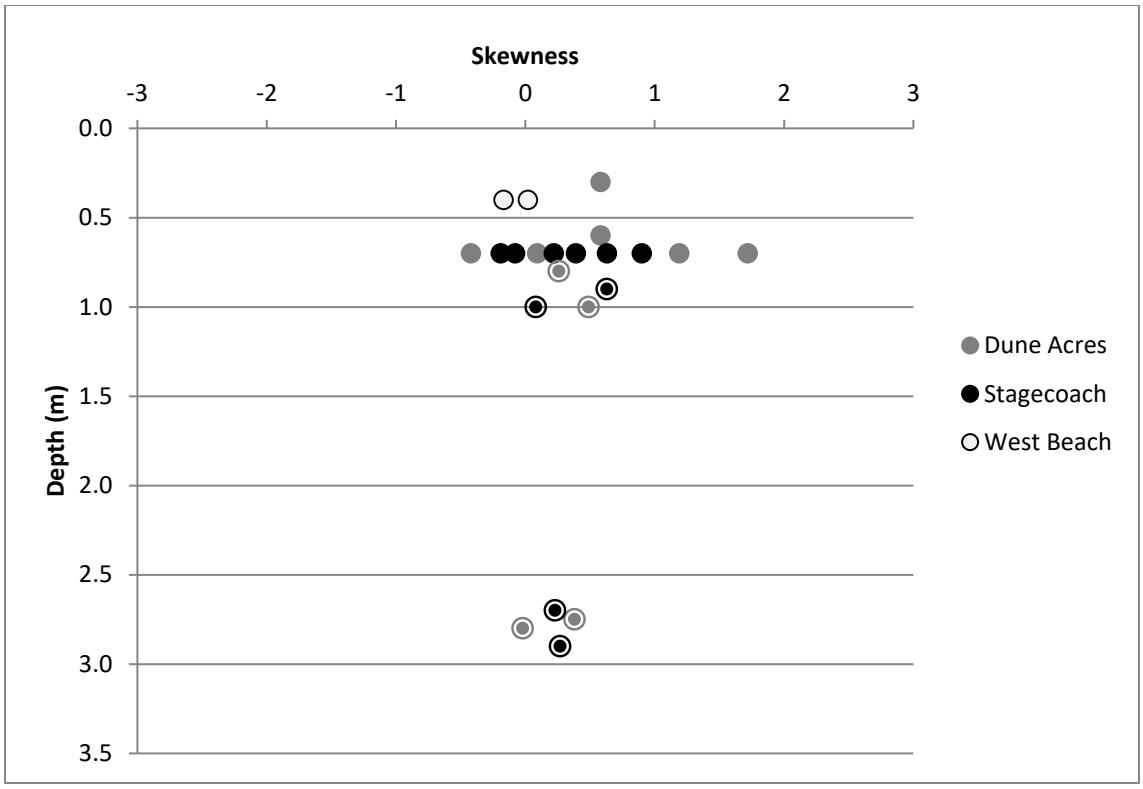

Figure 8. Skewness of D_e distribution vs. sample depth at Dune Acres, Stagecoach and West Beach. Vibracore samples are circled, other samples collected from shovel test pits.

Overdispersion, which represents the degree of spread in D_e values, could indicate a number of different problems, such as differential bleaching prior to burial or inconsistent dosing during burial (Bueno et al. 2013; Bateman 2007a; Hanson et al. 2015; Roberts et al. 2015). However, with fairly consistent environmental dose rates and a depositional setting likely to produce well bleached sediments, high overdispersion values could be attributed to post-depositional mixing of sediments, especially when coupled with the skewness data. Overdispersion values for the samples analyzed from Dune Acres (Figure 9) range from 12.1 to 24.9% which is quite typical for well-bleached eolian samples (Arnold and Roberts 2009; Hanson et al. 2015; Roberts et al. 2015). One outlier (UNL-4082)

has a value of 46.4% which possibly indicates some degree of post-depositional disturbance.

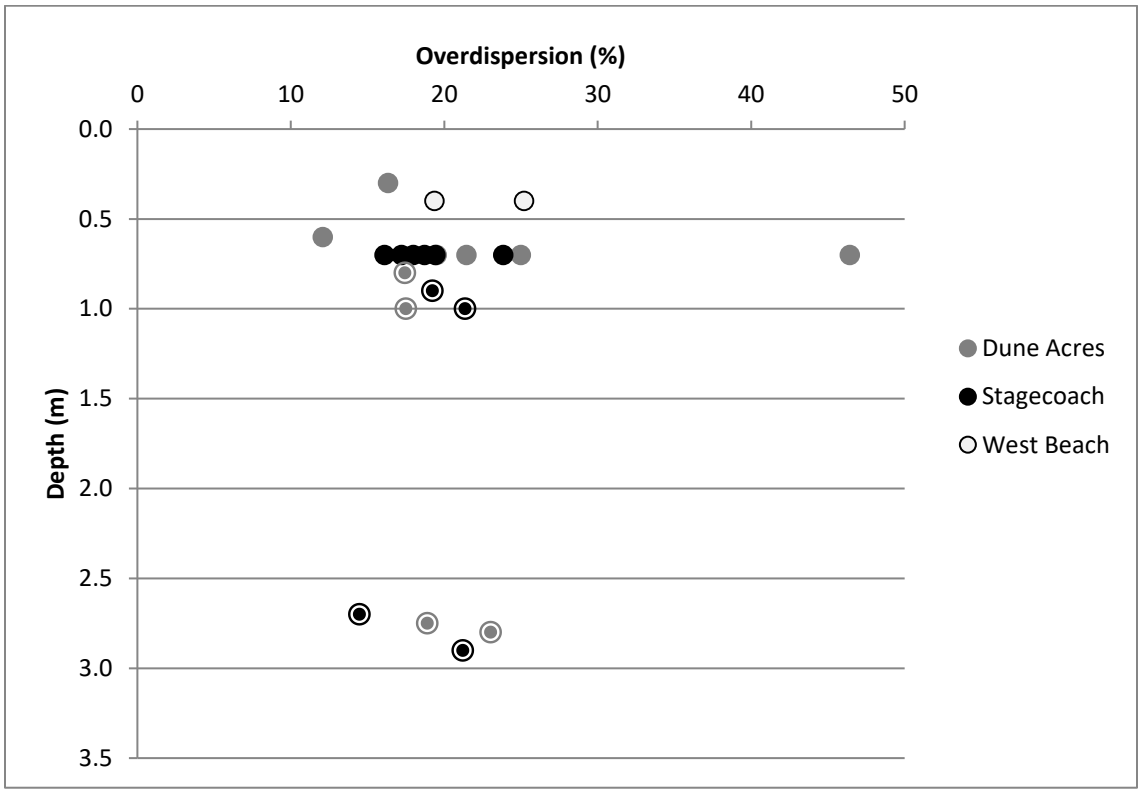

Figure 9. Overdispersion of OSL ages vs. sample depth at Dune Acres, Stagecoach and West Beach. Vibracore samples are circled, other samples collected from shovel test pits.

3.2 Stagecoach results

A total of 10 OSL samples were analyzed from the Stagecoach study area. The OSL age estimates range from 3.2 to 4.3 ka and came from depths between 0.7 and 2.9 m below ground surface (Table 1, Figure 5 and 10). Samples UNL-4083 through UNL-4092 were collected along the arms of two dunes at the depth of 0.7 m. The samples from the southern arm (UNL-4083 through UNL-4085) date between 3.2

and 3.9 ka, while the northern arm's samples (UNL-4090 through UNL-4092) produced slightly older ages of 3.9–4.2 ka (see Figure 10).

Two vibracores were also collected in the Stagecoach study area. VC3 (see Appendix 2) came from the middle of the southern arm, and showed similar weakly developed soil horizons. A thin surface soil consisting of very dark brown fine sand is followed by dark yellowish brown fine sand which grades into light yellowish brown fine sand. Although roots are not particularly abundant in the A horizon, occasional isolated rootlets are visible down to approx. 70 cm depth. Prominent horizontal to low angle laminations are preserved at approx. 1m depth and further traces of horizontal laminations are visible between 1.8 and 2.3 m depth. Two OSL samples, collected from 1.0 and 2.7 m depth (UNL-4297 and UNL-4298), yielded the same age estimates of 4.3 ± 0.4 ka. VC4 (see Appendix 2) was placed closer to the apex of the dune between the location of samples UNL-4084 and UNL-4085. A thin A horizon consisting of similar very dark brown fine sand with some roots is followed by a B horizon of dark yellowish brown fine sand which by approximately 70cm below surface grades into light yellowish brown fine sand. Clear low angle laminations are preserved at the depth of 1.9 m. Two OSL samples were collected from depths of 0.9 and 2.9 m (UNL-4299 and UNL-4300) and produced the same age estimate of 4.2 ± 0.4 ka .

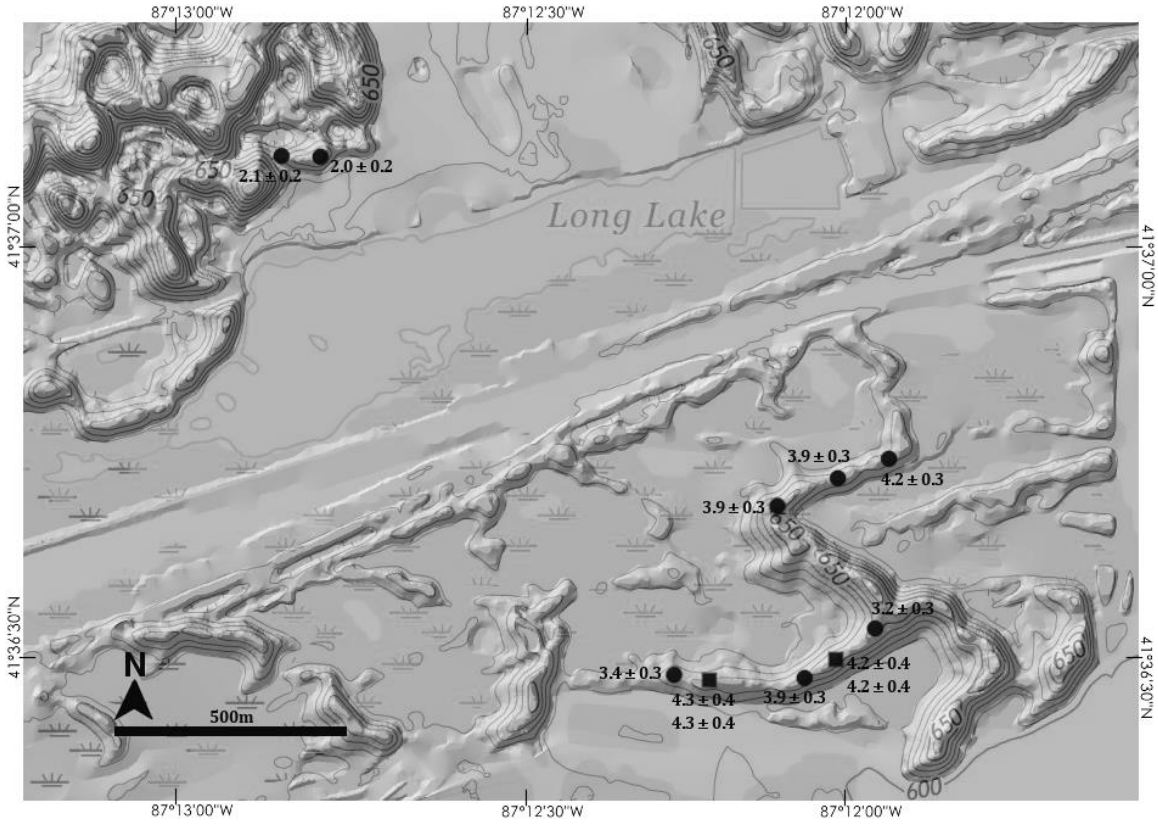

Figure 10. Sample locations with OSL ages at Stagecoach (lower right) and West Beach (upper left) study areas, overlain on a 1 m resolution LiDAR derived hillshade and a topographic map obtained from USGS's The National Map. Elevation is in feet, contour interval is 10 feet. Circles are shovel test and squares are vibracore locations.

Skewness values for Stagecoach samples range from -0.19 to 0.9 (Figure 8). Vibracore samples, again, are slightly less skewed (0.08 – 0.63) than the samples from shovel tests, although this pattern is much less obvious than at Dune Acres. Overdispersion values fit within the typically expected values for eolian sand between 14.5 and 23.9% (Figure 9).

3.3 West Beach results

Two samples (UNL-3995 and UNL-3996) were collected from the West Beach study area (Table 1, Figure 5 and 10). Their OSL ages range from 2.0 to 2.1 ka and

they were collected from the depth of 0.4 m. UNL-3995 was collected from a layer which contained archaeological artifacts. Both samples have very low skewness values (Figure 8), with UNL-3995 skewed slightly to the right (0.02) and UNL-3996 to the left (-0.17). Overdispersion values fall between 19.4 and 25.2% (Figure 9).

3.4 Summary

OSL ages obtained from the three study areas on the Tolleston Beach fall within two age clusters which could represent chronologically different depositional events (Figure 11). Alternatively, they could represent bioturbation. Samples at or

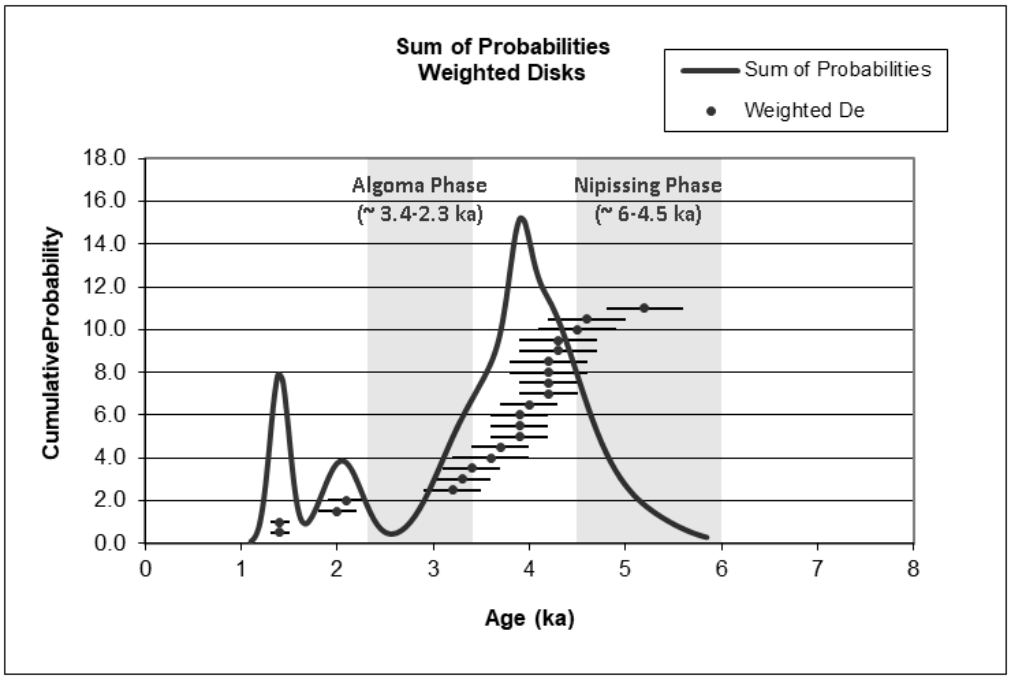

Figure 11. Probability distribution plot for all OSL age estimates in this study. Age estimates are indicated with their 1 σ errors, but the plot is constructed using summed probability values based on the 3 σ errors for the individual age estimates. Y-axis is arbitrary. The vertical gray bars indicate the timing of the Nipissing and Algoma phases after Baedke and Thompson (2000) and Thompson et al. (2011).

above 0.6 m fall within ~1.4 –2.1 ka, while samples at or below 0.7 m date between ~3.2 – 4.6 ka. The ages are stratigraphically consistent and increase with depth (Figure 5). However, numerous studies (Bueno et al. 2013; Bateman et al. 2007a, 2007b; Forrest et al. 2003; Hanson et al. 2015; Rink et al. 2013; Van Nest 2002) have shown that sediments within 1m below the ground surface are especially prone to post depositional disturbance that can be attributed to bioturbation and it is important to determine whether those ages reflect the actual burial age or perhaps a potential post-depositional disturbance. Even the occurrence of stratigraphically consistent ages does not preclude problems as those may simply reflect the intensity of bioturbation rather than be related to actual burial age (Bateman et al. 2007b). This question is especially critical for OSL applications in archaeological contexts, as those inevitably involve sampling in shallow deposits. Careful inspection of sediment characteristics as well as an evaluation of the quality of OSL data can help detect and account for post-depositional disturbance.

For the samples from shovel tests, while attention was paid to avoid visible roots and burrows, it was not possible to observe detailed characteristics of the sediment. Vibracores, however, allowed examination of sedimentary structures and also extended the stratigraphic context down to 3 m below surface. The stratigraphic profiles consist of 20 – 30 cm of organic soil horizons at the surface followed by dark to light yellowish brown eolian sand (Figure 7 and Appendix 2). No other buried soil horizons are present in the 3 m column. Traces of bedding were evident as shallow as at 0.7m depth in VC2, which would suggest that at least the samples from at or below 0.7 m depth came from undisturbed contexts. However,

relying on the presence of sedimentary structures alone is not a reliable strategy as Bateman et al. (2007b) have demonstrated. Neither is relying on the consistent vertical distribution of OSL ages without evaluating the quality of the OSL data. Overdispersion, which represents the degree of spread in D_e values, and skewness, which quantifies the asymmetry of statistical distribution, are both measures of variability within the OSL data. Some degree of overdispersion occurs due to variations in luminescence properties from grain to grain or variabilities in machine scatter (Bueno et al. 2013; Roberts et al. 2015) and are controlled in dose recovery, but any values greater than about 20% could be attributed to extrinsic factors such as differential dose rate, insufficient bleaching and bioturbation (Bateman et al. 2007a, 2007b; Bueno et al. 2013; Hanson et al. 2015; Roberts et al. 2015). Multimodal or highly skewed D_e distribution indicates the degree of mixing of grains into the sample that would be either older or younger than the depositional age. Low degree of overdispersion (10-25%; Figure 9) for all but one sample (UNL-4084) in this study and low values of skewness (-0.4 – 1.7; Figure 8) indicate that any potential post-depositional disturbance was likely minimal and therefore would not have been significant enough to affect the reliability of the OLS ages in this study.

4. Discussion

4.1 Dating the Tolleston

The older age cluster of eolian ages (Figure 5 and 11) falls between 3.2 and 5.2 ka and encompasses the period of the initial growth of the Tolleston dune field starting after the Nipissing peak in lake level (6 – 4.5 ka) and continuing up to its stabilization some time before the start of the Algoma phase highstand (3.4 – 2.3 ka). This is in accord with other studies around Lake Michigan (Argyilan et al. 2014; Hansen et al. 2010; Kilibarda et al. 2014; Lovis et al. 2009, 2012a; Rawling and Hanson 2014), which attribute most active dune building to the periods of lake level fall that immediately follow transgressive peaks. Vibracore samples consistently produced slightly older ages than the shallower samples from shovel tests that were collected at 0.7m depth. It appears that those deeper samples may represent the initial stages of Tolleston formation and correspond to the recession from the Nipissing peak at 4.7 ka (Chrzastowski and Thompson 1994; Hansel et al. 1985), while the shallower samples define the time when the parabolic dune field was stabilizing. One outlier is sample UNL-4081 at Dune Acres which yielded a date of 5.2 ± 0.4 ka. This dune is a compound nested dune and the sample came from the upwind end of a trailing arm. As the dune was migrating east, that arm likely stabilized early following the recession. If the sediment contained beach sediments that had only been transported by wind for a short distance, and thus had not been fully bleached, it may explain its older age. This sample has a higher value of positive

skewness which would be expected of a partially reset sample potentially containing grains that carry an older signal from previous burial (see Appendix 2).

These ages for the formation and stabilization of the Tolleston dune field are in agreement with other OSL studies conducted in the area. Argyilan et al. (2014) dated two dunes in the vicinity of the Dune Acres and Stagecoach study areas (Figure 12 and 13) as well as sediments from vibracores collected in adjacent wetlands. They concluded that the Tolleston Beach began to form around 4.4–4.2 ka and the dunes became stabilized by ~3.5 ka. That study targeted specific geomorphic components of the dunes with the purpose of identifying the most suitable sampling locations to represent the most recent period of dune migration. They sampled from below the soil's B horizons, between 1 and 2 m below surface, in an attempt to avoid zones which would contain potentially bioturbated sediments. Those ages correspond closely with the ages in the older cluster in this study (Figure 14). The slightly larger age range in this study may be explained by different sampling strategies. Argyilan et al. (2014) intentionally avoided dune crests, arguing that crestal ages may be indicative of short-term local disturbance and bedform movement rather than migration of the large dune form, which was the focus of their study. However, one of the purposes of this study was precisely to determine the extent of potential localized disturbance which would have affected shallow, near-surface deposits which are the target of archaeological investigations. For that reason, all samples for this analysis were collected from dune crests. A localized mobilization of sand would have exposed some grains to light and produced a younger age estimate while at the same time possibly placing older, previously

deeper, sediments closer to the surface and accessible to sampling at a shallower depth. If those localized events are indeed identifiable using OSL, a wider range of OSL ages is to be expected. Unsurprisingly then, vibracore samples show a less wide range of ages because of both greater depth and the fact that they come from only two locations on each dune and from the same stratigraphic column for each set of two samples.

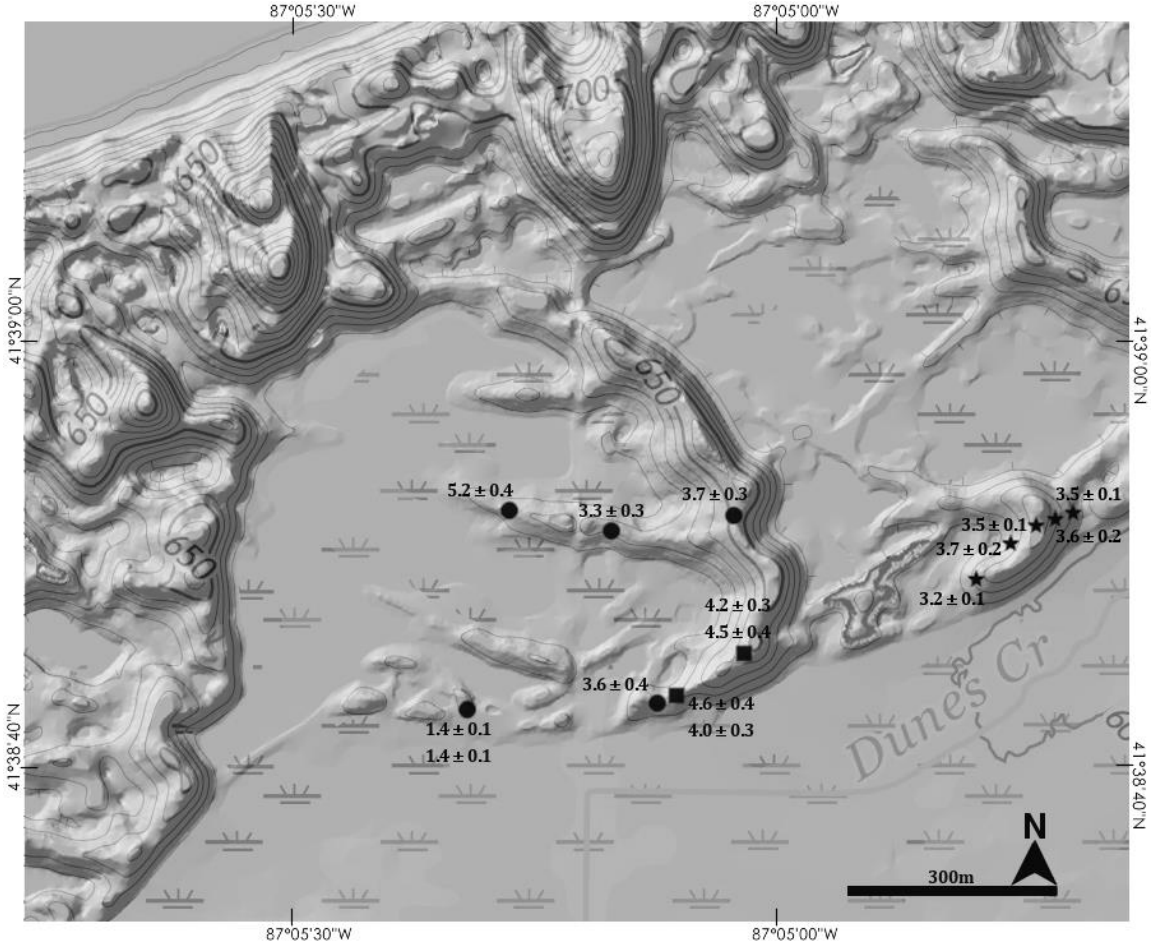

Figure 12. Dune Acres study areas with sampling locations from this study (black dots and squares) and that of Argyilan et al. (2014) (black stars; overlain on a 1 m resolution LiDAR derived hillshade and a topographic map obtained from USGS's The National Map. Lake Michigan is in the NW corner of the image. Elevation is in feet, contour interval is 10 feet. OSL ages are in thousands of years ago.

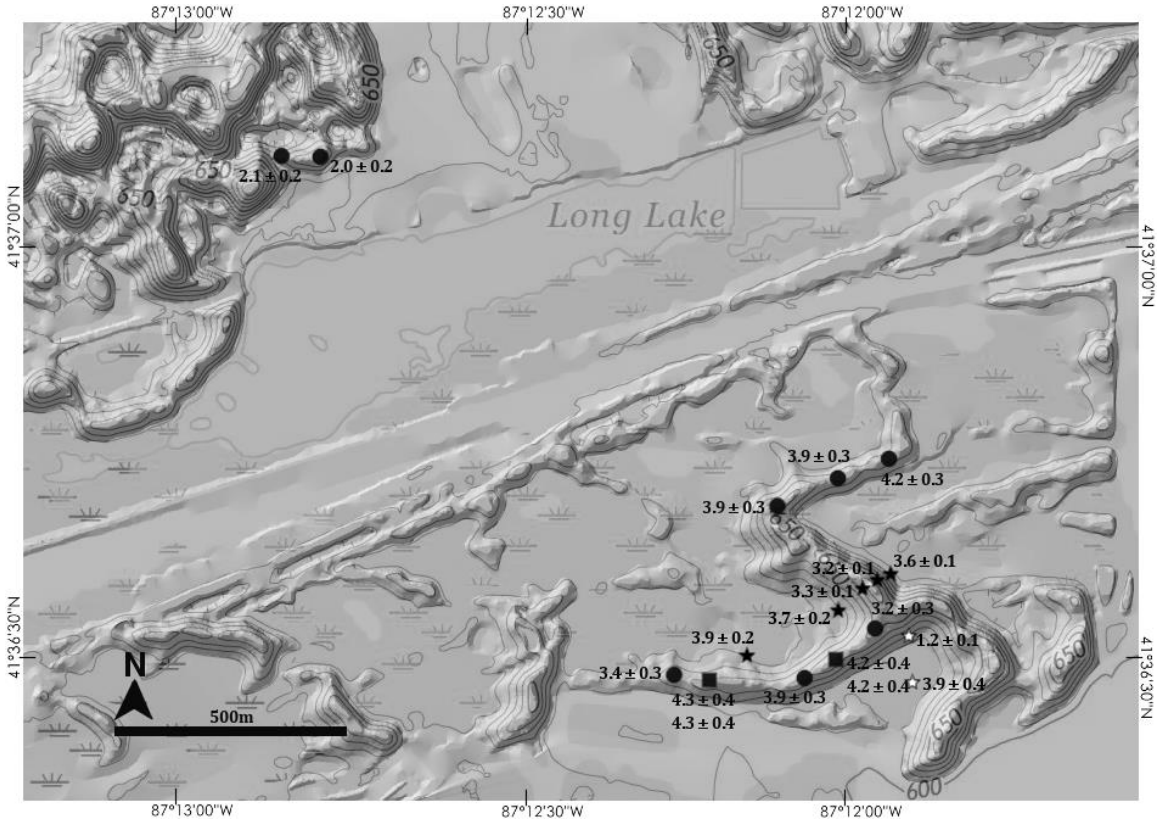

Figure 13. Stagecoach and West Beach study areas with sampling locations from this study (black dots and squares) and that of Argyilan et al. (2014) (black stars) and Bringelson et al. (2014) (white stars); overlain on a 1 m resolution LiDAR derived hillshade and a topographic map obtained from USGS's The National Map. Elevation is in feet, contour interval is 10 feet. OSL ages are in thousands of years ago.

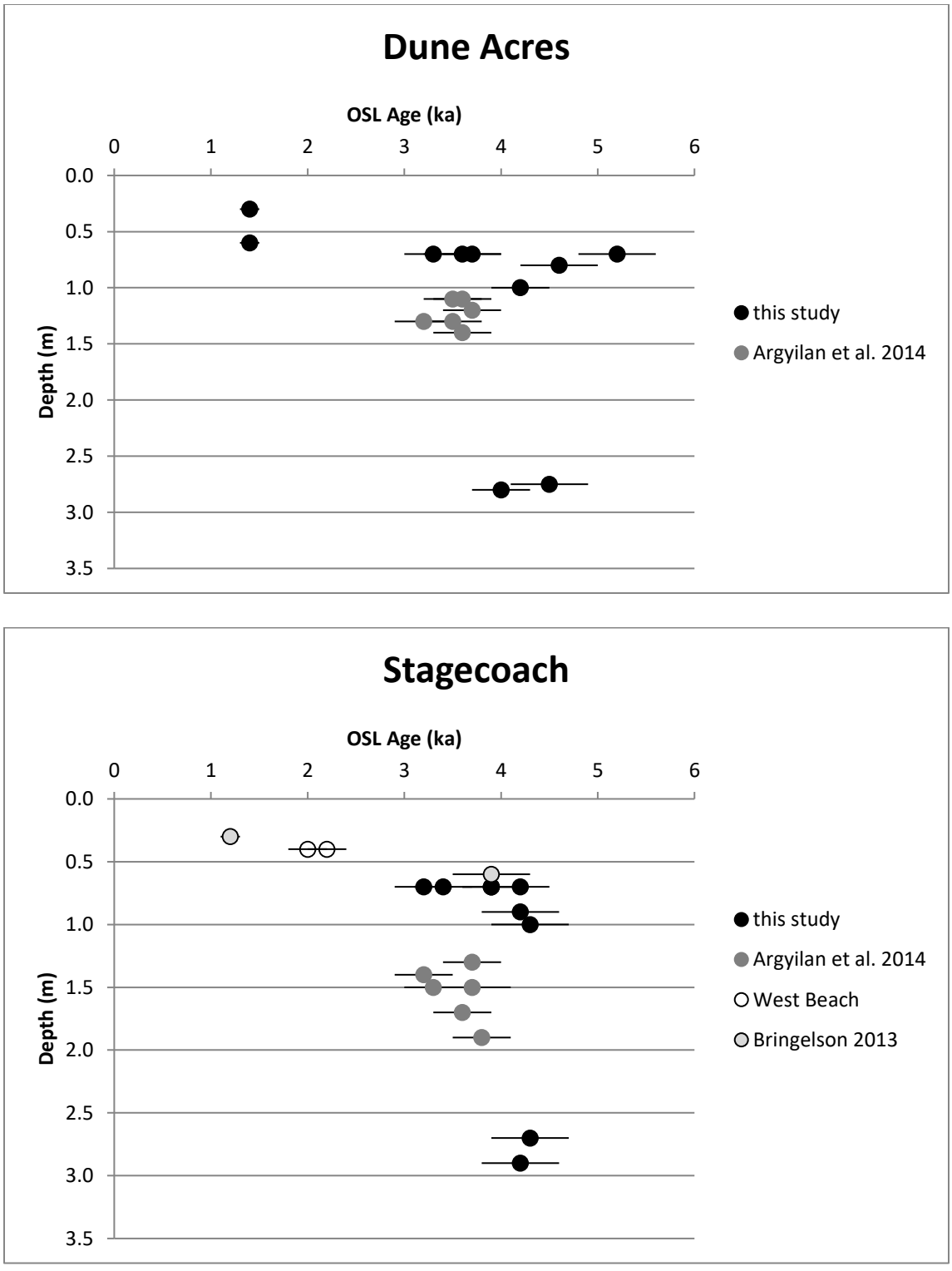

Figure 14. OSL ages with 1 σ errors at Dune Acres, Stagecoach and West Beach obtained in this study, in Argyilan et al. (2014) and in Bringelson et al. (2013).

One of the goals of this project was to determine the rate and extent of dune reactivation and how it might have affected the discoverability of archaeological sites. If the sediment reworking and the development of transgressive parabolic dunes were rapid enough, they might not be easily discernible using OSL dating as the progression of ages would fall within the ages' standard errors, especially within a single dune. However, it appears that any subsequent dune reactivation on the Tolleston (represented by the wider range of ages for the samples from 0.7 m depth, as well as the younger age cluster from shallower depth discussed below) was not sufficient to place the older sediments outside of the reach of standard archaeological methods. At both study sites, OSL ages indicate that at 0.7 m below surface, well within a feasible depth of a shovel test in this type of environment, it is possible to access deposits dated as far back as the Late Archaic. If there was in fact human occupation on landforms dating to the Tolleston at that time, it would be discoverable using this method of archaeological inventory.

The remaining four samples in this analysis come from shallower depth and their ages (1.4 – 2.1 ka) represent some kind of younger remobilization of sand on the Tolleston Beach. Even though sediments within the upper meter have been proven to be most prone to bioturbation (Bateman et al. 2003, 2007a, 2007b; Forrest et al. 2003; Hanson et al. 2015), these results suggest the impacts of bioturbation on OSL ages are minimal. This assessment appears to be the case for samples collected from 0.7 m depth, but perhaps also for samples collected from 0.3 or 0.4 m. All fours samples show acceptable degree of overdispersion (Table 1; Figure 9) and low skewness (Table 1; Figure 8). The slightly higher value of positive

skewness for the samples from Dune Acres (UNL-3994 and UNL-4301) might be explained by their association with archaeological deposits (which will be further discussed below). They came from the same shovel test at Dune Acres (Figure 6): UNL-3994 (at 0.3 m) was collected from a cultural layer which contained archaeological artifacts, while UNL-4301 was collected at 0.6 m – below the extent of the site as identified in 2008 (field documentation on file at the Midwest Archaeological Center). Surprisingly, both samples yielded the same age of 1.4 ± 0.1 ka. The two samples from West Beach came from a depth of 0.4 m. An archaeological site was recorded at this depth at the end of the dune's trailing arm (UNL-3995) and another sample from the same depth was collected at the apex (UNL-3996) to compare the ages of the different components of the dune, even though this layer did not yield archaeological material. Both samples yielded age estimates of ~2 ka. In both cases the ages do not show impacts of bioturbation and are interpreted to indicate eolian transport.

Recurrent episodes of dune building, attributed to lake level fluctuations as well as climatic shifts, are preserved all around the Lake Michigan basin (Baedtke et al. 2004; Hansen et al. 2010; Kilibarda et al. 2014; Lovis et al. 2009, 2012a; Rawling and Hanson 2014). A recent major reactivation of sand dunes occurred at ~1.0 ka and has been recorded throughout the Lake Michigan shoreline, but is usually limited to the most lakeward section of coastal dune complexes (Kilibarda et al. 2014, Lovis et al. 2012a; Hansen et al. 2010; Lovis et al. 2009, 2012a). For the Tolleston dune system, Kilibarda et al. (2014) identified four main phases of eolian development. They focused their sampling on areas of blowout activity throughout

the whole length of the shoreline in an attempt to pinpoint the main events in its initial formation and subsequent episodes of reactivation. Their analysis placed dune stabilization at around 3.0 ka, after which soils formed across the dune field. However, the wide range of OSL ages, as well as ^{14}C ages from paleosols embedded within eolian sand, were interpreted to indicate that localized blowouts were occurring on the Tolleston throughout this time period (Arbogast et al. 2004; Kilibarda et al. 2014). The last major reactivation began at ~1.0 ka and is preserved in blowouts that formed adjacent to the shoreline, where the change in wind direction is reflected in the NW-SE axis of these blowouts.

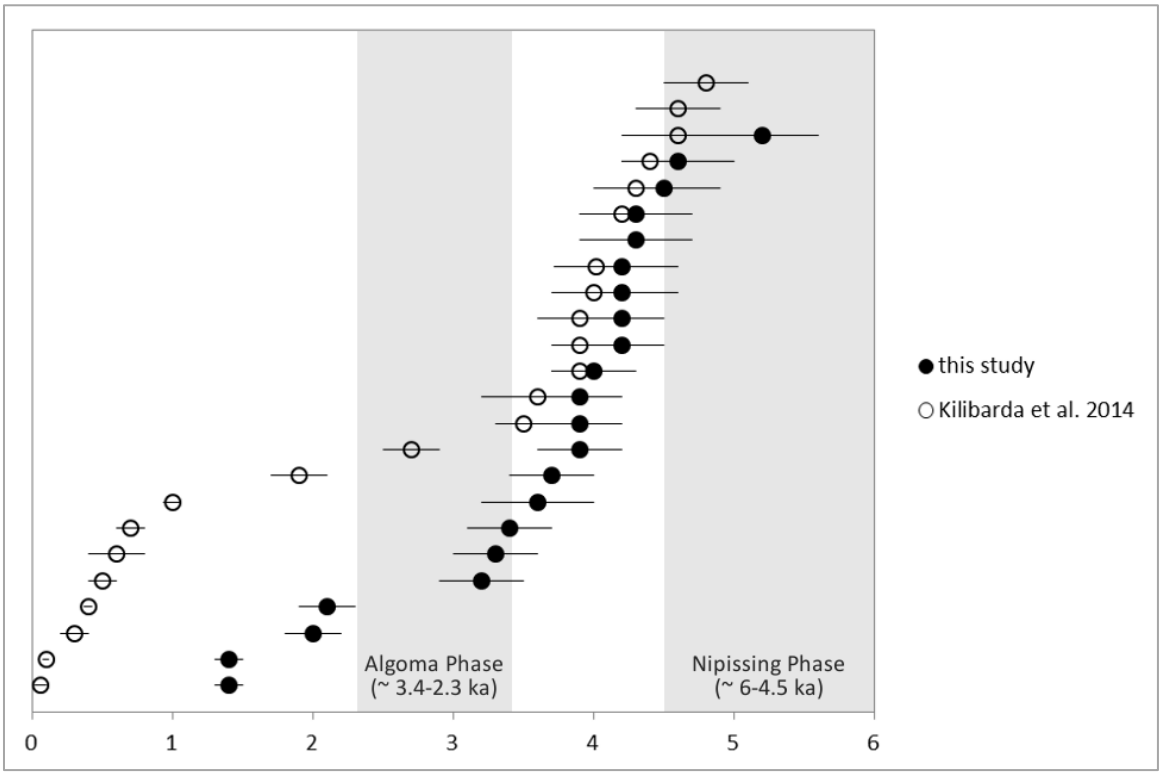

Figure 15. Summary of OSL ages with1 σ errors from this study and from Kilibarda et al. (2014). The vertical gray bars indicate the timing of the Nipissing and Algoma phases after Baedke and Thompson (2000) and Thompson et al. (2011).

Most of the OSL ages analyzed in this study overlap with the early stage of Tolleston dune field development (Figure 15) – stage 2 in Kilibarda et al. 2014, dated to ~4.5 – 3.0 ka, immediately following the Nipissing peak. These are the ages from the deeper samples collected at the depth 0.7 m or below. The ages for the four shallower samples fall within the period of localized blowout events between 3.0 and 1.0 ka (Kilibarda's Stage 3), which in turn follows the Algoma phase high. None are representative of Kilibarda's Stage 4. In their study, Kilibarda et al. sampled both from various depths and also different geomorphic locations within the dunes, as well as from different parts of the dune field, which included the blowouts closest to the modern shoreline. The samples in this study all come from the older, more landward part of the Tolleston, which may not have been affected by sand mobilization in the last one thousand years, so it is not surprising that even at the shallower depth the OSL ages do not reflect these events. With such a limited number of samples it is hard to add anything definitive to the interpretation of this period on the Tolleston. Records from the northern part of the Lake Michigan Basin (Arbogast et al. 2002; Lovis et al 2012a; Rawling and Hanson 2014) indicate a period of dune growth around 2 ka and correlate it to subtle high stands. However, this period on the southern shoreline, which did not experience the same kind of isostatic uplift as in the North, is much less well understood.

Two more OSL dates are available from INDU (Bringelson et al. 2013). They come from the interior portion of a dune just southwest of the Stagecoach location (Figure 13 and 14) and yielded ages of 1.2 ± 0.1at 0.3 m (UNL-3783) and 3.9 ± 0.4 at 0.6 m (UNL-3782) below surface. While the OSL age of the sample from 0.3 m depth

is close to the age obtained from the same depth at Dune Acres, the OSL age from 0.6 m depth correlates with the older ages collected from 0.7 m and deeper in these profiles. The question that arises, especially taking into consideration the ~ 2 ka ages from West Beach at 0.4 m depth, is whether these younger ages point to localized blowout events or if they represent a more extensive reactivation across the dune field. In either case, validating that we are potentially able to access several chronologically different events of dune reactivation at depths that are reached with shallow shovel test pits, and thus the ability to locate past human occupations from different time periods, would be of utmost importance for archaeological project planning. To answer this question, more sampling from shallow depths within the dunes is needed, combined with a careful analysis of the OSL data to assess the potential effects of bioturbation on these ages.

4.2 OSL and archaeology

When applying OSL dating in archaeology, one of the challenges is how to properly interpret the ages and their contexts. OSL could be used to date deposits that bracket otherwise defined cultural layers (Bueno et al. 2013; Sommerville et al. 2003, 2007), or deposits that are directly associated with cultural material, where it essentially dates human disturbance of that sediment. Consequently, in order to assess the reliability of an OSL age, a detailed understanding of the archaeological context is especially critical in order to be able to evaluate whether enough of that disturbance had occurred to fully reset the luminescence signal.

The archaeological site at the Dune Acres location (samples UNL-3994 and UNL-4301) is a fairly large site which contains numerous archaeological features and hundreds of lithic and ceramic artifacts (field documentation on file at the Midwest Archeological Center). This implies extensive and perhaps repeated use of that location by people in the past. Two ^{14}C dates were obtained from two hearth features located approximately 5 m apart: Feature 1 at 0.3 m depth (~1.0 – 1.1 ka) and Feature 2 at 0.5 m depth (~1.1 – 1.3 ka). The two OSL samples, which came from the same shovel test placed within 5 m west of these features, were dated to 1.4 ± 0.1 ka at both 0.3 and 0.6 m depth. While ^{14}C dates the event of burning materials in that hearth, OSL dates the disturbed sand deposit. It is not necessarily surprising that OSL ages are slightly older than ^{14}C ages. Assuming the samples were disturbed by human activity, the probable forested setting and the potential lack of complete sunlight exposure of the sand makes it likely that some residual signal may have been retained in the grains, causing some overestimation of the OSL age (Bateman et al. 2007b; Sommerville et al. 2001). Further work is needed to properly assess the chronological relationship between OSL and ^{14}C ages both in the study area and in archaeological contexts in sandy eolian environments, in general.

The archaeological site at the West Beach location consists of only 5 pieces of debitage (lithic debris from stone tool production) found at the depth of 0.4 m at the end of the dune's trailing arm. The sample UNL-3995, collected from the cultural layer, produced an OSL age of 2.1 ± 0.2 ka. The lack of evidence of more extensive human occupation makes its interpretation difficult, especially considering the fact that the sample UNL-3996, collected from the same depth at the apex of the dune,

was dated to 2.0 ± 0.2 ka and came from a shovel test devoid of any archaeological material. One thing to keep in mind is that our lack of broader archaeological context here might be due to the fact that, unlike at Dune Acres, this location has not been extensively excavated and our archaeological knowledge comes from a transect of 17 shovel test pits placed along the crest of the dune. On the other hand, since none of those shovel tests produced any archaeological material, it is possible that there was no more extensive human presence there and that the ~2 ka OSL ages may indicate some natural sand remobilization that occurred at that time. Although there is some evidence of dune reactivation associated with the end of the Algoma phase (~3.4 – 2.3 ka) from other locations around Lake Michigan (Lovis et al. 2009, 2012b; Rawling and Hanson 2014), eolian activation during the Algoma phase on the southern shoreline is not well understood. While localized dune formation cannot be discounted, it is not possible to fully interpret these dates without further archaeological testing as well as further OSL dating at the same shallow depth in other parts of the Tolleston dune field. This illustrates how important a broader archaeological and sedimentary context is for the interpretation of OSL data.

One more thing to consider is the question of the probability of the preservation of archaeological deposits in their original contexts. The presence of organic occupation horizons, often bracketed by eolian deposits, can help put the archaeological data in a chronological context (Lovis et al. 2009, 201 Bueno et al. 3023), but that unfortunately is not normally the case on the southern shore of Lake Michigan. More often than not, sparse artifact scatters are incorporated into sand

deposits without clear indication of whether they are in their original context, or perhaps within a buried lag surface, making interpretation of OSL dates and their relationship with the original occupation time extremely difficult to ascertain (see also Lovis et al. 2012b). Furthermore, just like sand grains themselves, archaeological artifacts can be subjected to processes of bioturbation which are usually attributed to small soil fauna, tree tips, as well as "anthroturbation" at multi-component sites, which further displaces original contexts and complicates chronological considerations (Bueno et al. 2013; Forrest et al. 2003; Van Nest 2002). Although the extent of this displacement is constrained by artifact size, research has shown that artifacts as big as gravel size can be moved as far down as 30 cm below ground surface (Van Nest 2002). While larger size artifacts are less likely to be brought up by burrowing fauna, instances have been reported of microdebitage being moved up the stratigraphic column by ant colonies (Bueno et al. 20123; Rink et al. 2013). Van Nest (2002) has noted that in the process of artifact burial by the formation of biomantle (organic-rich bioturbated upper part of the soil), much of the contextual data is preserved, and in some instances may even be spared by being removed from the near surface, but the reliability of numerical dating techniques in this case would have been compromised. The interpretation of OSL ages must take into account the fact that it dates displaced sediment grains as well. Fortunately, in most cases problems related to post-depositional mixing of grains are well indicated by variabilities within the OSL data, such as multi-modal D_e distributions and a notoriously high degree of overdispersion and skewness. The use of different OSL age models or the use of single grain dating protocols can help

mitigate the problems associated with dating mixed and bioturbated deposits, even if the numerical age may not be obtainable. Even if that is the case, careful examination of OSL data can help evaluate whether archaeological deposits may have been displaced along with surrounding sediment grains and, thus, OSL can provide insight into the contextual integrity of archaeological sites (Bueno et al. 2013; Roberts et al. 2013).

4.3 Archaeology at Indiana Dunes National Lakeshore

Despite years of extensive archaeological surveys which to date have covered close to 20% of the Tolleston Beach, the archaeological record remains sparse and past human occupation fairly elusive relative to other similar locations on Lake Michigan. Attempting to understand the nature and intensity of that occupation, or lack thereof, the concern has been that the eolian processes that occurred on the Tolleston since its stabilization may have buried archaeological resources below the reach of standard archaeological survey methods. However, that does not appear to be the case. OSL ages from sediments at 0.7 m depth produced dates that suggest that deposits as old as the Late Archaic can be reached within a shovel test, confirming it to be a valid and effective survey method in this particular environment. Whatever the extent of later reactivation may have been, sand accumulation was not deep enough to place those older deposits outside of the reach of standard archaeological field techniques.

The chronology and extent of more recent sand remobilization events within the Tolleston dunes is still not clear due to the limited number of shallower samples available for analysis in this study. The dates of 1.1 – 1.4 ka and 2.0 – 2.1 ka came from eolian dunes in locations that both contained archaeological sites as well as layers that were devoid of archaeological artifacts. Due to the limited number of ages available it is unclear if any extensive natural reactivation of the dunes took place during these times. Additional fieldwork has already been planned to supplement this study with a suite of samples from shallower depths (0.3 and 0.5 m) in hope of determining whether those dates reflect localized events or more wide-spread remobilization of sand across the dune field.

The Late Woodland date from the site at Dune Acres, collected at 0.6 m below surface, indicates that at a large-scale site, "anthroturbation" can reach quite deep, possibly disturbing older sediments that may contain older archaeological deposits. However, these results should be interpreted with caution and take into account the context of each sample and its placement within the dune's morphology. More dates from shallower depths, and from deposits devoid of archaeological artifacts, will help determine whether within one shovel test OSL dating can identify a stratified column of different depositional events which would allow archaeologists to identify different chronological stages of potential past human occupation.

Keeping in mind the sparse nature of archaeological resources recorded after decades of survey, the question that arises is whether the frequency and intensity of eolian processes on the Tolleston in the past perhaps created a landscape that

affected settlement patterns and occupation choices. The OSL ages from vibracores help decipher the early development of the Tolleston. It appears that the parabolic dune field developed relatively quickly. While the deposits from 0.7 m depth pinpoint the time of stabilization, the ages from vibracores, from just below 1 m and just above 3 m depth represent the early stages that fall closely after the Nippissing phase peak. It appears that the dunes built up rather quickly and most likely stabilized rapidly. The broader range of OSL ages from shovel test pits might be indicative of localized blowout events on dune crests, but they do not seem to have been substantial enough to deter human occupation of the area.

As has become clear in this analysis, the geologic context does not necessarily prevent archaeologists from accessing even older sediments. And yet, the archaeological history of the Tolleston, and especially in the West Unit of the park, remains elusive. It appears then, that it may have been a cultural choice made by people in the past to not occupy the dunes – at least not beyond some kind of ephemeral presence that would have left little to no trace in the archaeological record. Future work will hopefully aim to further investigate the archaeological history of the area.

5. Conclusions and recommendations for future work

The puzzling scarcity of archaeological sites on the Tolleston Beach at Indiana Dunes National Lakeshore prompted an investigation into the chronology of the development of this parabolic dune field and further, whether the distribution of known archaeological sites is governed by ancient human behaviors, or influenced by its dune setting which can affect site preservation and discoverability. Soil samples collected from shovel test pits and from vibracores on the crests of two compound parabolic dunes were dated using Optically Stimulated Luminescence to refine the chronology of the Tolleston and assess the variability of ages with depth. The use of vibracores in the dunes enabled the collection of samples from a 3 m long stratigraphic column and the capturing of the early stages of the Tolleston formation, immediately following the Nippissing high stand (OSL ages ~4.6–4.0 ka), while the OSL ages from 0.7 m depth represented the timing of its stabilization (OSL ages ~3.9–3.2 ka). The parabolic dune field appears to have formed relatively quickly and, within a thousand years, became stabilized with only localized episodes of dune reactivation occurring thereafter. The extent and chronology of these events will need to be refined through more dating of shallower deposits in the future. That will also help put into context the two OSL ages dating to ~2 ka, which may represent eolian remobilization of sand following the Algoma high stand. At this point, without further sampling at shallow depths from other parts of the Tolleston,

it is not possible to determine whether those ages represent a localized disturbance or a more wide spread dune reactivation following the Algoma phase.

One of the purposes of this study was to determine whether post-depositional disturbance related to bioturbation might obscure the true burial age of shallow near surface deposits which are often the target of OSL dating in archaeology. An examination of sedimentary structures within vibracores as well as an analysis of the variability within the OSL data has revealed that this is likely not the case in this particular context. The presence of preserved laminations as shallow as 0.7 m below the ground surface, stratigraphically consistent vertical distribution of OSL ages, and low values of overdispersion and skewness in the OSL data indicate that any potential post-depositional disturbance was likely minimal and therefore would not have been significant enough to affect the reliability of the OLS ages. Future work will need to address the depth to which OSL ages are adversely impacted by bioturbation.

The study also revealed that at the depth of 0.7 m below the ground surface, sediments as old as Late Archaic can be successfully accessed by archaeologists using traditional shovel test surveys. Whatever the extent of the more recent dune reactivation was in the study area, it was probably localized and not substantial enough to cause significant sand accumulation that would place archaeological deposits outside of the reach of standard archaeological methods. This validates the use of shovel test surveys as a method of inventorying cultural resources in this environment. Since the geologic setting does not appear to preclude the

archaeologists' access to potential archaeological resources, the sparse distribution pattern of human occupation on the Tolleston Beach might be better explained by exploring cultural habitation choices of past populations.

References cited

Aitken, M.J., 1998. An introduction to optical dating. New York, Oxford University Press.

Araujo A.G.M., 2013, Bioturbation and the upward movement of sediment particles and archaeological materials: comments on Bueno et al., Journal of Archaeological Science 40, 2124-2127

Arbogast, A.F., Schaetzl, R.J., Hupy, J.P., and Hansen, E.C., 2004, The Holland Paleosol: An informal pedostratigraphic unit in the coastal dunes of southeastern Lake Michigan. Canadian Journal of Earth Sciences, v. 41, 1385–1400.

Arbogast, A.F., Hansen, E.C., and Van Oort, M.D., 2002, Reconstructing the geomorphic evolution of large coastal dunes along the southeastern shore of Lake Michigan. Geomorphology, v. 46, 241–255.

Argyilan, E.P., Lepper, K., Thompson, T.A., 2014. Late Holocene coastal development along the southern shore of Lake Michigan determined by strategic dating of stabilized parabolic dunes and wetlands of the Tolleston Beach. In Fisher, T.G., and Hansen, E.C., (Eds.), Coastline and Dune Evolution along the Great Lakes. Geological Society of America Special Paper 508, 31–46.

Arnold, L.J., Roberts, R.G., 2009. Stochastic modelling of multi-grain equivalent dose (De) distributions: implications for OSL dating of sediment mixtures. Quaternary Geochronology 4, 204–230.

Baedke, S.J., Thompson, T.A., 2000. A 4,700-year record of lake level and isostasy for Lake Michigan. Journal of Great Lakes Research 26, 416–426.

Baedke, S.J., Thompson, T.A., Johnston, J.W. Wilcox, D.A., 2004. Reconstructing Paleo Lake Levels from Relict Shorelines along the Upper Great Lakes. Aquatic Ecosystem Health & Management, 7, 435–449.

Bateman, M.D., Frederick, C.D., Jaiswal, M.K., Singhvi, A.K., 2003. Investigations into the potential effects of pedoturbation on luminescence dating. Quaternary Science Reviews 22, 1169–1176.

Bateman, M.D., Boulter, C.H., Carr, A.S., Frederick, C.D., Peter, D. Wilder, M., 2007a. Detecting postdepositional sediment disturbance in sandy deposits using luminescence. Quaternary Geochronology 2, 57–64.

Bateman, M.D., Boulter, C.H., Carr, A.S., Frederick, C.D., Peter, D. Wilder, M., 2007b. Preserving the palaeoenvironmental record in Drylands: Bioturbation and its significance for luminescence derived chronologies. Sedimentary Geology 195, 5–19.

Bringelson, D., Mahoney G., Hanson, P.R., 2014. The Conundrum of the West Unit: Understanding Duneland Prehistory Along Southern Lake Michigan. Poster presented at the 79th Annual Meeting of the Society for American Archaeology, Austin, TX.

Bringelson, D., Sturdevant, J.T., 2007. An archeological overview and assessment of Indiana Dunes National Lakeshore, Indiana. Midwest Archeological Center Technical Report No. 97, National Park Service, Midwest Archeological Center, Lincoln, Nebraska.

Brose, D.S., 1970. The Archaeology of Summer Island: Changing Settlement Systems in Northern Lake Michigan. Anthropological Papers No. 41. Museum of Anthropology, University of Michigan, Ann Arbor.

Bueno, L., Feathers, J., De Blasis, P., 2013. The formation process of a paleoindian open-air site in Central Brazil: integrating lithic analysis, radiocarbon and luminescence dating. Journal of Archaeological Science 40, 190-203.

Capps, D.K., Thompson, T.A., Booth, R.K., 2007. A post-Calumet shoreline along southern Lake Michigan. Journal of Paleolimnology 37, p. 395–409.

Chrzastowski, M.J., Thompson, T.A., 1992. Late Wisconsinan and Holocene coastal evolution of the southern shore of Lake Michigan. In Fletcher, C.H., III, and Wehmiller, J.H. (Eds.), Quaternary Coasts of the United States: Marine and Lacustrine Systems, SEPM Special Publication No. 48, 397–413.

Chrzastowski, M.J., Thompson, T.A., 1994. Late Wisconsinan and Holocene geologic history of the Illinois-Indiana coast of Lake Michigan: Journal of Great Lakes Research, 20, 9–26.

Clarke M.L., Rendell H.M., Wintle A.G., 1999. Quality assurance in luminescence dating. Geomorphology 29, 173–185.

Durán, O., Herrmann, H.J., 2006. Vegetation against dune mobility: Physical Review Letters, 97, 188001–188004.

Forrest, B., Rink, W.J., Bicho, N., Ferring, C.R., 2003. OSL ages and possible bioturbation signals at the upper Palaeolithic site of Lagoa do Bordoal, Algarve, Portugal. Quaternary Science Reviews 22, 1279–1285.

Frederick, C. D., Bateman, M.D., Rogers, R., 2002. Evidence for eolian deposition in the sandy uplands of east Texas and the implications for archaeological site integrity. Geoarchaeology 17:191– 217.

Frost, F.L., 2001. Archeological inventory and evaluation of selected areas, Indiana Dunes National Lakeshore, Indiana: 1992-1995. US Department of the Interior, National Park Service, Midwest Archeological Center, Lincoln, Nebraska.

Galbraith, R., Roberts, R., Laslett, G., Yoshida, H., Olley, J., 1999. Optical dating of single and multiple grains of quartz from Jinmium rock shelter, northern Australia: Part I, experimental design and statistical models. Archaeometry 41, 339-364.

Gliganic, L. A., Cohen, T. J., Slack, M., and Feathers, J. K., 2016. Sediment mixing in aeolian sandsheets identified and quantified using single-grain optically stimulated luminescence. Quaternary Geochronology 32, 53-66.

Hansel A.K., Mickelson D.M., 1988. Reevaluation of the timing and causes of high lake phases in the Lake Michigan basin. Quaternary Research 29, 113–128.

Hansel, A. K., Mickelson, D. M., Schneider, A. F., and Larsen, C. E., 1985. Late Wisconsinan and Holocene history of the Lake Michigan basin. Geological Association of Canada Special Paper 30, 39–53.

Hansen, E.C., Fisher, T.G., Arbogast, A.F., and Bateman, M.D., 2010, Geomorphic history of low-perched, transgressive dune complexes along the southeastern shore of Lake Michigan. Aeolian Research, v. 1, p. 111–127.

Hanson, P.R., Mason, J.A., Jacobs, P.M., Young, A.R., 2015. Evidence for bioturbation of luminescence signals in eolian sand on upland ridgetops, southeastern Minnesota, USA. Quaternary International 362, 108–115.

Hesp, P., 2011. Dune Coasts. In: Wolanski, E. McLusky, D.S. (eds.), Treatise on Estuarine and Coastal Science, Vol 3, 193–221. Waltham: Academic Press.

Huntley, D.J., Godfrey-Smith, D.I., Thewalt, M.L.W., 1985. Optical dating of sediments. Nature 313, 105–107.

Indiana State Climate Office, https://climate.agry.purdue.edu/climate/narrative.asp accessed August 31, 2018.

Jeske, R.J., 1990. The Wabash-Erie divide and prehistoric cultural contact: The Northeast-Midwest transition in Northern Indiana. In: Proceedings of the

Indiana Academy of Sciences. Indiana Academy of Sciences, Bloomington, pp. 100-108.

Kilibarda, Z., Venturelli, R., Goble, R.J., 2014. Late Holocene dune development and shift in dune-building winds along southern Lake Michigan. in Fisher, T.G., Hansen, E.C. (Eds.), Coastline and Dune Evolution along the Great Lakes. Geological Society of America Special Paper 508, 47–64.

Lovis, W.A., 1990. Site Formation Processes and the Organization of Space at the Stratified Late Woodland O'Neil Site. In Gibbon, R. (Ed.), The Woodland Tradition in the Western Great Lakes: Papers Presented to Elden Johnson, Chapter 12, pp. 195–211. Publications in Anthropology No 4., University of Minnesota Press, Minneapolis.

Lovis, W.A., Rajnovich G., Bartley A., 1998. Exploratory Cluster Analysis, Temporal Change, and the Woodland Ceramics of the Portage Site at L'Arbre Croche. In Birmingham R., Cleland C. (Eds.), Papers in Honor of Ronald J. Mason, The Wisconsin Archeologist 79, 89–112.

Lovis, W.A., Arbogast A.F., Monaghan. G.W., 2009 Geoarchaeology and Taphonomy of Lake Michigan Coastal Dunes: Activation, Stabilization, Cycling and Archaeological Site Formation Processes. Report submitted to the Environmental Section, Michigan Department of Transportation (Contract IDS 2006-0034-Z1). Michigan State University, East Lansing, Michigan.

Lovis, W.A., Arbogast, A.F., Monaghan, G.W., 2012a. The geoarchaeology of Lake Michigan coastal dunes. Environmental Research Series No. 2, Michigan Department of Transportation, Michigan State University Press, East Lansing.

Lovis, W.A., Monaghan, G.W., Arbogast, A.F., Forman, S.L., 2012b. Deferential temporal and spatial preservation of archaeological sites in a Great Lakes coastal zone. American Antiquity 77, 591-608.

Lynot, M.J., Frost, F., Neff, H., Cogswell, J.W., Glascock, M.D., 1998. Prehistoric occupation of the Calumet Dune Ridge, Northwest Indiana. Midcontinental Journal of Archaeology 23, 221-260.

Muhs, D.R., Maat, P.B., 1993, The potential response of eolian sands to greenhouse warming and precipitation reduction on the Great Plains of the U.S.A: Journal of Arid Environments 25, 351–361.

Murray, A.S., Olley, J.M., 2002. Precision and accuracy in the optically stimulated luminescence dating of sedimentary quartz: a status review. Geochronometria 21, 1–16.

Murray, A.S., and Wintle, A.G., 2000a. Luminescence dating of quartz using an improved single-aliquot regenerative-dose protocol. Radiation Measurements 32, 57–73.

Murray, A.S., and Wintle, A.G., 2000b. Quartz OSL: Effects of thermal treatment and their relevance to laboratory dating procedures. Radiation Measurements 32, 387–400.

Murray, A. S., Wintle, A. G., 2003. The single aliquot regenerative dose protocol: potential for improvements in reliability. Radiation Measurements 37, 377-381.

Prescott, J.R., Hutton J.T., 1994. Cosmic ray contributions to dose rates for luminescence and ESR dating: large depths and long-term time variations. Radiation Measurements 23, 497–500.

Puta, R.A. Hanson, P.R., Young A.R., 2013. Late Holocene Activation History of the Stanton Dunes, Northeastern Nebraska. Great Plains Research 23, 11–23.

Pye, K., 1982. Morphological development of coastal dunes in a humid tropical environment, Cape Bedford and Cape Flattery, North Queensland: Geografiska Annaler, v. 64, p. 212–227.

Pye, K., 1983. Coastal dunes: Progress in Physical Geography 7, 531–557.

Pye, K., Tsoar, H., 1990. Aeolian Sand and Sand Dunes. Unwin Hyman, London.

Rawling, J.E. III, Hanson, P.R., 2014. Dune formation on late Holocene sandy bay barriers along Lake Michigan's Door Peninsula: The importance of increased sediment supply following the Nipissing and Algoma high lake-level phases. In: Fisher, T.G., and Hansen, E.C., eds., Coastline and Dune Evolution along the Great Lakes: Geological Society of America Special Paper 508,(2014)

Richards, J.D., Jeske, R.J., 2002. Location, location, location: The temporal and cultural context of late prehistoric settlement in Southeast Wisconsin. The Wisconsin Archeologist 83, 32-54.

Richner, J. J., 1973. Depositional history and tool industries at the Winter Site: A Lake Forest Middle Woodland cultural manifestation. Unpublished Master's thesis, Department of Anthropology, Western Michigan University, Kalamazoo.

Rink, W. Jack, James S. Dunbar, Walter R. Tschinkel, Christina Kwapich, Andrea Repp, William Stanton, and David K.Thulman, 2013. Subterranean Transport and Deposition of Quartz by Ants in Sandy Sites Relevant to Age Overestimation in Optical Luminescence Dating. Journal of Archaeological Science 40, 2217–2226.

Rhodes, E.J., 2011. Optically stimulated luminescence dating of sediments over the past 200,000 years. Annual Review of Earth Planetary Sciences 39, 461-488.

Roberts, R.G., Jacobs, Z., Li, B., Jankowski, N.R., Cunningham, A.C., Rosenfeld, A.B., 2015. Optical dating in archaeology: thirty years in retrospect and grand challenges for the future. Journal of Archaeological Science 56, 41–60.

Schurr, M.R., 2003. The late prehistory of Northwestern Indiana: New perspectives on an old model. In: Redmond, B.G., Jones, J.R. III (Eds.), Facing the final millennium: Studies in in the late prehistory of Indiana, A.D. 700 to 1700. Indiana Department of Natural Resources, Division of Historic Preservation and Archaeology, Indianapolis, pp. 4-31.

Sommerville, A.A., Sanderson, D.C.W., Hansom, J.D., Housley, R.A., 2001. Luminescence dating of Aeolian activity from archaeological sites in northern Britain: a preliminary study. Quaternary Science Reviews 20, 913–923.

Sommerville, A.A., Hansom, J.D., Sanderson, D C.W. and Housley, R.A., 2003. Optically stimulated luminescence dating of large storm events in northern Scotland. Quaternary Science Review 22, 1085–92.

Sommerville, A.A., Hansom, J., Housley, R., Sanderson, D.C.W., 2007. Optically stimulated luminescence (OSC) dating of coastal aeolian sand accumulation in Sanday, Orkney Islands, Scotland. Holocene. 17, 627–637.

Sturdevant, J.T., Bringelson, D. 2007. Archeological inventory and testing at sites along the Dunes Creek Corridor 2002-2005, Indiana Dunes National Lakeshore, Porter County, Indiana. Midwest Archeological Center Technical Report No. 101, US Department of the Interior, National Park Service, Midwest Archeological Center, Lincoln, Nebraska.

Thompson, T.A., 1990. Dune/beach complex and back-barrier sediments along the southeastern shore of Lake Michigan: Cowles Bog area of the Indiana Dunes National Lakeshore: Geological Society of America Special Paper 251, 9–19.

Thompson, T.A., 1992. Beach-ridge development and lake-level variation in southern Lake Michigan. Sedimentary Geology 80, 305–318.

Thompson, T.A., 1994. History and architecture of wetland development in the Indiana Dunes. Proceedings of the Indiana Academy of Science, 103 (3-4), 167-176.

Thompson, T.A., Baedke, S.J., 1997. Strand-plain evidence for late Holocene lake-level variations in Lake Michigan: Geological Society of America Bulletin 109, 666–682.

Thompson, T. A., Baedke, S. J., Johnston, J. W. 2004. Geomorphic expression of late Holocene lake levels and paleowinds in the upper Great Lakes. Michigan Academician 35, 355–371.

United States Geologic Survey, The National Map, https://nationalmap.gov/ accessed August 2018.

Van Nest J., 1997. The good earthworm: How natural processes preserve upland Archaic archaeological sites of western Illinois, U.S.A. Geoarchaeology 17(1):53–90.

White, D.R.M., 2000. Roots eternal and unshakable: An ethnographic overview of Indiana Dunes National Lakeshore. Report prepared for the National Park Service, Contract No. 1443-CX-6300-97033. Applied Cultural Dynamics, Santa Fe.

Wintle, A. G., Murray, A. S., 2006. A review of quartz optically stimulated luminescence characteristics and their relevance in single-aliquot regeneration dating protocols. Radiation Measurements 41, 369-391.

Appendix 1: Archaeological sites on the Tolleston Beach

State Site Number	Park Unit	Location	Site type
12LA419	West	in between beach ridges at western end of Tolleston Beach	isolated lithic find
12LA420	West	bench between Calumet River outlet and recent Tolleston dunes	lithic scatter
12LA421	West	bench between Calumet River outlet and recent Tolleston dunes	lithic scatter
12LA422	West	bench between Calumet River outlet and recent Tolleston dunes	lithic scatter
12LA423	West	arm of compound dune	ceramic scatter
12LA694	West	edge of wetland	isolated lithic find in disturbed context
12PR744	West	simple parabolic dune ridge	isolated lithic find
12PR770	West	end of trailing arm	lithic scatter
12PR248	West	beach ridge	lithic scatter on surface
12PR771	West	recent dune arm	historic and prehistoric artifact scatter
12PR497	West	end of dune ridge by inland marsh	lithic and ceramic scatter
12PR495	West	ridge overlooking marsh	lithic scatter
12PR746	West	in deflation basin	isolated ceramic find
12PR745	West	dune arm	isolated lithic find
12PR501	West	crest of high dune overlooking wetland to the south	isolated fire-cracked rock
12PR496	West	in slumped, disturbed context	lithic and ceramic artifacts
12PR398	East	end of trailing arm on edge of marsh	isolated lithic find
12PR413	East	compound dune ridge	isolated lithic find
12PR598	East	compound dune ridge	isolated lithic find
12PR391	East	low ridge of compound dune, next to bog	isolated lithic find
12PR392	East	low ridge of compound dune, next to bog	isolated lithic find
12PR393	East	low ridge of compound dune, next to bog	isolated lithic find
12PR394	East	low ridge of compound dune, next to bog	lithic, ceramic and historic artifacts
12PR406	East	low ridge overlooking wetland	lithic scatter
12PR407	East	low ridge overlooking wetland	isolated fire-cracked rock
12PR408	East	low ridge overlooking wetland	lithic scatter

12PR399	East	low ridge in between wetlands	isolated lithic find
12PR400	East	low ridge in between wetlands	lithic scatter
12PR401	East	low ridge in between wetlands	isolated lithic find
12PR395	East	low ridge in between wetlands	lithic and ceramic scatter
12PR396	East	small ridge next to wetland	lithic and ceramic scatter
12PR411	East	small ridge next to wetland	lithic scatter
12PR412	East	small ridge next to wetland	isolated lithic find
12PR402	East	high ridge of compound dune overlooking wetland	isolated lithic find
12PR397	East	high ridge of compound dune overlooking wetland	lithic scatter
12PR403	East	low ridge overlooking wetland	lithic scatter
12PR404	East	low ridge overlooking wetland	lithic, ceramic, and historic artifacts
12PR405	East	low ridge overlooking wetland	lithic and ceramics
12PR739	East	dune arm	isolated lithic find
12PR740	East	dune arm	isolated lithic find
12PR308	East	simple parabolic dune ridge	lithic scatter
12PR309	East	simple parabolic dune ridge	lithic scatter
12PR310	East	simple parabolic dune ridge	lithic scatter
12PR305	East	dune ridge along wetland	isolated lithic find
12PR306	East	dune ridge along wetland	lithic and ceramic scatter
12PR307	East	compound dune arm	isolated lithic find
12PR121	East	Big Blowout in state park	lithic scatter
12PR331	East	low ridge overlooking wetland	lithic scatter
12PR332	East	low ridge overlooking wetland	lithic scatter
12PR333	East	low ridge overlooking wetland	lithic scatter
12PR334	East	low ridge overlooking wetland	lithic and ceramic scatter
12PR335	East	low ridge overlooking wetland	lithic scatter
12PR336	East	low ridge overlooking wetland	lithic scatter
12PR337	East	low ridge overlooking wetland	lithic and ceramic scatter
12PR330	East	simple dune ridge along wetland	lithic scatter

12PR327	East	simple dune ridge along wetland	lithic scatter
12PR329	East	small ridge along wetland	lithic scatter
12PR328	East	small ridge along wetland	isolated lithic find
12PR326	East	small ridge along wetland	isolated lithic find
12PR325	East	small ridge one edge of wetland	lithic scatter
12PR324	East	small ridge on edge of wetland	isolated lithic find
12PR323	East	small dune ridge along wetland	lithic and ceramics, historic too
12PR312	East	low ridge on edge of wetland	lithic and ceramic scatter
12PR311	East	ridge intersected by road	lithic and ceramic scatter
12PR313	East	small ridge along wetland	isolated lithic find
12PR314	East	dune crest, near marsh	lithics and ceramics
12PR315	East	dune crest, near marsh	isolated lithic find
12PR316	East	dune crest, near marsh	isolated lithic find
12PR317	East	end of arm	lithic scatter
12PR318	East	compound dune ridge, further from marsh	lithic scatter
12PR319	East	compound dune ridge, further from marsh	lithic scatter
12PR320	East	compound dune ridge, further form marsh	lithic and ceramic artifacts
12PR321	East	ridge of compound dune, end of arm	lithic and ceramic artifacts
12PR352	East	compound dune arm	lithic scatter

Appendix 2: Vibracore photographs

Photograph of vibracore **VC1**, collected from Dune Acres. Depths are in meters below surface. The arrows indicate prominent laminations. Ages are in thousands of years ago.

Photograph of vibracore **VC2**, collected from Dune Acres. Depths are in meters below surface. The arrows indicate prominent laminations. Ages are in thousands of years ago.

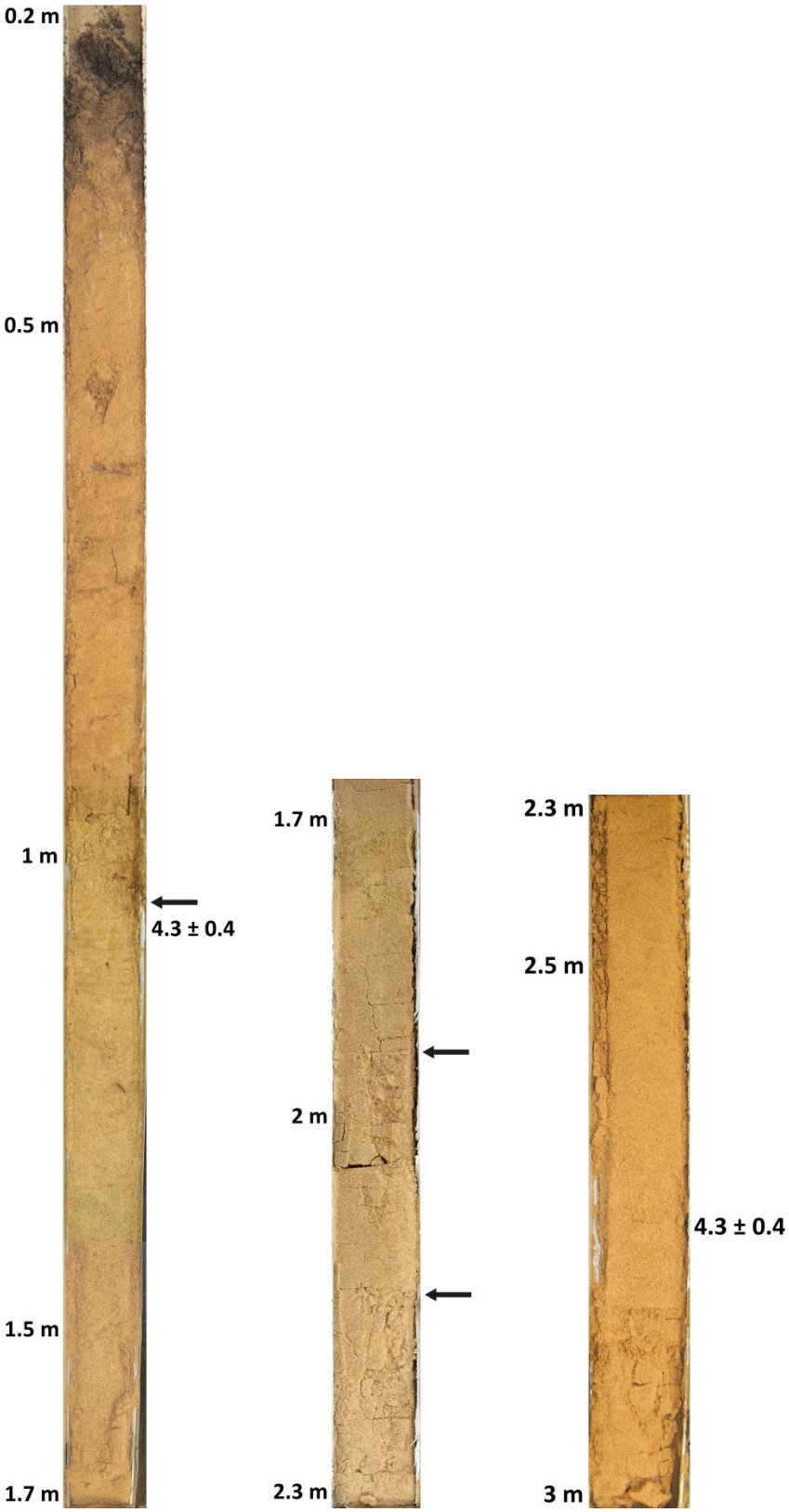

Photograph of vibracore **VC3**, collected from Dune Acres. Depths are in meters below surface. The arrows indicate prominent laminations. Ages are in thousands of years ago.

Photograph of vibracore **VC4**, collected from Dune Acres. Depths are in meters below surface. The arrows indicate prominent laminations. Ages are in thousands of years ago.

Appendix 3: OSL Data

UNL-3994

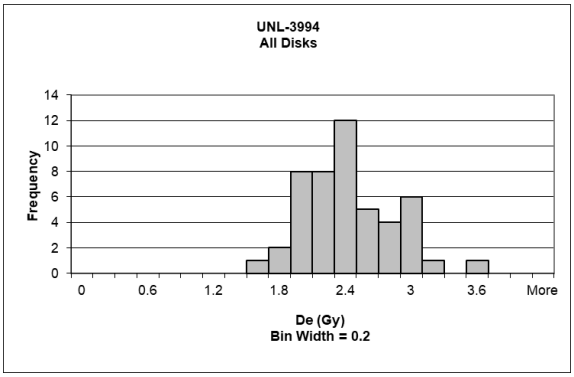

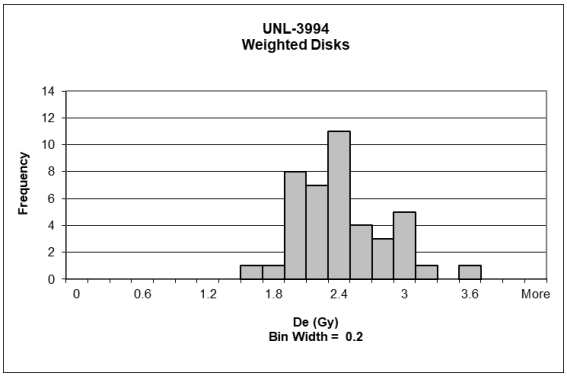

Disc	De	Error	Wt	Age	+/- 1 σ
1	1.927	0.08	1	1.146	0.94
2	1.927	0.08	1	1.146	0.94
3	2.956	0.02	1	1.758	1.47
4	2.191	0.12	1	1.303	0.32
5	2.777	0.06	1	1.652	1.05
6	2.568	0.10	1	1.527	0.56
7	2.307	0.13	1	1.372	0.05
8	1.514	0.24	1	0.901	1.91
9	2.711	0.21	1	1.612	0.89
10	3.524	0.01	1	2.096	2.80
11	2.293	0.09	1	1.364	0.09
12	2.842	0.10	1	1.690	1.20
13	2.225	0.13	1	1.324	0.24
14	2.229	0.16	1	1.326	0.24
15	2.062	0.20	1	1.226	0.63
16	2.345	0.11	1	1.395	0.04
17	2.107	0.23	1	1.253	0.52
18	2.217	0.13	1	1.318	0.27
19	2.171	0.07	1	1.291	0.37
20	2.071	0.21	1	1.232	0.61
21	2.015	0.11	1	1.199	0.74
22	2.493	0.17	1	1.483	0.38
23	1.888	0.06	1	1.123	1.04
24	2.018	0.09	1	1.201	0.73
25	2.205	0.07	1	1.312	0.29
26	2.299	0.23	1	1.367	0.07
27	2.577	0.19	1	1.533	0.58
28	1.906	0.17	1	1.134	0.99
29	2.541	0.06	1	1.511	0.49
30	1.813	0.07	1	1.078	1.21
31	2.763	0.02	1	1.643	1.01
32	2.884	0.09	1	1.715	1.30
33	2.922	0.07	1	1.738	1.39
34	2.340	0.13	1	1.392	0.02
35	2.323	0.04	1	1.382	0.02
36	1.929	0.05	1	1.147	0.94
37	1.947	0.03	1	1.158	0.90
38	2.470	0.13	1	1.469	0.33
39	1.861	0.21	1	1.107	1.10
40	1.644	0.24	1	0.978	1.61
41	1.726	0.18	1	1.027	1.41
42	2.896	0.07	1	1.723	1.33
43	2.862	0.20	1	1.702	1.24
44	2.388	0.04	1	1.420	0.14
45	2.166	0.19	1	1.289	0.38
46	2.719	0.24	1	1.617	0.91
47	2.350	0.08	1	1.398	0.05
48	3.121	0.20	1	1.856	1.85

Disc	De	Error	Wt	Age	+/- 1 σ
1	1.927	0.08	1	1.146	0.94
2	1.927	0.08	1	1.146	0.94
3	2.956	0.02	1	1.758	1.47
4	2.191	0.12	1	1.303	0.32
5	2.777	0.06	1	1.652	1.05
6	2.568	0.10	1	1.527	0.56
7	2.307	0.13	1	1.372	0.05
8	1.514	0.24	1	0.901	1.91
9	2.711	0.21	1	1.612	0.89
10	3.524	0.01	1	2.096	2.80
11	2.293	0.09	1	1.364	0.09
12	2.842	0.10	1	1.690	1.20
13	2.225	0.13	1	1.324	0.24
14	2.229	0.16	1	1.326	0.24
15	2.062	0.20	1	1.226	0.63
16	2.345	0.11	1	1.395	0.04
17	2.107	0.23	1	1.253	0.52
18	2.217	0.13	1	1.318	0.27
19	2.171	0.07	1	1.291	0.37
20	2.015	0.11	1	1.199	0.74
21	2.493	0.17	1	1.483	0.38
22	1.888	0.06	1	1.123	1.04
23	2.018	0.09	1	1.201	0.73
24	2.205	0.07	1	1.312	0.29
25	2.299	0.23	1	1.367	0.07
26	2.577	0.19	1	1.533	0.58
27	1.906	0.17	1	1.134	0.99
28	2.541	0.06	1	1.511	0.49
29	1.813	0.07	1	1.078	1.21
30	2.763	0.02	1	1.643	1.01
31	2.884	0.09	1	1.715	1.30
32	2.922	0.07	1	1.738	1.39
33	2.340	0.13	1	1.392	0.02
34	1.929	0.05	1	1.147	0.94
35	1.947	0.03	1	1.158	0.90
36	1.861	0.21	1	1.107	1.10
37	1.644	0.24	1	0.978	1.61
38	2.896	0.07	1	1.723	1.33
39	2.388	0.04	1	1.420	0.14
40	2.166	0.19	1	1.289	0.38
41	2.350	0.08	1	1.398	0.05
42	3.121	0.20	1	1.856	1.85
43					
44					
45					
46					
47					
48					

UNL-3995

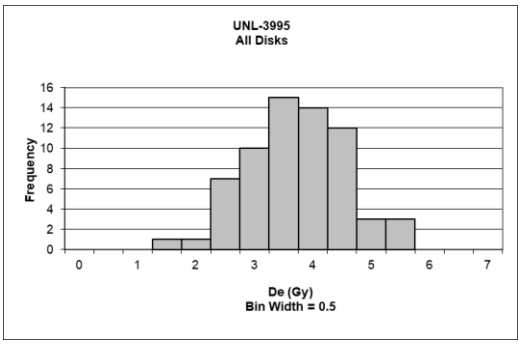

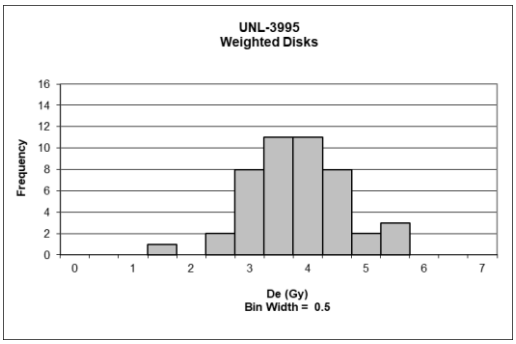

Disc	De	Error	Wt	Age	+/- 1 σ
1	4.643	0.23	1	2.814	1.42
2	3.049	0.02	1	1.848	0.59
3	2.521	0.35	1	1.528	1.25
4	3.577	0.32	1	2.168	0.08
5	3.906	0.16	1	2.367	0.49
6	2.202	0.33	1	1.334	1.65
7	2.438	0.72	1	1.477	1.36
8	3.424	0.00	1	2.075	0.11
9	2.675	0.27	1	1.621	1.06
10	5.213	0.03	1	3.159	2.14
11	5.030	0.14	1	3.048	1.91
12	2.328	0.44	1	1.411	1.49
13	3.124	0.15	1	1.893	0.49
14	3.150	0.30	1	1.909	0.46
15	3.460	0.38	1	2.097	0.07
16	4.484	0.14	1	2.717	1.22
17	3.490	0.21	1	2.115	0.03
18	2.065	0.44	1	1.251	1.83
19	3.655	0.10	1	2.215	0.18
20	3.513	0.37	1	2.129	0.00
21	3.707	0.19	1	2.246	0.24
22	1.785	0.48	1	1.082	2.18
23	3.841	0.27	1	2.328	0.41
24	4.221	0.27	1	2.558	0.89
25	3.649	0.02	1	2.212	0.17
26	3.230	0.45	1	1.957	0.36
27	2.924	0.16	1	1.772	0.74
28	3.179	0.31	1	1.926	0.42
29	4.155	0.15	1	2.518	0.81
30	2.532	0.14	1	1.535	1.24
31	2.870	0.11	1	1.739	0.81
32	4.204	0.21	1	2.548	0.87
33	3.055	0.28	1	1.852	0.58
34	4.216	0.11	1	2.555	0.89
35	4.067	0.06	1	2.465	0.70
36	3.512	0.30	1	2.128	0.00
37	2.692	0.11	1	1.631	1.04
38	2.779	0.16	1	1.684	0.93
39	2.946	0.19	1	1.785	0.72
40	3.206	0.09	1	1.943	0.39
41	3.658	0.30	1	2.217	0.18
42	3.243	0.21	1	1.965	0.34
43	4.709	0.14	1	2.854	1.51
44	3.188	0.17	1	1.932	0.41
45	3.573	0.02	1	2.166	0.07
46	2.167	0.56	1	1.313	1.70
47	5.131	0.17	1	3.109	2.04
48	2.454	0.46	1	1.487	1.34
49	4.043	0.03	1	2.450	0.67
50	4.058	0.08	1	2.459	0.69
51	4.125	0.40	1	2.500	0.77
52	4.236	0.01	1	2.567	0.91
53	1.348	0.27	1	0.817	2.73
54	4.275	0.25	1	2.591	0.96
55	4.815	0.94	1	2.918	1.64
56	3.514	0.38	1	2.130	0.00
57	3.634	0.35	1	2.202	0.15
58	4.223	0.05	1	2.559	0.89
59	2.119	0.44	1	1.284	1.76
60	3.143	0.19	1	1.905	0.47
61	2.749	0.59	1	1.666	0.96
62	3.224	0.24	1	1.954	0.36
63	3.448	0.27	1	2.089	0.08
64	3.606	0.43	1	2.185	0.12
65	3.542	0.12	1	2.147	0.04
66	2.851	0.31	1	1.728	0.83

Disc	De	Error	Wt	Age	+/- 1 σ
1	4.643	0.23	1	2.814	1.42
2	3.049	0.02	1	1.848	0.59
3	2.521	0.35	1	1.528	1.25
4	3.577	0.32	1	2.168	0.08
5	3.906	0.16	1	2.367	0.49
6	2.202	0.33	1	1.334	1.65
7	2.438	0.72	1	1.477	1.36
8	3.424	0.00	1	2.075	0.11
9	2.675	0.27	1	1.621	1.06
10	5.213	0.03	1	3.159	2.14
11	5.030	0.14	1	3.048	1.91
12	3.124	0.15	1	1.893	0.49
13	3.150	0.30	1	1.909	0.46
14	4.484	0.14	1	2.717	1.22
15	3.490	0.21	1	2.115	0.03
16	3.655	0.10	1	2.215	0.18
17	3.707	0.19	1	2.246	0.24
18	3.841	0.27	1	2.328	0.41
19	3.649	0.02	1	2.212	0.17
20	2.924	0.16	1	1.772	0.74
21	4.155	0.15	1	2.518	0.81
22	2.532	0.14	1	1.535	1.24
23	2.870	0.11	1	1.739	0.81
24	4.204	0.21	1	2.548	0.87
25	3.055	0.28	1	1.852	0.58
26	4.216	0.11	1	2.555	0.89
27	4.067	0.06	1	2.465	0.70
28	3.512	0.30	1	2.128	0.00
29	2.692	0.11	1	1.631	1.04
30	2.779	0.16	1	1.684	0.93
31	2.946	0.19	1	1.785	0.72
32	3.206	0.09	1	1.943	0.39
33	3.658	0.30	1	2.217	0.18
34	3.243	0.21	1	1.965	0.34
35	4.709	0.14	1	2.854	1.51
36	3.188	0.17	1	1.932	0.41
37	3.573	0.02	1	2.166	0.07
38	5.131	0.17	1	3.109	2.04
39	4.043	0.03	1	2.450	0.67
40	4.058	0.08	1	2.459	0.69
41	4.236	0.01	1	2.567	0.91
42	1.348	0.27	1	0.817	2.73
43	3.514	0.38	1	2.130	0.00
44	3.634	0.35	1	2.202	0.15
45	3.143	0.19	1	1.905	0.47
46	3.224	0.24	1	1.954	0.36
47					
48					
49					
50					
51					
52					
53					
54					

UNL-3996

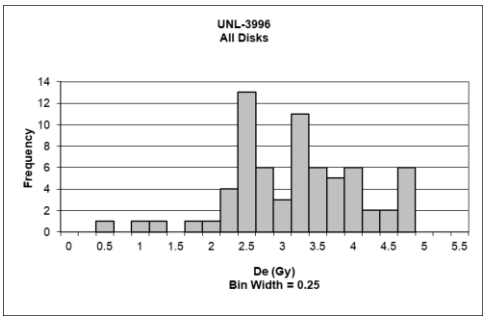

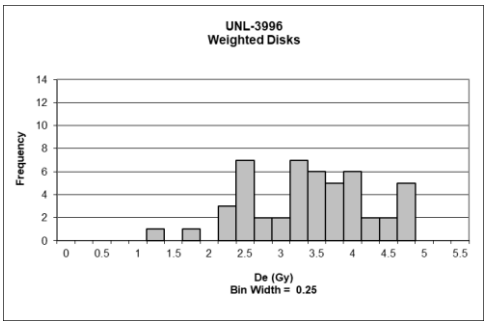

Disc	De	Error	Wt	Age	+/- 1 σ
1	4.685	0.19	1	2.964	1.69
2	3.944	0.24	1	2.495	0.81
3	2.271	0.22	1	1.437	1.19
4	0.874	0.25	1	0.553	2.86
5	4.568	0.24	1	2.890	1.56
6	2.550	0.28	1	1.613	0.86
7	2.856	0.22	1	1.807	0.49
8	1.851	0.39	1	1.171	1.69
9	2.493	0.17	1	1.577	0.93
10	1.182	0.19	1	0.748	2.49
11	4.434	0.07	1	2.805	1.39
12	4.002	0.02	1	2.531	0.88
13	2.370	0.38	1	1.499	1.07
14	3.088	0.14	1	1.953	0.21
15	3.825	0.07	1	2.420	0.67
16	3.103	0.01	1	1.963	0.20
17	3.639	0.19	1	2.302	0.44
18	2.858	0.56	1	1.808	0.49
19	3.075	0.58	1	1.945	0.23
20	3.934	0.30	1	2.489	0.80
21	3.513	0.16	1	2.222	0.29
22	3.318	0.37	1	2.099	0.06
23	2.642	0.56	1	1.671	0.75
24	2.437	0.35	1	1.541	0.99
25	2.434	0.04	1	1.540	1.00
26	4.080	0.00	1	2.581	0.97
27	2.435	0.42	1	1.540	1.00
28	2.660	0.59	1	1.682	0.73
29	1.612	0.26	1	1.020	1.98
30	4.697	0.32	1	2.971	1.71
31	3.341	0.33	1	2.113	0.09
32	3.792	0.28	1	2.399	0.63
33	0.269	1.55	1	0.170	3.59
34	4.677	0.30	1	2.959	1.69
35	2.655	0.35	1	1.680	0.73
36	2.096	0.11	1	1.326	1.40
37	2.374	0.06	1	1.502	1.07
38	4.382	0.16	1	2.772	1.33
39	2.549	0.09	1	1.612	0.86
40	3.232	0.28	1	2.045	0.04
41	4.590	0.28	1	2.904	1.58
42	3.676	0.15	1	2.326	0.49
43	4.566	0.01	1	2.889	1.55
44	2.098	0.20	1	1.327	1.40
45	3.175	0.20	1	2.008	0.11
46	3.149	0.32	1	1.992	0.14
47	2.879	0.05	1	1.821	0.47
48	2.305	0.10	1	1.458	1.15
49	3.629	0.11	1	2.296	0.43
50	2.377	0.20	1	1.504	1.06
51	2.651	0.40	1	1.677	0.74
52	3.057	0.32	1	1.934	0.25
53	3.157	0.04	1	1.997	0.13
54	3.252	0.06	1	2.057	0.02
55	2.153	0.31	1	1.362	1.33
56	2.349	0.30	1	1.486	1.10
57	3.734	0.05	1	2.362	0.56
58	3.258	0.14	1	2.061	0.01
59	3.305	0.03	1	2.091	0.05
60	3.432	0.46	1	2.171	0.20
61	3.091	0.05	1	1.955	0.21
62	3.095	0.19	1	1.958	0.21
63	2.400	0.45	1	1.518	1.04
64	3.771	0.20	1	2.386	0.60
65	2.391	0.10	1	1.513	1.05
66	2.463	0.20	1	1.558	0.96
67	3.885	0.13	1	2.457	0.74
68	2.248	0.15	1	1.422	1.22
69	3.054	0.22	1	1.932	0.26

Disc	De	Error	Wt	Age	+/- 1 σ
1	4.685	0.19	1	2.964	1.69
2	3.944	0.24	1	2.495	0.81
3	4.568	0.24	1	2.890	1.56
4	2.856	0.22	1	1.807	0.49
5	2.493	0.17	1	1.577	0.93
6	1.182	0.19	1	0.748	2.49
7	4.434	0.07	1	2.805	1.39
8	4.002	0.02	1	2.531	0.88
9	3.088	0.14	1	1.953	0.21
10	3.825	0.07	1	2.420	0.67
11	3.103	0.01	1	1.963	0.20
12	3.639	0.19	1	2.302	0.44
13	3.934	0.30	1	2.489	0.80
14	3.513	0.16	1	2.222	0.29
15	3.318	0.37	1	2.099	0.06
16	2.434	0.04	1	1.540	1.00
17	4.080	0.00	1	2.581	0.97
18	2.435	0.42	1	1.540	1.00
19	1.612	0.26	1	1.020	1.98
20	4.697	0.32	1	2.971	1.71
21	3.341	0.33	1	2.113	0.09
22	3.792	0.28	1	2.399	0.63
23	4.677	0.30	1	2.959	1.69
24	2.096	0.11	1	1.326	1.40
25	4.382	0.16	1	2.772	1.33
26	2.549	0.09	1	1.612	0.86
27	3.676	0.15	1	2.326	0.49
28	4.566	0.01	1	2.889	1.55
29	3.175	0.20	1	2.008	0.11
30	2.879	0.05	1	1.821	0.47
31	2.305	0.10	1	1.458	1.15
32	3.629	0.11	1	2.296	0.43
33	2.377	0.20	1	1.504	1.06
34	2.651	0.40	1	1.677	0.74
35	3.057	0.32	1	1.934	0.25
36	3.157	0.04	1	1.997	0.13
37	3.252	0.06	1	2.057	0.02
38	2.153	0.31	1	1.362	1.33
39	2.349	0.30	1	1.486	1.10
40	3.734	0.05	1	2.362	0.56
41	3.258	0.14	1	2.061	0.01
42	3.305	0.03	1	2.091	0.05
43	3.432	0.46	1	2.171	0.20
44	3.091	0.05	1	1.955	0.21
45	3.095	0.19	1	1.958	0.21
46	3.771	0.20	1	2.386	0.60
47	2.391	0.10	1	1.513	1.05
48	3.885	0.13	1	2.457	0.74
49	2.248	0.15	1	1.422	1.22
50					
51					
52					
53					
54					

UNL-4079

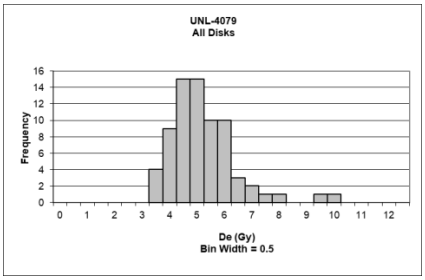

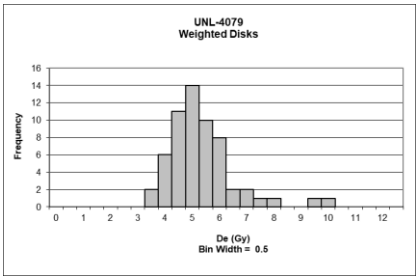

Disc	De	Error	Wt	Age	+/- 1 σ
1	3.768	0.27	1	2.455	1.07
2	5.740	0.15	1	3.740	0.50
3	7.330	0.07	1	4.776	1.77
4	5.890	0.08	1	3.838	0.62
5	3.663	0.20	1	2.386	1.15
6	5.248	0.16	1	3.419	0.11
7	4.645	0.11	1	3.027	0.37
8	5.254	0.10	1	3.423	0.12
9	4.982	0.19	1	3.246	0.10
10	5.823	0.05	1	3.794	0.57
11	4.419	0.01	1	2.880	0.55
12	4.379	0.02	1	2.853	0.58
13	4.410	0.07	1	2.873	0.56
14	4.920	0.10	1	3.206	0.15
15	4.562	0.06	1	2.972	0.44
16	4.862	0.03	1	3.168	0.20
17	3.979	0.22	1	2.593	0.90
18	4.844	0.06	1	3.156	0.21
19	5.232	0.04	1	3.409	0.10
20	5.208	0.01	1	3.393	0.08
21	4.330	0.02	1	2.822	0.62
22	4.602	0.09	1	2.999	0.40
23	4.406	0.03	1	2.871	0.56
24	3.178	0.26	1	2.070	1.54
25	4.279	0.22	1	2.788	0.66
26	4.209	0.11	1	2.742	0.72
27	3.694	0.18	1	2.407	1.13
28	5.323	0.07	1	3.468	0.17
29	5.040	0.05	1	3.284	0.05
30	4.778	0.05	1	3.113	0.26
31	9.654	0.02	1	6.290	3.62
32	22.337	0.61	1	14.554	13.72
33	5.207	0.12	1	3.393	0.08
34	5.978	0.12	1	3.895	0.69
35	7.980	0.03	1	5.200	2.29
36	4.702	0.12	1	3.064	0.32
37	5.348	0.13	1	3.484	0.19
38	5.683	0.07	1	3.703	0.46
39	5.084	0.04	1	3.313	0.02
40	3.903	0.08	1	2.543	0.96
41	4.149	0.30	1	2.704	0.76
42	6.027	0.08	1	3.927	0.73
43	5.923	0.15	1	3.859	0.65
44	5.677	0.02	1	3.699	0.45
45	5.320	0.04	1	3.467	0.17
46	4.210	0.01	1	2.743	0.72
47	4.239	0.18	1	2.762	0.69
48	5.610	0.01	1	3.655	0.40
49	6.727	0.12	1	4.383	1.29
50	3.753	0.33	1	2.445	1.08
51	4.147	0.21	1	2.702	0.77
52	3.437	0.50	1	2.240	1.33
53	3.581	0.13	1	2.333	1.22
54	4.698	0.15	1	3.061	0.33
55	6.336	0.22	1	4.128	0.98
56	4.720	0.12	1	3.076	0.31
57	4.114	0.11	1	2.681	0.79
58	5.645	0.06	1	3.678	0.43
59	4.915	0.25	1	3.202	0.15
60	9.273	0.03	1	6.042	3.32
61	4.138	0.26	1	2.696	0.77
62	6.252	0.15	1	4.074	0.91
63	4.014	0.06	1	2.615	0.87
64	3.494	0.05	1	2.277	1.29
65	4.093	0.15	1	2.667	0.81
66	6.840	0.06	1	4.457	1.38
67	4.682	0.08	1	3.051	0.34
68	3.922	0.03	1	2.556	0.94
69	4.806	0.12	1	3.132	0.24
70	3.684	0.11	1	2.401	1.13
71	5.558	0.03	1	3.621	0.36
72	4.953	0.05	1	3.227	0.12
73	3.406	0.08	1	2.219	1.36

Disc	De	Error	Wt	Age	+/- 1 σ
1	5.740	0.15	1	3.740	0.50
2	7.330	0.07	1	4.776	1.77
3	5.890	0.08	1	3.838	0.62
4	5.248	0.16	1	3.419	0.11
5	4.645	0.11	1	3.027	0.37
6	5.254	0.10	1	3.423	0.12
7	4.982	0.19	1	3.246	0.10
8	5.823	0.05	1	3.794	0.57
9	4.419	0.01	1	2.880	0.55
10	4.379	0.02	1	2.853	0.58
11	4.920	0.10	1	3.206	0.15
12	4.562	0.06	1	2.972	0.44
13	4.862	0.03	1	3.168	0.20
14	3.979	0.22	1	2.593	0.90
15	4.844	0.06	1	3.156	0.21
16	5.232	0.04	1	3.409	0.10
17	5.208	0.01	1	3.393	0.08
18	4.330	0.02	1	2.822	0.62
19	4.602	0.09	1	2.999	0.40
20	4.406	0.03	1	2.871	0.56
21	4.209	0.11	1	2.742	0.72
22	3.694	0.18	1	2.407	1.13
23	5.323	0.07	1	3.468	0.17
24	5.040	0.05	1	3.284	0.05
25	4.778	0.05	1	3.113	0.26
26	9.654	0.02	1	6.290	3.62
27	5.207	0.12	1	3.393	0.08
28	5.978	0.12	1	3.895	0.69
29	7.980	0.03	1	5.200	2.29
30	4.702	0.12	1	3.064	0.32
31	5.348	0.13	1	3.484	0.19
32	5.084	0.04	1	3.313	0.02
33	3.903	0.08	1	2.543	0.96
34	4.149	0.30	1	2.704	0.76
35	6.027	0.08	1	3.927	0.73
36	5.677	0.02	1	3.699	0.45
37	5.320	0.04	1	3.467	0.17
38	4.239	0.18	1	2.762	0.69
39	5.610	0.01	1	3.655	0.40
40	6.727	0.12	1	4.383	1.29
41	4.147	0.21	1	2.702	0.77
42	3.581	0.13	1	2.333	1.22
43	4.698	0.15	1	3.061	0.33
44	4.114	0.11	1	2.681	0.79
45	5.645	0.06	1	3.678	0.43
46	4.915	0.25	1	3.202	0.15
47	9.273	0.03	1	6.042	3.32
48	6.252	0.15	1	4.074	0.91
49	4.014	0.06	1	2.615	0.87
50	3.494	0.05	1	2.277	1.29
51	4.093	0.15	1	2.667	0.81
52	6.840	0.06	1	4.457	1.38
53	4.682	0.08	1	3.051	0.34
54	3.922	0.03	1	2.556	0.94
55	4.806	0.12	1	3.132	0.24
56	3.684	0.11	1	2.401	1.13
57	5.558	0.03	1	3.621	0.36
58	4.953	0.05	1	3.227	0.12
59	3.406	0.08	1	2.219	1.36
60					

UNL-4080

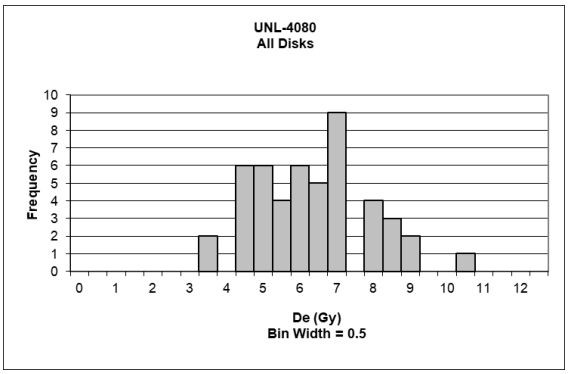

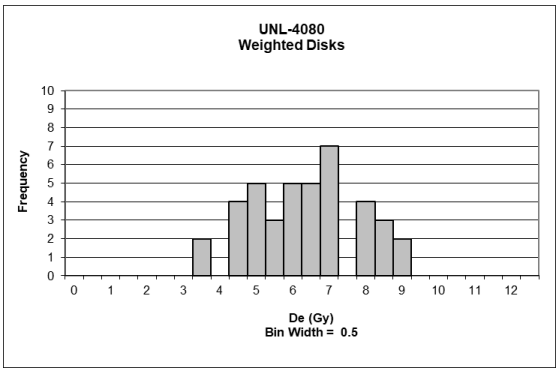

Disc	De	Error	Wt	Age	+/- 1 σ
1	4.056	0.22	1	2.545	1.40
2	5.907	0.27	1	3.707	0.12
3	5.837	0.06	1	3.663	0.16
4	5.143	0.14	1	3.227	0.65
5	4.364	0.39	1	2.738	1.19
6	6.762	0.08	1	4.243	0.48
7	5.221	0.24	1	3.276	0.59
8	4.489	0.18	1	2.817	1.10
9	4.806	0.05	1	3.016	0.88
10	6.901	0.09	1	4.330	0.57
11	3.494	0.29	1	2.192	1.79
12	6.649	0.09	1	4.172	0.40
13	4.536	0.12	1	2.846	1.07
14	6.706	0.07	1	4.208	0.44
15	5.952	0.10	1	3.735	0.09
16	8.776	0.19	1	5.507	1.88
17	6.767	0.13	1	4.246	0.48
18	7.645	0.00	1	4.797	1.09
19	8.263	0.05	1	5.185	1.52
20	6.608	0.20	1	4.146	0.37
21	7.964	0.02	1	4.997	1.31
22	6.634	0.18	1	4.162	0.39
23	4.135	0.17	1	2.594	1.35
24	4.447	0.08	1	2.790	1.13
25	6.049	0.20	1	3.795	0.02
26	8.371	0.14	1	5.252	1.59
27	6.097	0.18	1	3.826	0.02
28	5.563	0.15	1	3.491	0.36
29	6.071	0.15	1	3.809	0.00
30	5.131	0.08	1	3.220	0.65
31	5.886	0.00	1	3.693	0.13
32	7.904	0.10	1	4.959	1.27
33	3.314	0.14	1	2.079	1.92
34	10.018	0.03	1	6.286	2.74
35	6.667	0.23	1	4.183	0.41
36	8.032	0.13	1	5.040	1.36
37	7.513	0.10	1	4.714	1.00
38	4.189	0.11	1	2.628	1.31
39	5.751	0.04	1	3.609	0.22
40	6.210	0.20	1	3.897	0.09
41	4.680	0.16	1	2.936	0.97
42	4.501	0.02	1	2.824	1.09
43	4.594	0.14	1	2.883	1.03
44	5.375	0.04	1	3.372	0.49
45	4.906	0.12	1	3.078	0.81
46	8.525	0.01	1	5.349	1.70
47	6.218	0.11	1	3.902	0.10
48	6.699	0.18	1	4.203	0.43

Disc	De	Error	Wt	Age	+/- 1 σ
1	5.837	0.06	1	3.663	0.16
2	5.143	0.14	1	3.227	0.65
3	6.762	0.08	1	4.243	0.48
4	4.489	0.18	1	2.817	1.10
5	4.806	0.05	1	3.016	0.88
6	6.901	0.09	1	4.330	0.57
7	3.494	0.29	1	2.192	1.79
8	6.649	0.09	1	4.172	0.40
9	6.706	0.07	1	4.208	0.44
10	5.952	0.10	1	3.735	0.09
11	8.776	0.19	1	5.507	1.88
12	6.767	0.13	1	4.246	0.48
13	7.645	0.00	1	4.797	1.09
14	8.263	0.05	1	5.185	1.52
15	7.964	0.02	1	4.997	1.31
16	4.135	0.17	1	2.594	1.35
17	4.447	0.08	1	2.790	1.13
18	6.049	0.20	1	3.795	0.02
19	8.371	0.14	1	5.252	1.59
20	6.097	0.18	1	3.826	0.02
21	5.563	0.15	1	3.491	0.36
22	6.071	0.15	1	3.809	0.00
23	5.131	0.08	1	3.220	0.65
24	5.886	0.00	1	3.693	0.13
25	7.904	0.10	1	4.959	1.27
26	3.314	0.14	1	2.079	1.92
27	6.667	0.23	1	4.183	0.41
28	8.032	0.13	1	5.040	1.36
29	7.513	0.10	1	4.714	1.00
30	4.189	0.11	1	2.628	1.31
31	5.751	0.04	1	3.609	0.22
32	6.210	0.20	1	3.897	0.09
33	4.680	0.16	1	2.936	0.97
34	4.501	0.02	1	2.824	1.09
35	4.594	0.14	1	2.883	1.03
36	5.375	0.04	1	3.372	0.49
37	4.906	0.12	1	3.078	0.81
38	8.525	0.01	1	5.349	1.70
39	6.218	0.11	1	3.902	0.10
40	6.699	0.18	1	4.203	0.43
41					
42					
43					
44					
45					
46					
47					
48					

UNL-4081

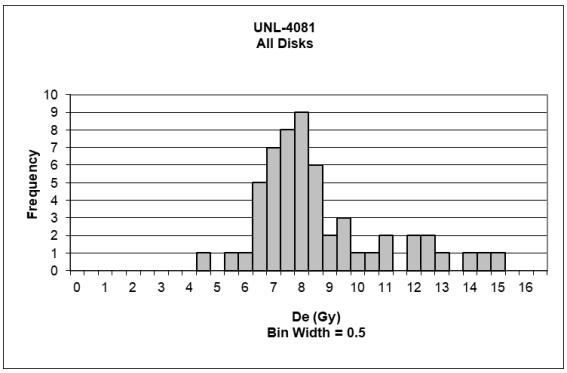

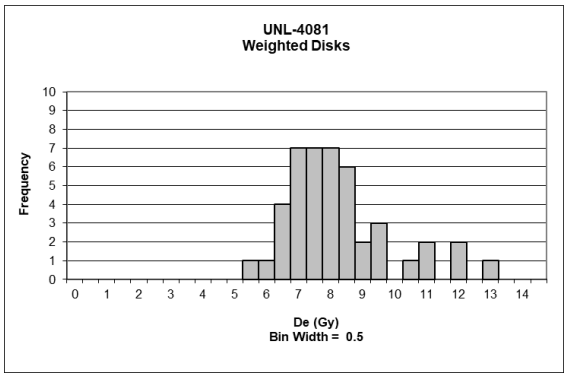

Disc	De	Error	Wt	Age	+/- 1 σ
1	11.848	0.30	1	7.854	2.29
2	14.694	0.11	1	9.741	3.97
3	9.259	0.22	1	6.137	0.76
4	7.520	0.33	1	4.985	0.26
5	12.290	0.28	1	8.147	2.55
6	9.658	0.17	1	6.402	1.00
7	10.862	0.02	1	7.200	1.71
8	12.777	0.16	1	8.470	2.84
9	13.841	0.46	1	9.175	3.47
10	10.723	0.12	1	7.108	1.63
11	7.566	0.24	1	5.016	0.23
12	12.424	0.38	1	8.236	2.63
13	10.414	0.04	1	6.904	1.45
14	11.993	0.05	1	7.950	2.38
15	14.356	0.06	1	9.516	3.77
16	8.491	0.20	1	5.628	0.31
17	7.965	0.12	1	5.280	0.00
18	6.677	0.12	1	4.426	0.76
19	7.149	1.12	1	4.739	0.48
20	7.672	0.09	1	5.086	0.17
21	6.639	0.14	1	4.401	0.78
22	7.526	0.15	1	4.989	0.26
23	8.251	0.04	1	5.470	0.17
24	6.230	0.21	1	4.130	1.02
25	6.710	0.22	1	4.448	0.74
26	5.492	0.09	1	3.640	1.46
27	4.008	0.32	1	2.657	2.33
28	7.746	0.12	1	5.135	0.13
29	6.073	0.22	1	4.025	1.11
30	8.912	0.09	1	5.907	0.56
31	8.149	0.05	1	5.402	0.11
32	8.123	0.01	1	5.385	0.10
33	6.692	0.20	1	4.436	0.75
34	7.001	0.23	1	4.641	0.57
35	6.645	0.27	1	4.405	0.78
36	9.224	0.08	1	6.114	0.74
37	7.179	0.26	1	4.759	0.46
38	9.220	0.18	1	6.112	0.74
39	7.015	0.14	1	4.650	0.56
40	6.257	0.11	1	4.148	1.01
41	6.180	0.17	1	4.096	1.05
42	7.219	0.02	1	4.785	0.44
43	7.460	0.10	1	4.945	0.30
44	6.294	0.15	1	4.172	0.98
45	8.399	0.15	1	5.568	0.26
46	7.785	0.04	1	5.160	0.10
47	7.366	0.00	1	4.883	0.35
48	7.239	0.01	1	4.799	0.43
49	8.177	0.14	1	5.420	0.13
50	6.572	0.12	1	4.357	0.82
51	8.709	0.34	1	5.773	0.44
52	7.654	0.02	1	5.074	0.18
53	7.803	0.06	1	5.172	0.09
54	6.556	0.22	1	4.346	0.83
55	5.883	0.20	1	3.900	1.23

Disc	De	Error	Wt	Age	+/- 1 σ
1	11.848	0.30	1	7.854	2.29
2	9.259	0.22	1	6.137	0.76
3	7.520	0.33	1	4.985	0.26
4	10.862	0.02	1	7.200	1.71
5	12.777	0.16	1	8.470	2.84
6	10.723	0.12	1	7.108	1.63
7	10.414	0.04	1	6.904	1.45
8	11.993	0.05	1	7.950	2.38
9	8.491	0.20	1	5.628	0.31
10	6.677	0.12	1	4.426	0.76
11	7.149	1.12	1	4.739	0.48
12	7.672	0.09	1	5.086	0.17
13	6.639	0.14	1	4.401	0.78
14	7.526	0.15	1	4.989	0.26
15	8.251	0.04	1	5.470	0.17
16	6.230	0.21	1	4.130	1.02
17	6.710	0.22	1	4.448	0.74
18	5.492	0.09	1	3.640	1.46
19	7.746	0.12	1	5.135	0.13
20	6.073	0.22	1	4.025	1.11
21	8.912	0.09	1	5.907	0.56
22	8.149	0.05	1	5.402	0.11
23	8.123	0.01	1	5.385	0.10
24	6.692	0.20	1	4.436	0.75
25	7.001	0.23	1	4.641	0.57
26	6.645	0.27	1	4.405	0.78
27	9.224	0.08	1	6.114	0.74
28	9.220	0.18	1	6.112	0.74
29	7.015	0.14	1	4.650	0.56
30	6.180	0.17	1	4.096	1.05
31	7.219	0.02	1	4.785	0.44
32	7.460	0.10	1	4.945	0.30
33	6.294	0.15	1	4.172	0.98
34	8.399	0.15	1	5.568	0.26
35	7.785	0.04	1	5.160	0.10
36	7.366	0.00	1	4.883	0.35
37	7.239	0.01	1	4.799	0.43
38	8.177	0.14	1	5.420	0.13
39	6.572	0.12	1	4.357	0.82
40	8.709	0.34	1	5.773	0.44
41	7.654	0.02	1	5.074	0.18
42	7.803	0.06	1	5.172	0.09
43	6.556	0.22	1	4.346	0.83
44	5.883	0.20	1	3.900	1.23
45					
46					
47					
48					
49					
50					
51					
52					
53					
54					

UNL-4082

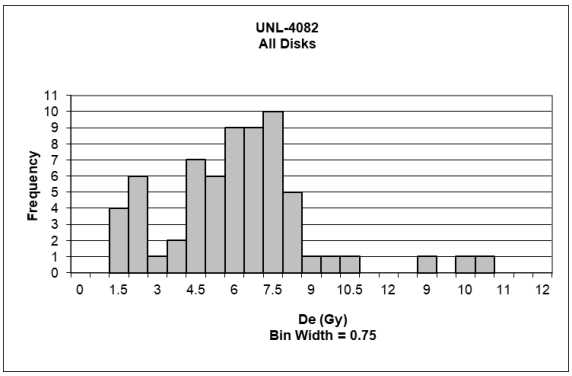

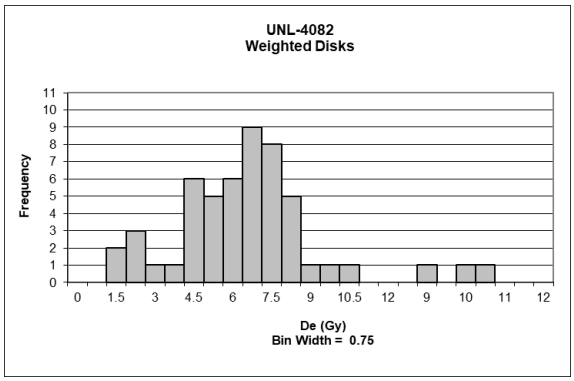

Disc	De	Error	Wt	Age	+/- 1 σ
1	8.826	0.09	1	6.125	1.54
2	5.469	0.10	1	3.795	0.11
3	1.618	0.04	1	1.123	1.99
4	5.941	0.08	1	4.123	0.13
5	1.806	0.07	1	1.253	1.90
6	7.987	0.23	1	5.543	1.13
7	6.646	0.04	1	4.612	0.47
8	7.158	0.38	1	4.967	0.72
9	3.881	0.17	1	2.693	0.88
10	5.289	0.02	1	3.670	0.19
11	5.681	0.05	1	3.942	0.00
12	2.015	0.40	1	1.398	1.80
13	4.023	0.38	1	2.791	0.81
14	4.854	0.14	1	3.368	0.41
15	6.521	0.12	1	4.525	0.41
16	0.917	0.21	1	0.636	2.33
17	4.701	0.11	1	3.262	0.48
18	5.123	0.20	1	3.555	0.27
19	7.068	0.16	1	4.905	0.68
20	2.789	0.21	1	1.935	1.42
21	0.985	0.11	1	0.684	2.30
22	6.605	0.07	1	4.584	0.45
23	4.368	0.06	1	3.031	0.64
24	4.335	0.32	1	3.008	0.66
25	4.868	0.42	1	3.378	0.40
26	0.940	0.04	1	0.652	2.32
27	7.911	0.07	1	5.490	1.09
28	5.806	0.07	1	4.029	0.06
29	7.438	0.39	1	5.162	0.86
30	6.807	0.28	1	4.724	0.55
31	2.051	0.16	1	1.424	1.78
32	9.619	0.07	1	6.675	1.93
33	6.361	0.06	1	4.415	0.33
34	6.244	0.13	1	4.333	0.27
35	5.074	0.12	1	3.521	0.30
36	7.018	0.12	1	4.870	0.65
37	1.252	0.11	1	0.869	2.17
38	7.263	0.08	1	5.040	0.77
39	2.058	0.17	1	1.428	1.77
40	6.814	0.14	1	4.728	0.55
41	1.941	0.10	1	1.347	1.83
42	7.860	0.18	1	5.455	1.06
43	5.690	0.19	1	3.949	0.00
44	5.545	0.28	1	3.848	0.07
45	4.805	0.02	1	3.335	0.43
46	4.118	0.21	1	2.857	0.77
47	7.118	0.25	1	4.940	0.70
48	6.013	0.05	1	4.173	0.16
49	7.507	0.03	1	5.209	0.89
50	6.030	0.24	1	4.185	0.17
51	6.411	0.11	1	4.449	0.36
52	3.357	0.05	1	2.330	1.14
53	4.416	0.15	1	3.065	0.62
54	5.960	0.26	1	4.136	0.13
55	5.662	0.38	1	3.929	0.01
56	6.868	0.27	1	4.766	0.58
57	6.002	0.02	1	4.165	0.16
58	10.008	0.05	1	6.945	2.12
59	7.624	0.10	1	5.291	0.95
60	7.329	0.26	1	5.086	0.80
61	3.819	0.05	1	2.650	0.91
62	3.557	0.12	1	2.468	1.04

Disc	De	Error	Wt	Age	+/- 1 σ
1	8.826	0.09	1	6.125	1.54
2	5.469	0.10	1	3.795	0.11
3	5.941	0.08	1	4.123	0.13
4	1.806	0.07	1	1.253	1.90
5	7.987	0.23	1	5.543	1.13
6	6.646	0.04	1	4.612	0.47
7	7.158	0.38	1	4.967	0.72
8	3.881	0.17	1	2.693	0.88
9	5.289	0.02	1	3.670	0.19
10	5.681	0.05	1	3.942	0.00
11	4.023	0.38	1	2.791	0.81
12	4.854	0.14	1	3.368	0.41
13	6.521	0.12	1	4.525	0.41
14	0.917	0.21	1	0.636	2.33
15	4.701	0.11	1	3.262	0.48
16	5.123	0.20	1	3.555	0.27
17	7.068	0.16	1	4.905	0.68
18	2.789	0.21	1	1.935	1.42
19	6.605	0.07	1	4.584	0.45
20	4.368	0.06	1	3.031	0.64
21	4.335	0.32	1	3.008	0.66
22	7.911	0.07	1	5.490	1.09
23	5.806	0.07	1	4.029	0.06
24	6.807	0.28	1	4.724	0.55
25	2.051	0.16	1	1.424	1.78
26	9.619	0.07	1	6.675	1.93
27	6.361	0.06	1	4.415	0.33
28	6.244	0.13	1	4.333	0.27
29	5.074	0.12	1	3.521	0.30
30	7.018	0.12	1	4.870	0.65
31	1.252	0.11	1	0.869	2.17
32	7.263	0.08	1	5.040	0.77
33	2.058	0.17	1	1.428	1.77
34	6.814	0.14	1	4.728	0.55
35	7.860	0.18	1	5.455	1.06
36	4.805	0.02	1	3.335	0.43
37	4.118	0.21	1	2.857	0.77
38	7.118	0.25	1	4.940	0.70
39	6.013	0.05	1	4.173	0.16
40	7.507	0.03	1	5.209	0.89
41	6.030	0.24	1	4.185	0.17
42	6.411	0.11	1	4.449	0.36
43	3.357	0.05	1	2.330	1.14
44	4.416	0.15	1	3.065	0.62
45	5.662	0.38	1	3.929	0.01
46	6.002	0.02	1	4.165	0.16
47	10.008	0.05	1	6.945	2.12
48	7.624	0.10	1	5.291	0.95
49	7.329	0.26	1	5.086	0.80
50					
51					
52					
53					
54					

UNL-4083

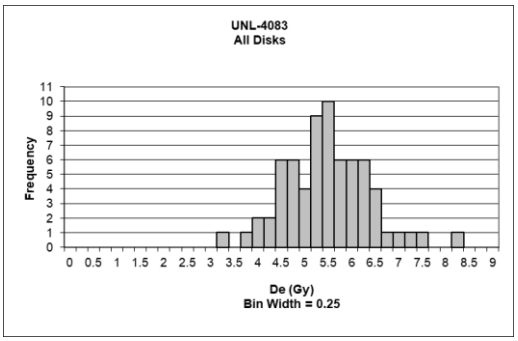

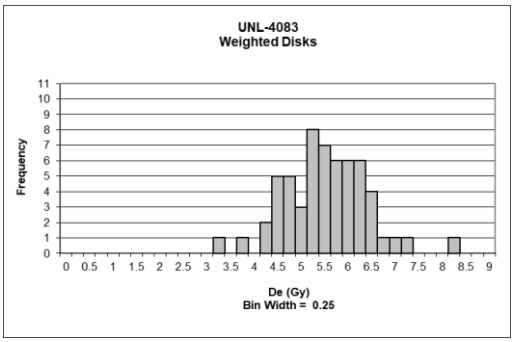

Disc	De	Error	Wt	Age	+/- 1 σ
1	5.318	0.10	1	3.368	0.11
2	5.313	0.02	1	3.364	0.12
3	8.058	0.10	1	5.103	3.12
4	5.165	0.10	1	3.271	0.29
5	7.308	0.08	1	4.628	2.24
6	4.163	0.14	1	2.637	1.47
7	7.165	0.15	1	4.538	2.07
8	6.019	0.13	1	3.811	0.72
9	3.939	0.36	1	2.494	1.74
10	5.958	0.02	1	3.773	0.65
11	5.996	0.12	1	3.797	0.69
12	4.371	0.14	1	2.768	1.23
13	5.829	0.19	1	3.692	0.49
14	6.117	0.03	1	3.874	0.83
15	6.691	0.05	1	4.237	1.51
16	5.369	0.05	1	3.400	0.05
17	6.314	0.05	1	3.998	1.06
18	5.363	0.11	1	3.396	0.06
19	4.739	0.18	1	3.001	0.79
20	5.313	0.30	1	3.364	0.12
21	4.341	0.14	1	2.749	1.26
22	5.341	0.10	1	3.382	0.08
23	6.185	0.05	1	3.917	0.91
24	5.784	0.09	1	3.663	0.44
25	4.628	0.25	1	2.931	0.93
26	5.147	0.08	1	3.260	0.31
27	6.488	0.06	1	4.109	1.27
28	4.824	0.04	1	3.055	0.69
29	5.050	0.09	1	3.198	0.43
30	4.952	0.16	1	3.136	0.54
31	6.086	0.14	1	3.854	0.80
32	5.415	0.03	1	3.429	0.00
33	4.111	0.03	1	2.604	1.54
34	5.504	0.16	1	3.485	0.11
35	5.036	0.08	1	3.189	0.44
36	5.946	0.00	1	3.765	0.63
37	5.220	0.01	1	3.306	0.23
38	6.341	0.09	1	4.016	1.10
39	5.614	0.14	1	3.555	0.24
40	5.983	0.01	1	3.789	0.67
41	3.155	0.03	1	1.998	2.66
42	6.228	0.02	1	3.944	0.96
43	4.663	0.13	1	2.953	0.88
44	5.718	0.01	1	3.621	0.36
45	4.716	0.06	1	2.987	0.82
46	6.990	0.02	1	4.427	1.86
47	5.374	0.11	1	3.403	0.05
48	5.433	0.09	1	3.441	0.03
49	5.119	0.06	1	3.242	0.35
50	6.295	0.04	1	3.986	1.04
51	4.849	0.05	1	3.071	0.66
52	5.138	0.06	1	3.254	0.32
53	4.807	0.19	1	3.044	0.71
54	5.614	0.02	1	3.555	0.24
55	5.246	0.20	1	3.322	0.20
56	5.650	0.04	1	3.578	0.28
57	5.294	0.33	1	3.353	0.14
58	6.074	0.05	1	3.846	0.78
59	4.436	0.21	1	2.809	1.15
60	4.393	0.25	1	2.782	1.20
61	5.557	0.13	1	3.519	0.17
62	3.813	0.24	1	2.415	1.89
63	4.673	0.20	1	2.960	0.87
64	3.705	0.24	1	2.346	2.02
65	5.010	0.11	1	3.172	0.47
66	4.637	1.20	1	2.936	0.92
67	4.498	0.02	1	2.848	1.08
68	4.358	0.11	1	2.760	1.24

Disc	De	Error	Wt	Age	+/- 1 σ
1	5.318	0.10	1	3.368	0.11
2	8.058	0.10	1	5.103	3.12
3	5.165	0.10	1	3.271	0.29
4	4.163	0.14	1	2.637	1.47
5	7.165	0.15	1	4.538	2.07
6	6.019	0.13	1	3.811	0.72
7	5.958	0.02	1	3.773	0.65
8	5.996	0.12	1	3.797	0.69
9	4.371	0.14	1	2.768	1.23
10	5.829	0.19	1	3.692	0.49
11	6.117	0.03	1	3.874	0.83
12	6.691	0.05	1	4.237	1.51
13	5.369	0.05	1	3.400	0.05
14	6.314	0.05	1	3.998	1.06
15	5.363	0.11	1	3.396	0.06
16	4.739	0.18	1	3.001	0.79
17	4.341	0.14	1	2.749	1.26
18	5.341	0.10	1	3.382	0.08
19	6.185	0.05	1	3.917	0.91
20	5.784	0.09	1	3.663	0.44
21	4.628	0.25	1	2.931	0.93
22	5.147	0.08	1	3.260	0.31
23	6.488	0.06	1	4.109	1.27
24	4.824	0.04	1	3.055	0.69
25	5.050	0.09	1	3.198	0.43
26	4.952	0.16	1	3.136	0.54
27	6.086	0.14	1	3.854	0.80
28	5.415	0.03	1	3.429	0.00
29	4.111	0.03	1	2.604	1.54
30	5.504	0.16	1	3.485	0.11
31	5.036	0.08	1	3.189	0.44
32	5.946	0.00	1	3.765	0.63
33	5.220	0.01	1	3.306	0.23
34	6.341	0.09	1	4.016	1.10
35	5.614	0.14	1	3.555	0.24
36	5.983	0.01	1	3.789	0.67
37	3.155	0.03	1	1.998	2.66
38	6.228	0.02	1	3.944	0.96
39	4.663	0.13	1	2.953	0.88
40	5.718	0.01	1	3.621	0.36
41	4.716	0.06	1	2.987	0.82
42	6.990	0.02	1	4.427	1.86
43	5.374	0.11	1	3.403	0.05
44	5.433	0.09	1	3.441	0.03
45	5.119	0.06	1	3.242	0.35
46	6.295	0.04	1	3.986	1.04
47	4.849	0.05	1	3.071	0.66
48	5.138	0.06	1	3.254	0.32
49	5.614	0.02	1	3.555	0.24
50	5.650	0.04	1	3.578	0.28
51	6.074	0.05	1	3.846	0.78
52	4.436	0.21	1	2.809	1.15
53	5.557	0.13	1	3.519	0.17
54	4.673	0.20	1	2.960	0.87
55	3.705	0.24	1	2.346	2.02
56	5.010	0.11	1	3.172	0.47
57	4.498	0.02	1	2.848	1.08
58	4.358	0.11	1	2.760	1.24

UNL-4084

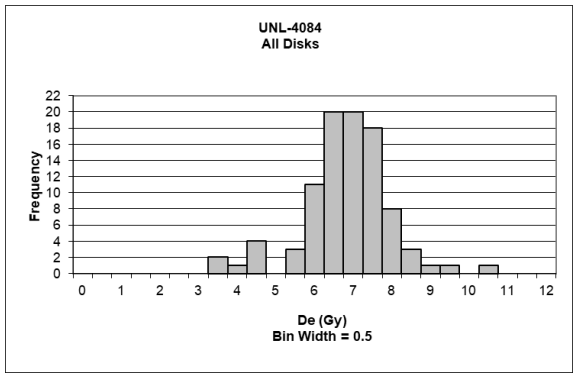
UNL-4084
All Disks
Frequency
0 2 4 6 8 10 12 14 16 18 20 22
0 1 2 3 4 5 6 7 8 9 10 11 12
De (Gy)
Bin Width = 0.5

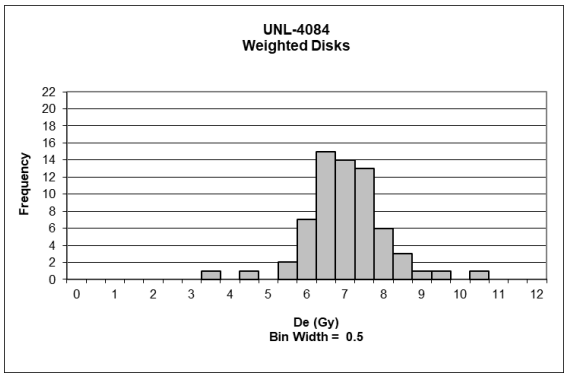
UNL-4084
Weighted Disks
Frequency
0 2 4 6 8 10 12 14 16 18 20 22
0 1 2 3 4 5 6 7 8 9 10 11 12
De (Gy)
Bin Width = 0.5

UNL-4084 contd.

Disc	De	Error	Wt	Age	+/- 1 σ
1	6.664	0.08	1	3.908	0.12
2	5.898	0.09	1	3.459	0.82
3	6.498	0.02	1	3.810	0.27
4	7.488	0.01	1	4.391	0.62
5	7.647	0.05	1	4.484	0.76
6	4.348	0.03	1	2.549	2.21
7	7.390	0.08	1	4.333	0.53
8	6.547	0.03	1	3.839	0.23
9	7.116	0.15	1	4.173	0.28
10	7.829	0.01	1	4.591	0.93
11	6.939	0.10	1	4.069	0.12
12	5.792	0.09	1	3.396	0.91
13	7.847	0.04	1	4.601	0.94
14	6.409	0.13	1	3.758	0.35
15	7.512	0.01	1	4.405	0.64
16	4.412	0.05	1	2.587	2.16
17	8.224	0.10	1	4.822	1.28
18	9.193	0.12	1	5.390	2.16
19	5.667	0.08	1	3.323	1.02
20	6.987	0.02	1	4.097	0.17
21	3.265	0.07	1	1.915	3.19
22	7.208	0.04	1	4.226	0.37
23	6.547	0.03	1	3.839	0.23
24	10.162	0.07	1	5.958	3.03
25	7.499	0.05	1	4.397	0.63
26	3.866	0.03	1	2.267	2.65
27	5.750	0.02	1	3.372	0.95
28	8.052	0.05	1	4.722	1.13
29	6.164	0.00	1	3.614	0.58
30	7.985	0.05	1	4.682	1.07
31	6.642	0.06	1	3.894	0.14
32	4.099	0.13	1	2.403	2.44
33	7.155	0.10	1	4.195	0.32
34	8.306	0.18	1	4.870	1.36
35	6.201	0.04	1	3.636	0.54
36	6.806	0.04	1	3.991	0.00
37	5.763	0.15	1	3.379	0.94
38	7.131	0.16	1	4.181	0.30
39	6.305	0.04	1	3.697	0.45
40	6.284	0.12	1	3.685	0.47
41	7.386	0.05	1	4.331	0.53
42	6.950	0.13	1	4.075	0.13
43	6.265	0.08	1	3.673	0.49
44	7.896	0.02	1	4.630	0.99
45	6.125	0.14	1	3.591	0.61
46	7.480	0.12	1	4.386	0.61
47	7.313	0.11	1	4.288	0.46
48	7.384	0.01	1	4.330	0.52
49	5.139	0.10	1	3.013	1.50
50	6.928	0.12	1	4.062	0.11
51	5.935	0.04	1	3.480	0.78
52	5.358	0.04	1	3.142	1.30
53	6.655	0.10	1	3.902	0.13
54	6.136	0.06	1	3.598	0.60
55	5.727	0.21	1	3.358	0.97
56	6.539	0.22	1	3.834	0.24
57	6.123	0.05	1	3.590	0.61
58	6.001	0.09	1	3.519	0.72
59	7.699	0.03	1	4.514	0.81
60	4.182	0.01	1	2.452	2.36
61	6.026	0.11	1	3.533	0.70
62	5.884	0.22	1	3.450	0.83
63	7.421	0.02	1	4.352	0.56
64	6.500	0.01	1	3.812	0.27
65	7.146	0.31	1	4.190	0.31
66	6.221	0.03	1	3.648	0.52
67	7.008	0.12	1	4.109	0.19
68	6.681	0.07	1	3.918	0.11
69	5.573	0.07	1	3.268	1.11
70	6.849	0.03	1	4.016	0.04
71	3.027	0.02	1	1.775	3.41
72	6.267	0.02	1	3.675	0.48
73	7.633	0.03	1	4.476	0.75
74	5.967	0.02	1	3.499	0.75
75	6.297	0.06	1	3.692	0.46
76	6.993	0.01	1	4.100	0.17
77	7.277	0.07	1	4.267	0.43
78	6.466	0.07	1	3.792	0.30
79	5.837	0.07	1	3.422	0.87
80	6.869	0.46	1	4.028	0.06
81	6.396	0.01	1	3.751	0.37
82	7.455	0.01	1	4.371	0.59
83	7.237	0.02	1	4.244	0.39
84	7.297	0.08	1	4.279	0.45
85	6.868	0.11	1	4.027	0.06
86	6.990	0.07	1	4.098	0.17
87	5.102	0.13	1	2.992	1.53
88	6.385	0.06	1	3.744	0.38
89	6.171	0.11	1	3.619	0.57
90	6.754	0.07	1	3.960	0.04
91	8.641	0.08	1	5.067	1.66
92	6.406	0.07	1	3.756	0.36
93	6.578	0.09	1	3.857	0.20

Disc	De	Error	Wt	Age	+/- 1 σ
1	6.664	0.08	1	3.908	0.12
2	5.898	0.09	1	3.459	0.82
3	6.498	0.02	1	3.810	0.27
4	7.488	0.01	1	4.391	0.62
5	7.647	0.05	1	4.484	0.76
6	4.348	0.03	1	2.549	2.21
7	7.390	0.08	1	4.333	0.53
8	7.116	0.15	1	4.173	0.28
9	7.829	0.01	1	4.591	0.93
10	6.939	0.10	1	4.069	0.12
11	5.792	0.09	1	3.396	0.91
12	7.847	0.04	1	4.601	0.94
13	6.409	0.13	1	3.758	0.35
14	7.512	0.01	1	4.405	0.64
15	8.224	0.10	1	4.822	1.28
16	9.193	0.12	1	5.390	2.16
17	6.987	0.02	1	4.097	0.17
18	7.208	0.04	1	4.226	0.37
19	6.547	0.03	1	3.839	0.23
20	10.162	0.07	1	5.958	3.03
21	7.499	0.05	1	4.397	0.63
22	5.750	0.02	1	3.372	0.95
23	8.052	0.05	1	4.722	1.13
24	6.164	0.00	1	3.614	0.58
25	6.642	0.06	1	3.894	0.14
26	7.155	0.10	1	4.195	0.32
27	8.306	0.18	1	4.870	1.36
28	6.201	0.04	1	3.636	0.54
29	6.806	0.04	1	3.991	0.00
30	5.763	0.15	1	3.379	0.94
31	6.284	0.12	1	3.685	0.47
32	7.386	0.05	1	4.331	0.53
33	6.950	0.13	1	4.075	0.13
34	6.265	0.08	1	3.673	0.49
35	7.896	0.02	1	4.630	0.99
36	6.125	0.14	1	3.591	0.61
37	7.480	0.12	1	4.386	0.61
38	7.313	0.11	1	4.288	0.46
39	7.384	0.01	1	4.330	0.52
40	5.139	0.10	1	3.013	1.50
41	6.928	0.12	1	4.062	0.11
42	6.655	0.10	1	3.902	0.13
43	6.136	0.06	1	3.598	0.60
44	5.573	0.07	1	3.268	1.11
45	6.849	0.03	1	4.016	0.04
46	3.027	0.02	1	1.775	3.41
47	6.267	0.02	1	3.675	0.48
48	7.633	0.03	1	4.476	0.75
49	5.967	0.02	1	3.499	0.75
50	6.297	0.06	1	3.692	0.46
51	7.277	0.07	1	4.267	0.43
52	6.466	0.07	1	3.792	0.30
53	5.837	0.07	1	3.422	0.87
54	6.396	0.01	1	3.751	0.37
55	7.455	0.01	1	4.371	0.59
56	7.237	0.02	1	4.244	0.39
57	6.868	0.11	1	4.027	0.06
58	6.990	0.07	1	4.098	0.17
59	5.102	0.13	1	2.992	1.53
60	6.385	0.06	1	3.744	0.38
61	6.171	0.11	1	3.619	0.57
62	6.754	0.07	1	3.960	0.04
63	8.641	0.08	1	5.067	1.66
64	6.406	0.07	1	3.756	0.36
65	6.578	0.09	1	3.857	0.20

UNL-4085

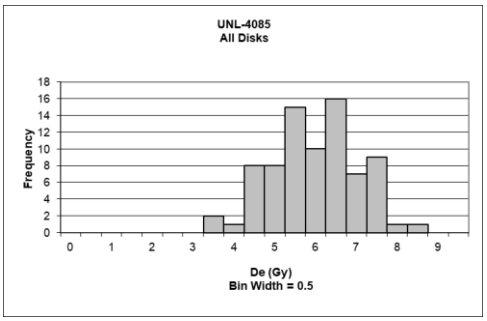

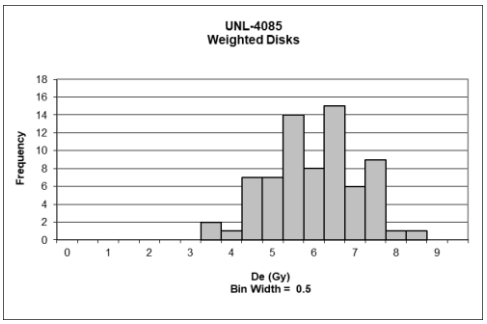

Disc	De	Error	Wt	Age	+/- 1 σ
1	6.412	0.05	1	3.566	0.64
2	6.130	0.04	1	3.409	0.36
3	5.427	0.07	1	3.018	0.32
4	5.189	0.03	1	2.886	0.55
5	6.904	0.01	1	3.840	1.12
6	4.741	0.14	1	2.637	0.99
7	6.854	0.07	1	3.812	1.07
8	5.020	0.05	1	2.792	0.72
9	5.162	0.05	1	2.871	0.58
10	6.514	0.08	1	3.623	0.74
11	7.362	0.07	1	4.094	1.56
12	5.214	0.45	1	2.900	0.53
13	6.437	0.03	1	3.580	0.66
14	4.202	0.34	1	2.337	1.51
15	5.646	0.20	1	3.140	0.11
16	5.796	0.09	1	3.223	0.04
17	3.817	0.17	1	2.123	1.89
18	6.721	0.09	1	3.738	0.94
19	4.255	0.16	1	2.367	1.46
20	5.216	0.33	1	2.901	0.53
21	6.133	0.06	1	3.411	0.37
22	6.262	0.03	1	3.483	0.49
23	4.608	0.20	1	2.562	1.12
24	7.405	0.03	1	4.118	1.61
25	4.113	0.10	1	2.287	1.60
26	6.726	0.00	1	3.741	0.94
27	4.796	0.11	1	2.667	0.94
28	7.266	0.07	1	4.041	1.47
29	7.499	0.14	1	4.170	1.70
30	5.669	0.08	1	3.153	0.08
31	4.230	0.14	1	2.352	1.49
32	4.444	0.23	1	2.472	1.28
33	4.860	0.06	1	2.703	0.87
34	5.268	0.11	1	2.930	0.48
35	6.053	0.21	1	3.366	0.29
36	5.369	0.02	1	2.986	0.38
37	4.728	0.15	1	2.629	1.00
38	7.113	0.09	1	3.955	1.32
39	7.126	0.05	1	3.963	1.33
40	6.724	0.09	1	3.740	0.94
41	4.834	0.19	1	2.688	0.90
42	6.131	0.12	1	3.410	0.37
43	3.408	0.13	1	1.895	2.29
44	6.147	0.17	1	3.418	0.38
45	6.438	0.24	1	3.580	0.66
46	4.211	0.32	1	2.342	1.50
47	6.119	0.17	1	3.403	0.35
48	5.820	0.17	1	3.236	0.06
49	7.360	0.00	1	4.093	1.56
50	6.273	0.03	1	3.488	0.50
51	5.829	0.08	1	3.242	0.07
52	5.471	0.57	1	3.042	0.28
53	5.532	0.11	1	3.077	0.22
54	5.697	0.38	1	3.168	0.06
55	5.340	0.04	1	2.970	0.40
56	6.162	0.08	1	3.427	0.39
57	5.047	0.30	1	2.807	0.69
58	6.071	0.10	1	3.376	0.31
59	6.151	0.29	1	3.421	0.38
60	7.006	0.03	1	3.896	1.22
61	4.984	0.07	1	2.772	0.75
62	4.048	0.07	1	2.251	1.66
63	5.478	0.17	1	3.047	0.27
64	7.196	0.13	1	4.002	1.40
65	6.959	0.11	1	3.870	1.17
66	4.968	0.28	1	2.763	0.77
67	5.384	0.08	1	2.994	0.36
68	5.062	0.06	1	2.815	0.68
69	5.752	0.01	1	3.199	0.00
70	5.474	0.06	1	3.044	0.28
71	8.261	0.05	1	4.594	2.44
72	5.655	0.08	1	3.145	0.10
73	7.700	0.15	1	4.282	1.89
74	4.384	0.04	1	2.438	1.34
75	6.121	0.05	1	3.404	0.35
76	6.442	0.13	1	3.583	0.67
77	3.246	0.07	1	1.805	2.44
78	5.819	0.21	1	3.236	0.06

Disc	De	Error	Wt	Age	+/- 1 σ
1	6.412	0.05	1	3.566	0.64
2	6.130	0.04	1	3.409	0.36
3	5.427	0.07	1	3.018	0.32
4	5.189	0.03	1	2.886	0.55
5	6.904	0.01	1	3.840	1.12
6	4.741	0.14	1	2.637	0.99
7	6.854	0.07	1	3.812	1.07
8	5.020	0.05	1	2.792	0.72
9	5.162	0.05	1	2.871	0.58
10	6.514	0.08	1	3.623	0.74
11	7.362	0.07	1	4.094	1.56
12	5.214	0.45	1	2.900	0.53
13	6.437	0.03	1	3.580	0.66
14	4.202	0.34	1	2.337	1.51
15	5.646	0.20	1	3.140	0.11
16	5.796	0.09	1	3.223	0.04
17	3.817	0.17	1	2.123	1.89
18	6.721	0.09	1	3.738	0.94
19	4.255	0.16	1	2.367	1.46
20	5.216	0.33	1	2.901	0.53
21	6.133	0.06	1	3.411	0.37
22	6.262	0.03	1	3.483	0.49
23	4.608	0.20	1	2.562	1.12
24	7.405	0.03	1	4.118	1.61
25	4.113	0.10	1	2.287	1.60
26	6.726	0.00	1	3.741	0.94
27	7.266	0.07	1	4.041	1.47
28	7.499	0.14	1	4.170	1.70
29	5.669	0.08	1	3.153	0.08
30	4.230	0.14	1	2.352	1.49
31	4.860	0.06	1	2.703	0.87
32	5.268	0.11	1	2.930	0.48
33	6.053	0.21	1	3.366	0.29
34	5.369	0.02	1	2.986	0.38
35	4.728	0.15	1	2.629	1.00
36	7.113	0.09	1	3.955	1.32
37	7.126	0.05	1	3.963	1.33
38	4.834	0.19	1	2.688	0.90
39	6.131	0.12	1	3.410	0.37
40	3.408	0.13	1	1.895	2.29
41	6.147	0.17	1	3.418	0.38
42	6.438	0.24	1	3.580	0.66
43	4.211	0.32	1	2.342	1.50
44	6.119	0.17	1	3.403	0.35
45	5.820	0.17	1	3.236	0.06
46	7.360	0.00	1	4.093	1.56
47	6.273	0.03	1	3.488	0.50
48	5.471	0.57	1	3.042	0.28
49	5.532	0.11	1	3.077	0.22
50	5.340	0.04	1	2.970	0.40
51	6.162	0.08	1	3.427	0.39
52	5.047	0.30	1	2.807	0.69
53	6.071	0.10	1	3.376	0.31
54	7.006	0.03	1	3.896	1.22
55	4.984	0.07	1	2.772	0.75
56	4.048	0.07	1	2.251	1.66
57	5.478	0.17	1	3.047	0.27
58	7.196	0.13	1	4.002	1.40
59	6.959	0.11	1	3.870	1.17
60	4.968	0.28	1	2.763	0.77
61	5.384	0.08	1	2.994	0.36
62	5.752	0.01	1	3.199	0.00
63	5.474	0.06	1	3.044	0.28
64	8.261	0.05	1	4.594	2.44
65	5.655	0.08	1	3.145	0.10
66	7.700	0.15	1	4.282	1.89
67	4.384	0.04	1	2.438	1.34
68	6.121	0.05	1	3.404	0.35
69	6.442	0.13	1	3.583	0.67
70	3.246	0.07	1	1.805	2.44
71	5.819	0.21	1	3.236	0.06

UNL-4090

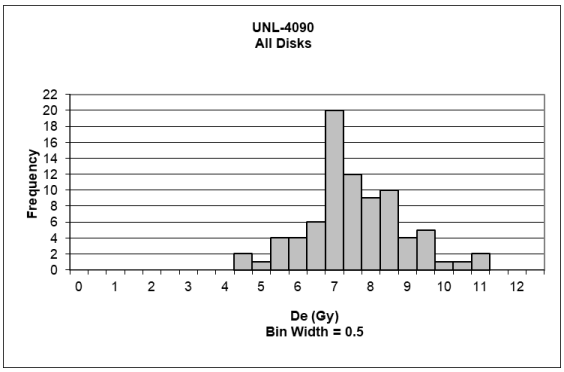
UNL-4090
All Disks
Frequency
0
2
4
6
8
10
12
14
16
18
20
22
0 1 2 3 4 5 6 7 8 9 10 11 12
De (Gy)
Bin Width = 0.5

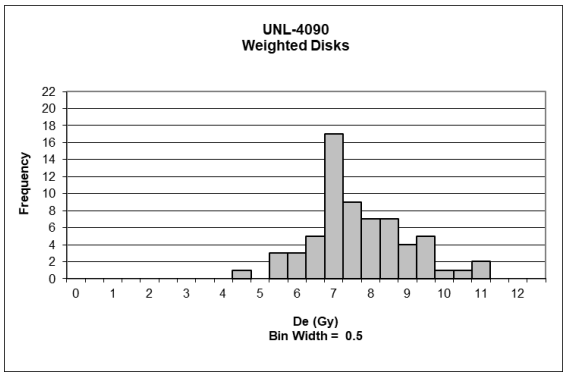
UNL-4090
Weighted Disks
Frequency
0
2
4
6
8
10
12
14
16
18
20
22
0 1 2 3 4 5 6 7 8 9 10 11 12
De (Gy)
Bin Width = 0.5

UNL-4090 contd.

Disc	De	Error	Wt	Age	+/- 1 σ	Disc	De	Error	Wt	Age	+/- 1 σ
1	7.220	0.21	1	4.122	0.19	1	7.220	0.21	1	4.122	0.19
2	7.676	0.28	1	4.382	0.21	2	9.059	0.01	1	5.172	1.45
3	5.069	0.22	1	2.894	2.12	3	6.944	0.17	1	3.965	0.44
4	9.059	0.01	1	5.172	1.45	4	8.245	0.01	1	4.707	0.72
5	6.944	0.17	1	3.965	0.44	5	7.714	0.13	1	4.404	0.25
6	8.245	0.01	1	4.707	0.72	6	6.939	0.23	1	3.962	0.45
7	7.714	0.13	1	4.404	0.25	7	5.460	0.19	1	3.117	1.77
8	6.939	0.23	1	3.962	0.45	8	6.776	0.05	1	3.868	0.59
9	5.460	0.19	1	3.117	1.77	9	6.544	0.05	1	3.736	0.80
10	6.776	0.05	1	3.868	0.59	10	6.348	0.15	1	3.624	0.98
11	6.544	0.05	1	3.736	0.80	11	5.859	0.09	1	3.345	1.41
12	6.348	0.15	1	3.624	0.98	12	8.284	0.01	1	4.730	0.76
13	5.859	0.09	1	3.345	1.41	13	9.039	0.07	1	5.161	1.44
14	8.284	0.01	1	4.730	0.76	14	6.991	0.06	1	3.991	0.40
15	9.039	0.07	1	5.161	1.44	15	7.181	0.21	1	4.100	0.23
16	6.991	0.06	1	3.991	0.40	16	7.037	0.03	1	4.017	0.36
17	7.181	0.21	1	4.100	0.23	17	6.527	0.23	1	3.726	0.82
18	7.037	0.03	1	4.017	0.36	18	6.573	0.11	1	3.753	0.77
19	6.527	0.23	1	3.726	0.82	19	10.142	0.25	1	5.790	2.42
20	8.457	0.17	1	4.828	0.91	20	5.424	0.06	1	3.097	1.80
21	6.573	0.11	1	3.753	0.77	21	8.729	0.06	1	4.983	1.16
22	10.142	0.25	1	5.790	2.42	22	9.149	0.07	1	5.223	1.53
23	5.424	0.06	1	3.097	1.80	23	8.612	0.20	1	4.917	1.05
24	8.729	0.06	1	4.983	1.16	24	7.982	0.07	1	4.557	0.49
25	7.347	0.26	1	4.195	0.08	25	6.736	0.14	1	3.846	0.63
26	9.149	0.07	1	5.223	1.53	26	6.835	0.13	1	3.902	0.54
27	8.612	0.20	1	4.917	1.05	27	8.581	0.26	1	4.899	1.03
28	7.982	0.07	1	4.557	0.49	28	8.283	0.38	1	4.729	0.76
29	6.736	0.14	1	3.846	0.63	29	8.287	0.03	1	4.731	0.76
30	6.835	0.13	1	3.902	0.54	30	8.934	0.05	1	5.101	1.34
31	8.581	0.26	1	4.899	1.03	31	9.111	0.03	1	5.201	1.50
32	6.891	0.25	1	3.934	0.49	32	6.438	0.04	1	3.676	0.89
33	8.283	0.38	1	4.729	0.76	33	8.125	0.05	1	4.639	0.62
34	6.741	0.09	1	3.849	0.62	34	9.622	0.02	1	5.493	1.96
35	5.626	0.21	1	3.212	1.62	35	7.067	0.02	1	4.035	0.33
36	8.287	0.03	1	4.731	0.76	36	6.839	0.19	1	3.904	0.54
37	8.934	0.05	1	5.101	1.34	37	7.832	0.04	1	4.471	0.35
38	9.111	0.03	1	5.201	1.50	38	6.945	0.07	1	3.965	0.44
39	4.238	0.31	1	2.420	2.87	39	6.684	0.17	1	3.816	0.67
40	7.453	0.29	1	4.255	0.01	40	8.293	0.06	1	4.735	0.77
41	6.438	0.04	1	3.676	0.89	41	5.062	0.17	1	2.890	2.13
42	8.125	0.05	1	4.639	0.62	42	5.883	0.16	1	3.359	1.39
43	9.622	0.02	1	5.493	1.96	43	7.548	0.05	1	4.309	0.10
44	7.067	0.02	1	4.035	0.33	44	7.153	0.20	1	4.084	0.25
45	6.839	0.19	1	3.904	0.54	45	5.959	0.07	1	3.402	1.32
46	7.832	0.04	1	4.471	0.35	46	7.866	0.11	1	4.491	0.38
47	6.945	0.07	1	3.965	0.44	47	7.460	0.01	1	4.259	0.02
48	6.684	0.17	1	3.816	0.67	48	6.986	0.06	1	3.988	0.40
49	8.293	0.06	1	4.735	0.77	49	8.100	0.30	1	4.624	0.59
50	5.062	0.17	1	2.890	2.13	50	6.468	0.05	1	3.693	0.87
51	5.883	0.16	1	3.359	1.39	51	7.829	0.07	1	4.470	0.35
52	7.548	0.05	1	4.309	0.10	52	6.970	0.14	1	3.980	0.42
53	7.153	0.20	1	4.084	0.25	53	7.112	0.11	1	4.060	0.29
54	5.959	0.07	1	3.402	1.32	54	6.571	0.08	1	3.751	0.78
55	7.866	0.11	1	4.491	0.38	55	6.678	0.18	1	3.813	0.68
56	7.460	0.01	1	4.259	0.02	56	4.140	0.07	1	2.363	2.95
57	6.986	0.06	1	3.988	0.40	57	7.119	0.04	1	4.064	0.28
58	8.100	0.30	1	4.624	0.59	58	6.641	0.16	1	3.792	0.71
59	6.468	0.05	1	3.693	0.87	59	6.423	0.13	1	3.667	0.91
60	7.829	0.07	1	4.470	0.35	60	6.410	0.23	1	3.660	0.92
61	6.970	0.14	1	3.980	0.42	61	10.608	0.09	1	6.056	2.84
62	7.112	0.11	1	4.060	0.29	62	9.211	0.08	1	5.259	1.59
63	6.571	0.08	1	3.751	0.78	63	10.854	0.05	1	6.197	3.06
64	8.486	0.08	1	4.845	0.94	64	7.129	0.12	1	4.070	0.28
65	7.409	0.20	1	4.230	0.02	65	7.822	0.02	1	4.466	0.35
66	7.590	0.52	1	4.334	0.14						
67	6.678	0.18	1	3.813	0.68						
68	4.140	0.07	1	2.363	2.95						
69	7.119	0.04	1	4.064	0.28						
70	6.641	0.16	1	3.792	0.71						
71	6.423	0.13	1	3.667	0.91						
72	6.410	0.23	1	3.660	0.92						
73	10.608	0.09	1	6.056	2.84						
74	9.211	0.08	1	5.259	1.59						
75	8.308	0.06	1	4.743	0.78						
76	4.973	0.06	1	2.839	2.21						
77	6.611	0.03	1	3.774	0.74						
78	10.854	0.05	1	6.197	3.06						
79	7.129	0.12	1	4.070	0.28						
80	6.431	0.13	1	3.671	0.90						
81	7.822	0.02	1	4.466	0.35						

UNL-4091

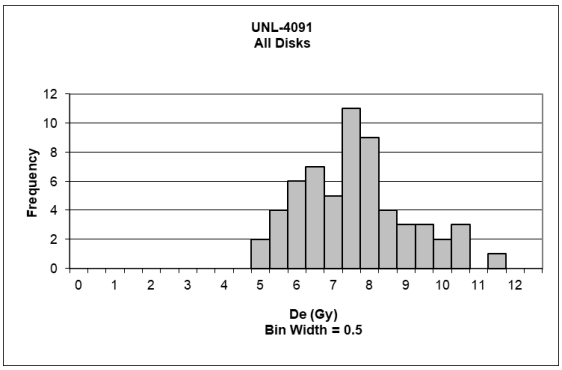

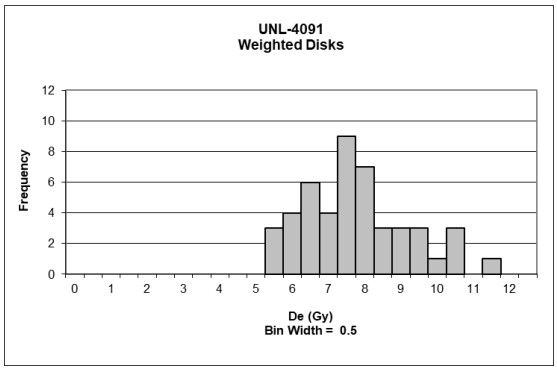

Disc	De	Error	Wt	Age	+/- 1 σ
1	10.226	0.04	1	5.413	1.85
2	8.284	0.46	1	4.385	0.53
3	6.814	0.23	1	3.607	0.47
4	4.635	0.22	1	2.454	1.96
5	6.523	0.36	1	3.453	0.67
6	8.139	0.27	1	4.308	0.43
7	7.043	0.01	1	3.728	0.32
8	7.991	0.11	1	4.230	0.33
9	5.805	0.17	1	3.073	1.16
10	5.895	0.05	1	3.120	1.10
11	6.445	0.05	1	3.412	0.73
12	6.774	0.21	1	3.586	0.50
13	7.631	0.04	1	4.039	0.08
14	7.288	0.14	1	3.858	0.15
15	9.288	0.18	1	4.917	1.21
16	7.609	0.14	1	4.028	0.07
17	5.277	0.32	1	2.793	1.52
18	8.239	0.04	1	4.361	0.50
19	6.105	0.20	1	3.232	0.96
20	6.068	0.08	1	3.212	0.98
21	8.613	0.29	1	4.559	0.75
22	7.995	0.11	1	4.232	0.33
23	8.911	0.08	1	4.717	0.96
24	5.227	0.02	1	2.767	1.56
25	7.292	0.07	1	3.860	0.15
26	8.177	0.38	1	4.328	0.46
27	9.379	0.07	1	4.965	1.28
28	4.693	0.27	1	2.484	1.92
29	9.518	0.05	1	5.038	1.37
30	5.377	0.09	1	2.847	1.45
31	8.956	0.14	1	4.741	0.99
32	7.948	0.04	1	4.207	0.30
33	6.022	0.18	1	3.188	1.01
34	7.005	0.05	1	3.708	0.34
35	10.430	0.04	1	5.521	1.99
36	10.049	0.03	1	5.319	1.73
37	11.447	0.17	1	6.059	2.69
38	7.703	0.19	1	4.078	0.13
39	7.725	0.16	1	4.089	0.15
40	7.297	0.09	1	3.863	0.14
41	7.216	0.18	1	3.820	0.20
42	7.068	0.52	1	3.741	0.30
43	5.880	0.43	1	3.112	1.11
44	6.924	0.40	1	3.665	0.40
45	7.177	0.24	1	3.799	0.23
46	7.641	0.13	1	4.045	0.09
47	5.564	0.27	1	2.945	1.33
48	6.094	0.01	1	3.226	0.96
49	6.170	0.20	1	3.266	0.91
50	5.860	0.14	1	3.102	1.12
51	5.250	0.27	1	2.779	1.54
52	7.590	0.03	1	4.018	0.06
53	7.166	0.16	1	3.793	0.23
54	9.866	0.13	1	5.222	1.61
55	6.903	0.03	1	3.654	0.41
56	7.242	0.15	1	3.834	0.18
57	7.481	0.22	1	3.960	0.02
58	5.750	0.09	1	3.044	1.20
59	9.158	0.04	1	4.848	1.13
60	6.107	0.26	1	3.233	0.96

Disc	De	Error	Wt	Age	+/- 1 σ
1	10.226	0.04	1	5.413	1.85
2	8.284	0.46	1	4.385	0.53
3	6.814	0.23	1	3.607	0.47
4	6.523	0.36	1	3.453	0.67
5	7.043	0.01	1	3.728	0.32
6	5.805	0.17	1	3.073	1.16
7	5.895	0.05	1	3.120	1.10
8	6.445	0.05	1	3.412	0.73
9	6.774	0.21	1	3.586	0.50
10	7.631	0.04	1	4.039	0.08
11	7.288	0.14	1	3.858	0.15
12	9.288	0.18	1	4.917	1.21
13	7.609	0.14	1	4.028	0.07
14	5.277	0.32	1	2.793	1.52
15	8.239	0.04	1	4.361	0.50
16	6.105	0.20	1	3.232	0.96
17	6.068	0.08	1	3.212	0.98
18	8.613	0.29	1	4.559	0.75
19	7.995	0.11	1	4.232	0.33
20	8.911	0.08	1	4.717	0.96
21	5.227	0.02	1	2.767	1.56
22	7.292	0.07	1	3.860	0.15
23	8.177	0.38	1	4.328	0.46
24	9.379	0.07	1	4.965	1.28
25	9.518	0.05	1	5.038	1.37
26	5.377	0.09	1	2.847	1.45
27	8.956	0.14	1	4.741	0.99
28	7.948	0.04	1	4.207	0.30
29	6.022	0.18	1	3.188	1.01
30	7.005	0.05	1	3.708	0.34
31	10.430	0.04	1	5.521	1.99
32	10.049	0.03	1	5.319	1.73
33	11.447	0.17	1	6.059	2.69
34	7.703	0.19	1	4.078	0.13
35	7.725	0.16	1	4.089	0.15
36	7.297	0.09	1	3.863	0.14
37	7.216	0.18	1	3.820	0.20
38	5.880	0.43	1	3.112	1.11
39	7.177	0.24	1	3.799	0.23
40	7.641	0.13	1	4.045	0.09
41	6.094	0.01	1	3.226	0.96
42	6.170	0.20	1	3.266	0.91
43	5.860	0.14	1	3.102	1.12
44	7.166	0.16	1	3.793	0.23
45	6.903	0.03	1	3.654	0.41
46	7.242	0.15	1	3.834	0.18
47	9.158	0.04	1	4.848	1.13
48					
49					
50					
51					
52					
53					
54					

UNL-4092

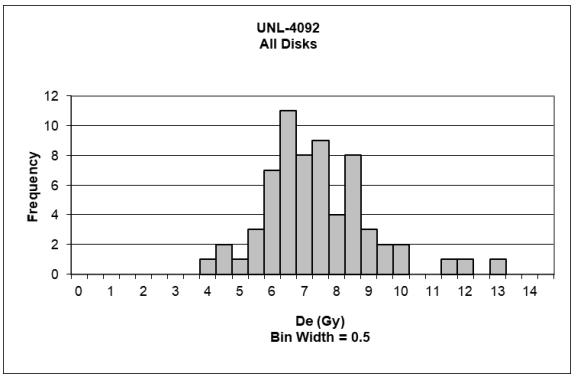

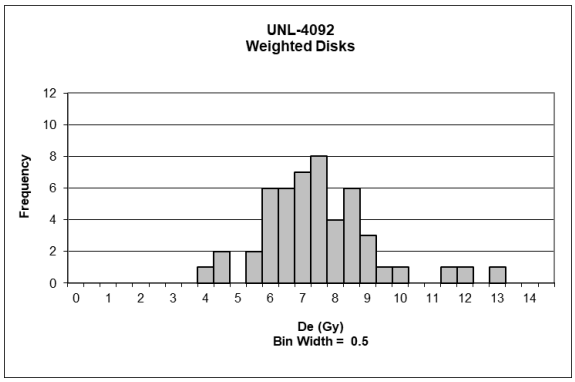

Disc	De	Error	Wt	Age	+/- 1 σ
1	9.817	0.05	1	5.388	1.50
2	6.386	0.20	1	3.505	0.48
3	6.285	0.20	1	3.450	0.54
4	8.029	0.20	1	4.407	0.47
5	4.392	0.34	1	2.411	1.63
6	6.740	0.05	1	3.699	0.28
7	7.310	0.06	1	4.013	0.05
8	6.353	0.27	1	3.487	0.50
9	8.262	0.10	1	4.535	0.60
10	6.841	0.02	1	3.755	0.22
11	7.195	0.05	1	3.949	0.01
12	6.659	0.18	1	3.655	0.32
13	7.971	0.14	1	4.376	0.44
14	6.277	0.12	1	3.446	0.54
15	7.028	0.10	1	3.857	0.11
16	5.272	0.25	1	2.894	1.12
17	6.157	0.15	1	3.380	0.61
18	8.073	0.24	1	4.432	0.49
19	6.626	0.20	1	3.637	0.34
20	9.238	0.24	1	5.071	1.17
21	5.468	0.08	1	3.001	1.01
22	6.332	0.06	1	3.476	0.51
23	8.292	0.26	1	4.552	0.62
24	5.526	0.50	1	3.033	0.98
25	6.698	0.13	1	3.676	0.30
26	5.586	0.11	1	3.066	0.94
27	6.117	0.19	1	3.358	0.64
28	7.723	0.11	1	4.239	0.29
29	7.069	0.09	1	3.880	0.09
30	3.733	0.27	1	2.049	2.01
31	8.194	0.19	1	4.498	0.56
32	11.617	0.01	1	6.377	2.54
33	8.634	0.04	1	4.739	0.82
34	6.591	0.11	1	3.618	0.36
35	5.524	0.14	1	3.032	0.98
36	7.362	0.07	1	4.041	0.08
37	7.321	0.12	1	4.018	0.06
38	7.178	0.07	1	3.940	0.02
39	7.791	0.17	1	4.276	0.33
40	12.761	0.00	1	7.005	3.20
41	8.167	0.02	1	4.483	0.55
42	5.846	0.13	1	3.209	0.79
43	8.594	0.13	1	4.717	0.80
44	8.637	0.01	1	4.741	0.82
45	5.672	0.23	1	3.113	0.89
46	6.014	0.32	1	3.301	0.70
47	8.060	0.06	1	4.424	0.49
48	7.281	0.35	1	3.996	0.04
49	9.550	0.05	1	5.242	1.35
50	6.976	0.21	1	3.829	0.14
51	5.842	0.44	1	3.207	0.79
52	6.355	0.03	1	3.489	0.50
53	7.339	0.09	1	4.028	0.07
54	8.483	0.13	1	4.656	0.73
55	9.319	0.61	1	5.115	1.21
56	6.752	0.22	1	3.706	0.27
57	11.044	0.16	1	6.062	2.21
58	6.243	0.21	1	3.427	0.56
59	4.221	0.11	1	2.317	1.73
60	6.356	0.03	1	3.489	0.50
61	5.977	0.15	1	3.281	0.72
62	7.736	0.30	1	4.246	0.30
63	4.677	0.34	1	2.567	1.47
64	5.013	0.16	1	2.752	1.27

Disc	De	Error	Wt	Age	+/- 1 σ
1	9.817	0.05	1	5.388	1.50
2	8.029	0.20	1	4.407	0.47
3	4.392	0.34	1	2.411	1.63
4	7.310	0.06	1	4.013	0.05
5	8.262	0.10	1	4.535	0.60
6	6.841	0.02	1	3.755	0.22
7	7.195	0.05	1	3.949	0.01
8	6.659	0.18	1	3.655	0.32
9	7.971	0.14	1	4.376	0.44
10	6.277	0.12	1	3.446	0.54
11	7.028	0.10	1	3.857	0.11
12	6.626	0.20	1	3.637	0.34
13	5.468	0.08	1	3.001	1.01
14	6.332	0.06	1	3.476	0.51
15	8.292	0.26	1	4.552	0.62
16	6.698	0.13	1	3.676	0.30
17	5.586	0.11	1	3.066	0.94
18	6.117	0.19	1	3.358	0.64
19	7.723	0.11	1	4.239	0.29
20	7.069	0.09	1	3.880	0.09
21	3.733	0.27	1	2.049	2.01
22	11.617	0.01	1	6.377	2.54
23	8.634	0.04	1	4.739	0.82
24	6.591	0.11	1	3.618	0.36
25	5.524	0.14	1	3.032	0.98
26	7.362	0.07	1	4.041	0.08
27	7.321	0.12	1	4.018	0.06
28	7.178	0.07	1	3.940	0.02
29	7.791	0.17	1	4.276	0.33
30	12.761	0.00	1	7.005	3.20
31	8.167	0.02	1	4.483	0.55
32	5.846	0.13	1	3.209	0.79
33	8.594	0.13	1	4.717	0.80
34	8.637	0.01	1	4.741	0.82
35	5.672	0.23	1	3.113	0.89
36	8.060	0.06	1	4.424	0.49
37	6.976	0.21	1	3.829	0.14
38	5.842	0.44	1	3.207	0.79
39	6.355	0.03	1	3.489	0.50
40	7.339	0.09	1	4.028	0.07
41	8.483	0.13	1	4.656	0.73
42	9.319	0.61	1	5.115	1.21
43	6.752	0.22	1	3.706	0.27
44	11.044	0.16	1	6.062	2.21
45	6.243	0.21	1	3.427	0.56
46	4.221	0.11	1	2.317	1.73
47	6.356	0.03	1	3.489	0.50
48	5.977	0.15	1	3.281	0.72
49	7.736	0.30	1	4.246	0.30
50	5.013	0.16	1	2.752	1.27
51					
52					
53					
54					

UNL-4244

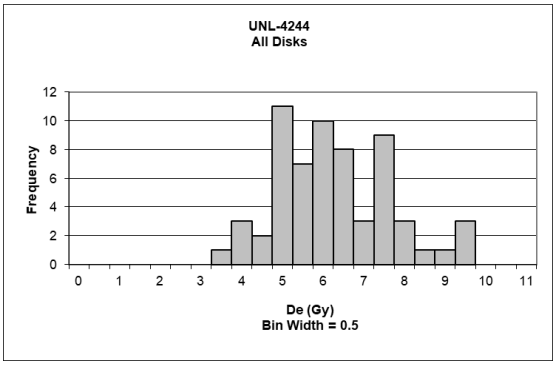

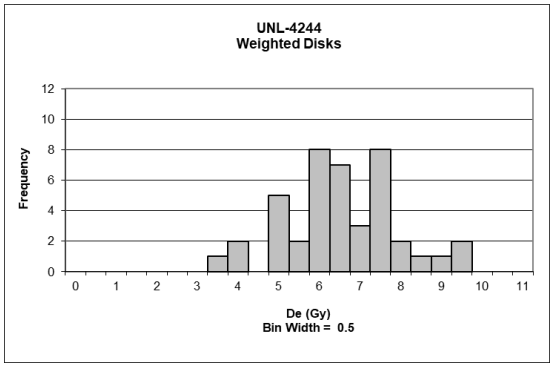

Disc	De	Error	Wt	Age	+/- 1 σ
1	6.703	0.34	1	4.356	0.30
2	8.409	0.35	1	5.465	1.53
3	5.927	0.41	1	3.852	0.25
4	4.850	0.18	1	3.152	1.02
5	3.032	0.21	1	1.971	2.32
6	5.583	0.23	1	3.629	0.50
7	5.597	0.13	1	3.637	0.49
8	7.464	0.05	1	4.851	0.85
9	7.423	0.08	1	4.824	0.82
10	4.935	0.42	1	3.207	0.96
11	7.619	0.42	1	4.951	0.96
12	3.856	0.15	1	2.506	1.73
13	5.690	0.02	1	3.698	0.42
14	5.584	0.10	1	3.629	0.50
15	9.223	0.29	1	5.994	2.11
16	7.211	0.04	1	4.687	0.67
17	9.206	0.09	1	5.983	2.10
18	7.432	0.08	1	4.830	0.83
19	4.782	0.49	1	3.108	1.07
20	3.646	0.11	1	2.370	1.88
21	8.592	0.06	1	5.584	1.66
22	5.772	0.07	1	3.751	0.36
23	5.691	0.13	1	3.698	0.42
24	7.401	0.09	1	4.810	0.80
25	5.369	0.39	1	3.489	0.65
26	7.278	0.06	1	4.730	0.72
27	5.063	0.35	1	3.290	0.87
28	5.746	0.07	1	3.734	0.38
29	9.137	0.02	1	5.938	2.05
30	5.037	0.19	1	3.273	0.89
31	7.613	0.02	1	4.947	0.96
32	5.862	0.29	1	3.810	0.30
33	4.078	0.39	1	2.650	1.58
34	7.030	0.25	1	4.569	0.54
35	4.742	0.21	1	3.082	1.10
36	6.136	0.12	1	3.988	0.10
37	6.015	0.07	1	3.909	0.19
38	4.836	0.37	1	3.143	1.03
39	6.803	0.20	1	4.421	0.38
40	7.452	0.20	1	4.843	0.84
41	6.497	0.15	1	4.222	0.16
42	5.137	0.23	1	3.339	0.82
43	6.186	0.05	1	4.020	0.07
44	4.602	0.09	1	2.991	1.20
45	6.204	0.03	1	4.032	0.05
46	4.144	0.41	1	2.693	1.53
47	5.804	0.30	1	3.772	0.34
48	4.988	0.31	1	3.241	0.92
49	4.973	0.56	1	3.232	0.93
50	3.831	0.27	1	2.489	1.75
51	5.453	0.08	1	3.544	0.59
52	7.560	0.45	1	4.913	0.92
53	4.690	0.25	1	3.048	1.14
54	4.966	0.18	1	3.227	0.94
55	6.099	0.18	1	3.964	0.13
56	7.388	0.11	1	4.802	0.79
57	6.466	0.19	1	4.202	0.13
58	5.120	0.27	1	3.328	0.83
59	6.200	0.51	1	4.029	0.06
60	4.744	0.37	1	3.083	1.10
61	5.237	0.62	1	3.404	0.75
62	6.922	0.28	1	4.498	0.46

Disc	De	Error	Wt	Age	+/- 1 σ
1	6.703	0.34	1	4.356	0.30
2	8.409	0.35	1	5.465	1.53
3	5.927	0.41	1	3.852	0.25
4	4.850	0.18	1	3.152	1.02
5	3.032	0.21	1	1.971	2.32
6	5.583	0.23	1	3.629	0.50
7	5.597	0.13	1	3.637	0.49
8	7.464	0.05	1	4.851	0.85
9	7.423	0.08	1	4.824	0.82
10	4.935	0.42	1	3.207	0.96
11	7.619	0.42	1	4.951	0.96
12	3.856	0.15	1	2.506	1.73
13	5.690	0.02	1	3.698	0.42
14	5.584	0.10	1	3.629	0.50
15	7.211	0.04	1	4.687	0.67
16	9.206	0.09	1	5.983	2.10
17	7.432	0.08	1	4.830	0.83
18	3.646	0.11	1	2.370	1.88
19	8.592	0.06	1	5.584	1.66
20	5.772	0.07	1	3.751	0.36
21	5.691	0.13	1	3.698	0.42
22	7.401	0.09	1	4.810	0.80
23	7.278	0.06	1	4.730	0.72
24	5.746	0.07	1	3.734	0.38
25	9.137	0.02	1	5.938	2.05
26	5.037	0.19	1	3.273	0.89
27	7.613	0.02	1	4.947	0.96
28	7.030	0.25	1	4.569	0.54
29	4.742	0.21	1	3.082	1.10
30	6.136	0.12	1	3.988	0.10
31	6.015	0.07	1	3.909	0.19
32	6.803	0.20	1	4.421	0.38
33	6.497	0.15	1	4.222	0.16
34	6.186	0.05	1	4.020	0.07
35	4.602	0.09	1	2.991	1.20
36	6.204	0.03	1	4.032	0.05
37	4.966	0.18	1	3.227	0.94
38	7.388	0.11	1	4.802	0.79
39	6.466	0.19	1	4.202	0.13
40	5.120	0.27	1	3.328	0.83
41	6.200	0.51	1	4.029	0.06
42	6.922	0.28	1	4.498	0.46
43					
44					
45					
46					
47					
48					
49					
50					
51					
52					
53					
54					

UNL-4294

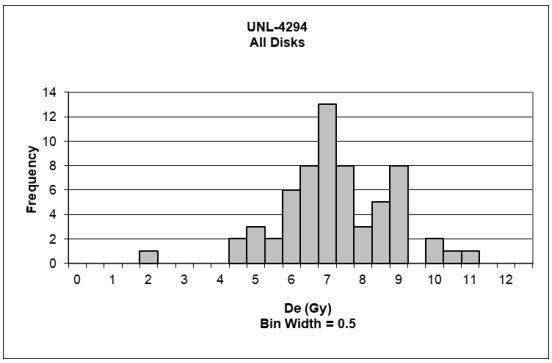

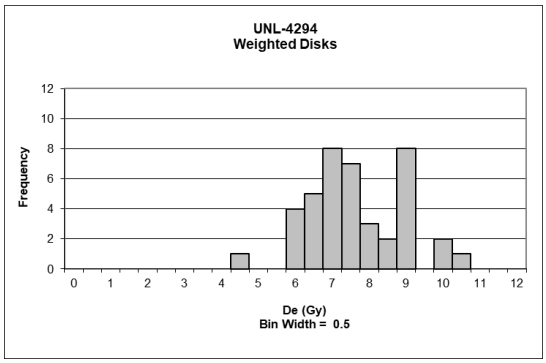

Disc	De	Error	Wt	Age	+/- 1 σ
1	5.606	0.09	1	3.533	1.36
2	6.681	0.03	1	4.211	0.55
3	7.282	0.10	1	4.590	0.09
4	6.902	0.19	1	4.350	0.38
5	7.282	0.02	1	4.590	0.09
6	6.919	0.21	1	4.361	0.37
7	10.524	0.08	1	6.633	2.36
8	6.594	0.02	1	4.156	0.61
9	6.835	0.29	1	4.308	0.43
10	8.418	0.16	1	5.306	0.77
11	5.336	0.23	1	3.363	1.57
12	4.642	0.19	1	2.926	2.09
13	1.690	0.83	1	1.065	4.33
14	6.840	0.38	1	4.311	0.43
15	7.080	0.01	1	4.463	0.24
16	6.169	0.08	1	3.888	0.93
17	5.604	0.11	1	3.532	1.36
18	7.494	0.07	1	4.723	0.07
19	5.719	0.11	1	3.605	1.28
20	6.057	0.30	1	3.818	1.02
21	9.857	0.05	1	6.212	1.86
22	6.576	0.21	1	4.145	0.63
23	6.835	0.16	1	4.308	0.43
24	8.609	0.10	1	5.426	0.91
25	8.680	0.21	1	5.471	0.97
26	5.953	0.19	1	3.752	1.10
27	6.360	0.31	1	4.009	0.79
28	5.376	0.39	1	3.388	1.54
29	8.794	0.07	1	5.543	1.05
30	4.800	0.16	1	3.026	1.97
31	4.778	0.26	1	3.011	1.99
32	7.024	0.28	1	4.427	0.29
33	8.132	0.30	1	5.126	0.55
34	7.766	0.26	1	4.895	0.27
35	4.333	0.29	1	2.731	2.32
36	5.570	0.35	1	3.511	1.39
37	7.767	0.06	1	4.895	0.27
38	6.377	0.23	1	4.019	0.78
39	7.671	0.15	1	4.835	0.20
40	5.520	0.07	1	3.479	1.43
41	7.067	0.21	1	4.454	0.26
42	8.911	0.20	1	5.617	1.14
43	6.853	0.02	1	4.319	0.42
44	6.913	0.16	1	4.357	0.37
45	7.123	0.13	1	4.489	0.21
46	8.434	0.05	1	5.316	0.78
47	9.983	0.16	1	6.292	1.95
48	8.498	0.22	1	5.356	0.83
49	6.274	0.07	1	3.955	0.85
50	6.829	0.25	1	4.304	0.44
51	8.941	0.02	1	5.635	1.16
52	4.460	0.30	1	2.811	2.23
53	8.759	0.08	1	5.521	1.03
54	6.900	0.04	1	4.349	0.38
55	6.269	0.14	1	3.951	0.86
56	8.012	0.06	1	5.050	0.46
57	10.493	0.03	1	6.614	2.34
58	7.465	0.06	1	4.705	0.05
59	6.659	0.40	1	4.197	0.56
60	8.605	0.03	1	5.424	0.91
61	6.269	0.31	1	3.952	0.86
62	8.673	0.12	1	5.467	0.96
63	6.457	0.04	1	4.070	0.72

Disc	De	Error	Wt	Age	+/- 1 σ
1	5.606	0.09	1	3.533	1.36
2	6.681	0.03	1	4.211	0.55
3	7.282	0.10	1	4.590	0.09
4	6.902	0.19	1	4.350	0.38
5	7.282	0.02	1	4.590	0.09
6	6.594	0.02	1	4.156	0.61
7	7.080	0.01	1	4.463	0.24
8	6.169	0.08	1	3.888	0.93
9	5.604	0.11	1	3.532	1.36
10	7.494	0.07	1	4.723	0.07
11	9.857	0.05	1	6.212	1.86
12	6.835	0.16	1	4.308	0.43
13	8.609	0.10	1	5.426	0.91
14	8.680	0.21	1	5.471	0.97
15	5.953	0.19	1	3.752	1.10
16	8.794	0.07	1	5.543	1.05
17	7.766	0.26	1	4.895	0.27
18	4.333	0.29	1	2.731	2.32
19	7.767	0.06	1	4.895	0.27
20	7.671	0.15	1	4.835	0.20
21	5.520	0.07	1	3.479	1.43
22	7.067	0.21	1	4.454	0.26
23	8.911	0.20	1	5.617	1.14
24	6.853	0.02	1	4.319	0.42
25	6.913	0.16	1	4.357	0.37
26	7.123	0.13	1	4.489	0.21
27	8.434	0.05	1	5.316	0.78
28	9.983	0.16	1	6.292	1.95
29	6.274	0.07	1	3.955	0.85
30	8.941	0.02	1	5.635	1.16
31	8.759	0.08	1	5.521	1.03
32	6.900	0.04	1	4.349	0.38
33	6.269	0.14	1	3.951	0.86
34	8.012	0.06	1	5.050	0.46
35	10.493	0.03	1	6.614	2.34
36	7.465	0.06	1	4.705	0.05
37	6.659	0.40	1	4.197	0.56
38	8.605	0.03	1	5.424	0.91
39	6.269	0.31	1	3.952	0.86
40	8.673	0.12	1	5.467	0.96
41	6.457	0.04	1	4.070	0.72
42					
43					
44					
45					
46					
47					
48					
49					
50					
51					
52					
53					
54					

UNL-4295

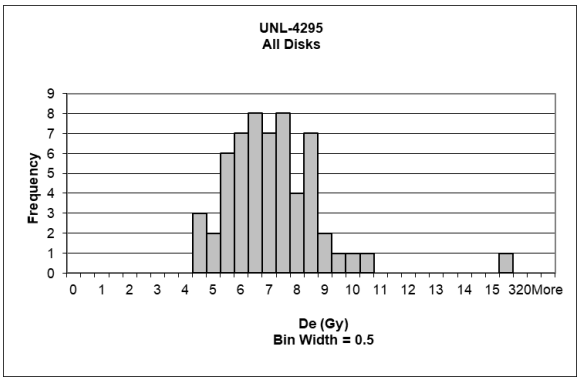

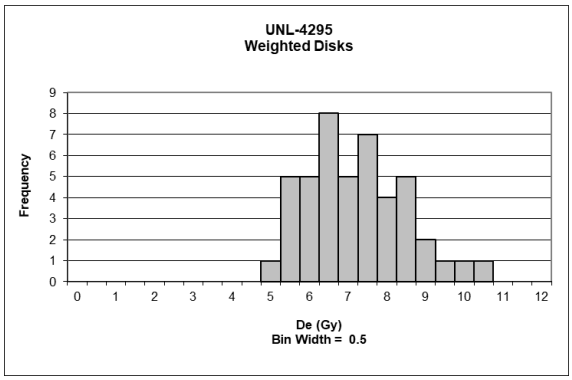

Disc	De	Error	Wt	Age	+/- 1 σ
1	7.969	0.20	1	4.858	0.78
2	7.117	0.04	1	4.338	0.12
3	7.871	0.33	1	4.798	0.70
4	9.509	0.10	1	5.796	1.97
5	6.408	0.16	1	3.906	0.43
6	6.190	0.03	1	3.773	0.60
7	4.704	0.51	1	2.867	1.75
8	6.025	0.18	1	3.673	0.73
9	7.411	0.16	1	4.518	0.34
10	5.925	0.18	1	3.612	0.81
11	5.710	0.26	1	3.481	0.97
12	7.303	0.31	1	4.452	0.26
13	4.971	0.13	1	3.030	1.55
14	6.522	0.39	1	3.976	0.34
15	8.104	0.13	1	4.940	0.88
16	8.130	0.02	1	4.956	0.90
17	5.671	0.31	1	3.457	1.00
18	6.720	0.12	1	4.097	0.19
19	8.898	0.35	1	5.424	1.50
20	5.395	0.12	1	3.289	1.22
21	4.057	0.35	1	2.473	2.26
22	4.171	0.18	1	2.543	2.17
23	6.649	0.22	1	4.053	0.25
24	7.452	0.11	1	4.542	0.38
25	35.639	0.16	1	21.726	22.24
26	6.946	0.07	1	4.234	0.02
27	5.587	0.54	1	3.406	1.07
28	5.376	0.16	1	3.277	1.23
29	8.870	0.03	1	5.407	1.48
30	7.060	0.07	1	4.304	0.07
31	6.480	0.11	1	3.950	0.38
32	5.382	0.27	1	3.281	1.23
33	6.368	0.17	1	3.882	0.46
34	5.153	0.22	1	3.141	1.41
35	5.708	0.08	1	3.480	0.98
36	5.782	0.03	1	3.524	0.92
37	6.039	0.24	1	3.681	0.72
38	5.180	0.05	1	3.157	1.39
39	7.482	0.10	1	4.561	0.40
40	7.078	0.03	1	4.315	0.09
41	7.660	0.11	1	4.669	0.54
42	6.973	0.21	1	4.251	0.01
43	9.463	0.14	1	5.769	1.94
44	7.961	0.20	1	4.853	0.77
45	6.182	0.16	1	3.769	0.61
46	8.064	0.06	1	4.916	0.85
47	10.241	0.12	1	6.243	2.54
48	8.050	0.12	1	4.907	0.84
49	8.023	0.16	1	4.891	0.82
50	8.240	0.32	1	5.023	0.99
51	6.322	0.04	1	3.854	0.50
52	6.539	0.21	1	3.986	0.33
53	5.329	0.27	1	3.249	1.27
54	8.331	0.18	1	5.078	1.06
55	5.616	0.37	1	3.423	1.05
56	4.098	0.41	1	2.498	2.22
57	6.565	0.22	1	4.002	0.31
58	7.126	0.36	1	4.344	0.12

Disc	De	Error	Wt	Age	+/- 1 σ
1	7.969	0.20	1	4.858	0.78
2	7.117	0.04	1	4.338	0.12
3	7.871	0.33	1	4.798	0.70
4	9.509	0.10	1	5.796	1.97
5	6.408	0.16	1	3.906	0.43
6	6.190	0.03	1	3.773	0.60
7	4.704	0.51	1	2.867	1.75
8	6.025	0.18	1	3.673	0.73
9	7.411	0.16	1	4.518	0.34
10	5.925	0.18	1	3.612	0.81
11	5.710	0.26	1	3.481	0.97
12	6.522	0.39	1	3.976	0.34
13	8.104	0.13	1	4.940	0.88
14	8.130	0.02	1	4.956	0.90
15	6.720	0.12	1	4.097	0.19
16	8.898	0.35	1	5.424	1.50
17	5.395	0.12	1	3.289	1.22
18	6.649	0.22	1	4.053	0.25
19	7.452	0.11	1	4.542	0.38
20	6.946	0.07	1	4.234	0.02
21	5.587	0.54	1	3.406	1.07
22	5.376	0.16	1	3.277	1.23
23	8.870	0.03	1	5.407	1.48
24	7.060	0.07	1	4.304	0.07
25	6.480	0.11	1	3.950	0.38
26	6.368	0.17	1	3.882	0.46
27	5.153	0.22	1	3.141	1.41
28	5.708	0.08	1	3.480	0.98
29	5.782	0.03	1	3.524	0.92
30	6.039	0.24	1	3.681	0.72
31	5.180	0.05	1	3.157	1.39
32	7.482	0.10	1	4.561	0.40
33	7.078	0.03	1	4.315	0.09
34	7.660	0.11	1	4.669	0.54
35	6.973	0.21	1	4.251	0.01
36	9.463	0.14	1	5.769	1.94
37	7.961	0.20	1	4.853	0.77
38	6.182	0.16	1	3.769	0.61
39	8.064	0.06	1	4.916	0.85
40	10.241	0.12	1	6.243	2.54
41	8.023	0.16	1	4.891	0.82
42	6.322	0.04	1	3.854	0.50
43	5.329	0.27	1	3.249	1.27
44	8.331	0.18	1	5.078	1.06
45	7.126	0.36	1	4.344	0.12
46					
47					
48					
49					
50					
51					
52					
53					
54					

UNL-4296

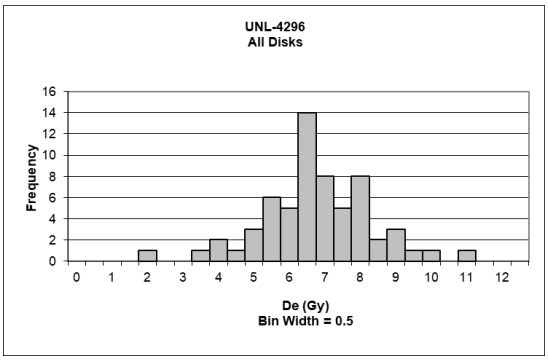

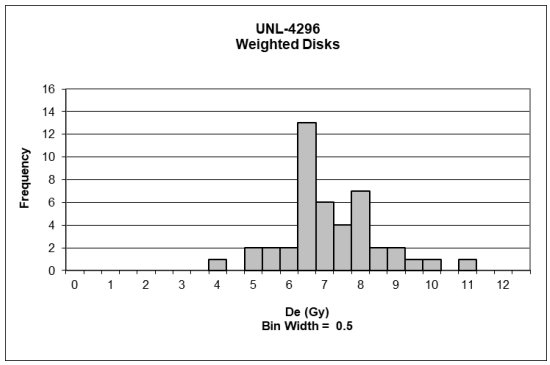

Disc	De	Error	Wt	Age	+/- 1 σ
1	6.394	0.13	1	4.253	0.39
2	6.474	0.03	1	4.306	0.33
3	10.552	0.12	1	7.019	2.72
4	3.163	0.30	1	2.104	2.80
5	7.777	0.11	1	5.173	0.65
6	4.597	0.51	1	3.058	1.73
7	6.630	0.15	1	4.410	0.21
8	7.343	0.36	1	4.884	0.32
9	6.383	0.02	1	4.245	0.40
10	6.415	0.11	1	4.267	0.37
11	7.718	0.04	1	5.133	0.60
12	6.028	0.31	1	4.009	0.66
13	3.720	0.70	1	2.474	2.39
14	6.752	0.23	1	4.491	0.12
15	5.663	0.25	1	3.767	0.93
16	6.224	0.06	1	4.140	0.51
17	9.452	0.09	1	6.287	1.90
18	7.633	0.20	1	5.077	0.54
19	4.299	0.55	1	2.859	1.95
20	7.324	0.22	1	4.871	0.31
21	8.648	0.33	1	5.752	1.30
22	7.844	0.21	1	5.217	0.70
23	6.965	0.14	1	4.633	0.04
24	6.325	0.16	1	4.207	0.44
25	5.347	0.29	1	3.557	1.17
26	5.000	0.77	1	3.326	1.43
27	6.552	0.71	1	4.358	0.27
28	4.786	0.82	1	3.183	1.59
29	5.059	0.40	1	3.365	1.39
30	8.236	0.35	1	5.478	0.99
31	6.268	0.18	1	4.169	0.48
32	6.173	0.13	1	4.106	0.55
33	7.888	0.12	1	5.246	0.73
34	8.083	0.10	1	5.376	0.87
35	4.978	0.17	1	3.311	1.45
36	9.792	0.11	1	6.513	2.15
37	6.103	0.22	1	4.059	0.61
38	6.367	0.18	1	4.235	0.41
39	7.872	0.21	1	5.236	0.72
40	6.893	0.09	1	4.584	0.02
41	6.243	0.21	1	4.152	0.50
42	8.749	0.02	1	5.819	1.37
43	1.846	0.87	1	1.228	3.79
44	8.966	0.37	1	5.963	1.53
45	7.520	0.31	1	5.002	0.45
46	6.539	0.22	1	4.349	0.28
47	7.666	0.10	1	5.099	0.56
48	5.533	0.24	1	3.680	1.03
49	6.914	0.10	1	4.599	0.00
50	6.236	0.30	1	4.148	0.51
51	7.369	0.11	1	4.902	0.34
52	5.884	0.43	1	3.913	0.77
53	5.646	0.41	1	3.755	0.95
54	5.995	0.39	1	3.987	0.69
55	5.212	0.41	1	3.467	1.27
56	7.395	0.24	1	4.919	0.36
57	3.612	0.14	1	2.402	2.47
58	5.129	0.16	1	3.412	1.33
59	5.048	0.28	1	3.357	1.39
60	6.655	0.03	1	4.426	0.19
61	6.020	0.12	1	4.004	0.67
62	7.388	0.06	1	4.914	0.35

Disc	De	Error	Wt	Age	+/- 1 σ
1	6.394	0.13	1	4.253	0.39
2	6.474	0.03	1	4.306	0.33
3	10.552	0.12	1	7.019	2.72
4	7.777	0.11	1	5.173	0.65
5	6.630	0.15	1	4.410	0.21
6	6.383	0.02	1	4.245	0.40
7	6.415	0.11	1	4.267	0.37
8	7.718	0.04	1	5.133	0.60
9	6.752	0.23	1	4.491	0.12
10	5.663	0.25	1	3.767	0.93
11	6.224	0.06	1	4.140	0.51
12	9.452	0.09	1	6.287	1.90
13	7.633	0.20	1	5.077	0.54
14	7.324	0.22	1	4.871	0.31
15	8.648	0.33	1	5.752	1.30
16	7.844	0.21	1	5.217	0.70
17	6.965	0.14	1	4.633	0.04
18	6.325	0.16	1	4.207	0.44
19	5.347	0.29	1	3.557	1.17
20	4.786	0.82	1	3.183	1.59
21	8.236	0.35	1	5.478	0.99
22	6.268	0.18	1	4.169	0.48
23	6.173	0.13	1	4.106	0.55
24	7.888	0.12	1	5.246	0.73
25	8.083	0.10	1	5.376	0.87
26	4.978	0.17	1	3.311	1.45
27	9.792	0.11	1	6.513	2.15
28	6.103	0.22	1	4.059	0.61
29	6.367	0.18	1	4.235	0.41
30	6.243	0.21	1	4.152	0.50
31	8.749	0.02	1	5.819	1.37
32	7.520	0.31	1	5.002	0.45
33	6.539	0.22	1	4.349	0.28
34	7.666	0.10	1	5.099	0.56
35	5.533	0.24	1	3.680	1.03
36	6.914	0.10	1	4.599	0.00
37	6.236	0.30	1	4.148	0.51
38	7.369	0.11	1	4.902	0.34
39	7.395	0.24	1	4.919	0.36
40	3.612	0.14	1	2.402	2.47
41	5.129	0.16	1	3.412	1.33
42	6.655	0.03	1	4.426	0.19
43	6.020	0.12	1	4.004	0.67
44	7.388	0.06	1	4.914	0.35
45					
46					
47					
48					
49					
50					
51					
52					
53					
54					

UNL-4297

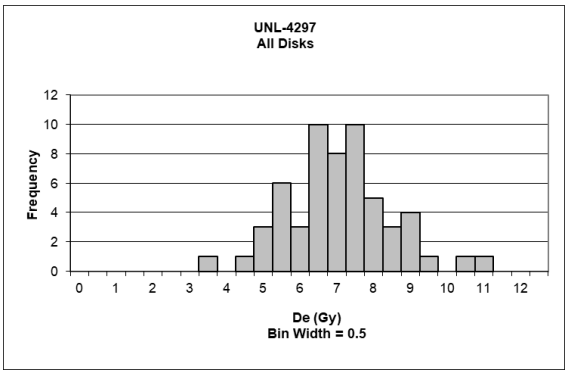

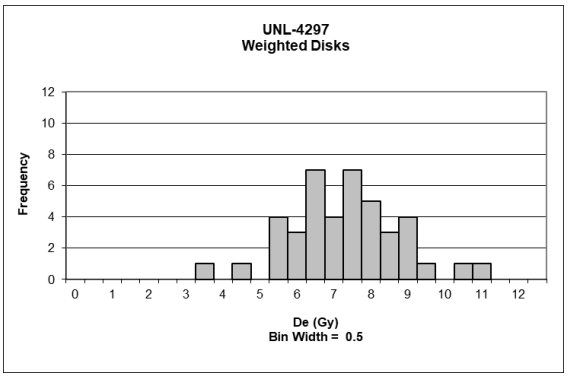

Disc	De	Error	Wt	Age	+/- 1 σ
1	6.382	0.05	1	3.974	0.46
2	5.778	0.16	1	3.598	0.86
3	5.817	0.04	1	3.623	0.84
4	8.877	0.18	1	5.528	1.23
5	5.478	0.39	1	3.411	1.07
6	4.420	0.19	1	2.752	1.78
7	6.022	0.19	1	3.751	0.70
8	3.270	0.25	1	2.036	2.56
9	6.518	0.02	1	4.059	0.36
10	6.361	0.29	1	3.961	0.47
11	8.839	0.11	1	5.505	1.20
12	7.737	0.05	1	4.818	0.46
13	5.444	0.03	1	3.390	1.09
14	7.011	0.06	1	4.366	0.03
15	7.639	0.08	1	4.757	0.39
16	7.098	0.04	1	4.420	0.03
17	8.786	0.05	1	5.471	1.16
18	7.879	0.03	1	4.906	0.55
19	6.198	0.22	1	3.860	0.58
20	9.072	0.02	1	5.650	1.36
21	5.300	0.20	1	3.301	1.19
22	7.890	0.19	1	4.914	0.56
23	5.146	0.13	1	3.204	1.29
24	6.395	0.13	1	3.983	0.45
25	7.495	0.11	1	4.667	0.29
26	4.521	0.21	1	2.816	1.71
27	8.562	0.08	1	5.332	1.01
28	7.879	0.06	1	4.906	0.55
29	6.365	0.07	1	3.964	0.47
30	8.420	0.06	1	5.243	0.92
31	5.260	0.08	1	3.276	1.21
32	7.116	0.12	1	4.432	0.04
33	6.627	0.16	1	4.127	0.29
34	6.616	0.09	1	4.120	0.30
35	6.211	0.02	1	3.868	0.57
36	8.259	0.02	1	5.143	0.81
37	6.213	0.28	1	3.869	0.57
38	10.741	0.13	1	6.689	2.48
39	6.932	0.26	1	4.317	0.09
40	10.089	0.03	1	6.283	2.04
41	6.671	0.02	1	4.154	0.26
42	7.019	0.17	1	4.371	0.03
43	7.085	0.08	1	4.412	0.02
44	7.137	0.08	1	4.445	0.05
45	7.452	0.08	1	4.641	0.27
46	5.144	0.37	1	3.203	1.29
47	7.298	0.10	1	4.545	0.16
48	4.886	0.26	1	3.043	1.47
49	8.365	0.06	1	5.209	0.88
50	6.863	0.44	1	4.274	0.13
51	6.704	0.27	1	4.175	0.24
52	4.539	0.38	1	2.827	1.70
53	7.242	0.22	1	4.510	0.12
54	5.772	0.11	1	3.595	0.87
55	6.695	0.14	1	4.169	0.25
56	6.389	0.04	1	3.979	0.45
57	6.272	0.21	1	3.906	0.53

Disc	De	Error	Wt	Age	+/- 1 σ
1	6.382	0.05	1	3.974	0.46
2	5.778	0.16	1	3.598	0.86
3	5.817	0.04	1	3.623	0.84
4	8.877	0.18	1	5.528	1.23
5	4.420	0.19	1	2.752	1.78
6	3.270	0.25	1	2.036	2.56
7	6.518	0.02	1	4.059	0.36
8	8.839	0.11	1	5.505	1.20
9	7.737	0.05	1	4.818	0.46
10	5.444	0.03	1	3.390	1.09
11	7.011	0.06	1	4.366	0.03
12	7.639	0.08	1	4.757	0.39
13	8.786	0.05	1	5.471	1.16
14	7.879	0.03	1	4.906	0.55
15	6.198	0.22	1	3.860	0.58
16	9.072	0.02	1	5.650	1.36
17	5.300	0.20	1	3.301	1.19
18	7.890	0.19	1	4.914	0.56
19	5.146	0.13	1	3.204	1.29
20	6.395	0.13	1	3.983	0.45
21	7.495	0.11	1	4.667	0.29
22	8.562	0.08	1	5.332	1.01
23	7.879	0.06	1	4.906	0.55
24	6.365	0.07	1	3.964	0.47
25	8.420	0.06	1	5.243	0.92
26	5.260	0.08	1	3.276	1.21
27	6.616	0.09	1	4.120	0.30
28	6.211	0.02	1	3.868	0.57
29	8.259	0.02	1	5.143	0.81
30	10.741	0.13	1	6.689	2.48
31	10.089	0.03	1	6.283	2.04
32	7.019	0.17	1	4.371	0.03
33	7.085	0.08	1	4.412	0.02
34	7.137	0.08	1	4.445	0.05
35	7.452	0.08	1	4.641	0.27
36	7.298	0.10	1	4.545	0.16
37	8.365	0.06	1	5.209	0.88
38	6.704	0.27	1	4.175	0.24
39	5.772	0.11	1	3.595	0.87
40	6.695	0.14	1	4.169	0.25
41	6.389	0.04	1	3.979	0.45
42	6.272	0.21	1	3.906	0.53
43					
44					
45					
46					
47					
48					
49					
50					
51					
52					
53					
54					

UNL-4298

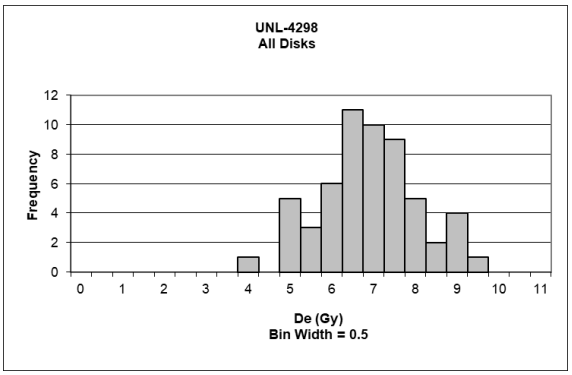

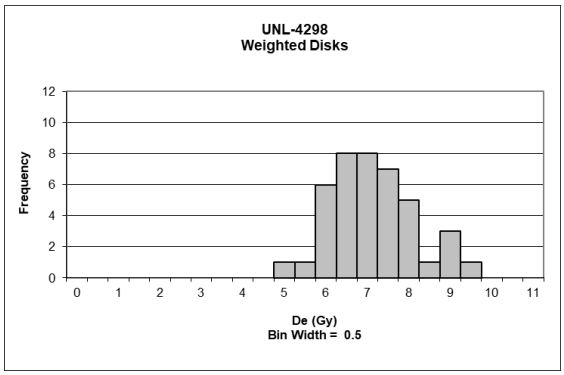

Disc	De	Error	Wt	Age	+/- 1 σ
1	7.002	0.01	1	4.407	0.16
2	8.592	0.07	1	5.407	1.72
3	5.149	0.30	1	3.241	1.66
4	7.706	0.03	1	4.850	0.85
5	4.694	0.20	1	2.955	2.11
6	5.936	0.11	1	3.736	0.89
7	6.160	0.25	1	3.877	0.67
8	6.350	0.34	1	3.997	0.48
9	6.989	0.05	1	4.399	0.14
10	4.527	0.15	1	2.849	2.28
11	6.626	0.07	1	4.170	0.21
12	6.036	0.15	1	3.799	0.79
13	6.937	0.12	1	4.366	0.09
14	5.453	0.27	1	3.432	1.37
15	4.514	0.19	1	2.841	2.29
16	7.712	0.14	1	4.854	0.85
17	6.062	0.14	1	3.815	0.77
18	5.116	0.27	1	3.220	1.70
19	7.501	0.05	1	4.721	0.65
20	5.864	0.10	1	3.690	0.96
21	8.630	0.33	1	5.432	1.76
22	7.695	0.17	1	4.843	0.84
23	6.084	0.53	1	3.829	0.75
24	6.254	0.01	1	3.936	0.58
25	6.462	0.15	1	4.067	0.37
26	7.511	0.05	1	4.728	0.66
27	5.590	0.23	1	3.518	1.23
28	9.055	0.06	1	5.699	2.17
29	7.245	0.10	1	4.560	0.39
30	6.200	0.24	1	3.902	0.63
31	6.368	0.18	1	4.008	0.47
32	6.878	0.10	1	4.329	0.03
33	6.842	0.36	1	4.307	0.00
34	6.574	0.10	1	4.138	0.26
35	7.102	0.06	1	4.470	0.25
36	8.286	0.00	1	5.215	1.42
37	7.475	0.09	1	4.705	0.62
38	5.562	0.04	1	3.501	1.26
39	4.658	0.14	1	2.932	2.15
40	7.207	1.46	1	4.536	0.36
41	6.618	0.05	1	4.165	0.22
42	4.952	0.14	1	3.117	1.86
43	8.982	0.13	1	5.653	2.10
44	7.267	0.03	1	4.573	0.42
45	6.762	0.12	1	4.256	0.08
46	8.614	0.04	1	5.422	1.74
47	6.902	0.17	1	4.344	0.06
48	7.472	0.07	1	4.703	0.62
49	5.794	0.11	1	3.647	1.03
50	6.404	0.12	1	4.031	0.43
51	6.959	0.01	1	4.380	0.11
52	5.610	0.13	1	3.531	1.21
53	6.300	0.13	1	3.965	0.53
54	3.858	0.26	1	2.428	2.93
55	7.362	0.21	1	4.633	0.51
56	8.299	0.01	1	5.223	1.43
57	7.289	0.07	1	4.588	0.44

Disc	De	Error	Wt	Age	+/- 1 σ
1	7.002	0.01	1	4.407	0.16
2	8.592	0.07	1	5.407	1.72
3	5.149	0.30	1	3.241	1.66
4	7.706	0.03	1	4.850	0.85
5	5.936	0.11	1	3.736	0.89
6	6.989	0.05	1	4.399	0.14
7	6.626	0.07	1	4.170	0.21
8	6.036	0.15	1	3.799	0.79
9	6.937	0.12	1	4.366	0.09
10	4.514	0.19	1	2.841	2.29
11	7.712	0.14	1	4.854	0.85
12	6.062	0.14	1	3.815	0.77
13	7.501	0.05	1	4.721	0.65
14	5.864	0.10	1	3.690	0.96
15	7.695	0.17	1	4.843	0.84
16	6.084	0.53	1	3.829	0.75
17	6.254	0.01	1	3.936	0.58
18	6.462	0.15	1	4.067	0.37
19	7.511	0.05	1	4.728	0.66
20	5.590	0.23	1	3.518	1.23
21	9.055	0.06	1	5.699	2.17
22	7.245	0.10	1	4.560	0.39
23	6.200	0.24	1	3.902	0.63
24	6.368	0.18	1	4.008	0.47
25	6.878	0.10	1	4.329	0.03
26	6.574	0.10	1	4.138	0.26
27	7.102	0.06	1	4.470	0.25
28	8.286	0.00	1	5.215	1.42
29	5.562	0.04	1	3.501	1.26
30	6.618	0.05	1	4.165	0.22
31	8.982	0.13	1	5.653	2.10
32	7.267	0.03	1	4.573	0.42
33	6.762	0.12	1	4.256	0.08
34	8.614	0.04	1	5.422	1.74
35	6.902	0.17	1	4.344	0.06
36	7.472	0.07	1	4.703	0.62
37	5.794	0.11	1	3.647	1.03
38	6.404	0.12	1	4.031	0.43
39	5.610	0.13	1	3.531	1.21
40	7.362	0.21	1	4.633	0.51
41	7.289	0.07	1	4.588	0.44
42					
43					
44					
45					
46					
47					
48					
49					
50					
51					
52					
53					
54					

UNL-4299

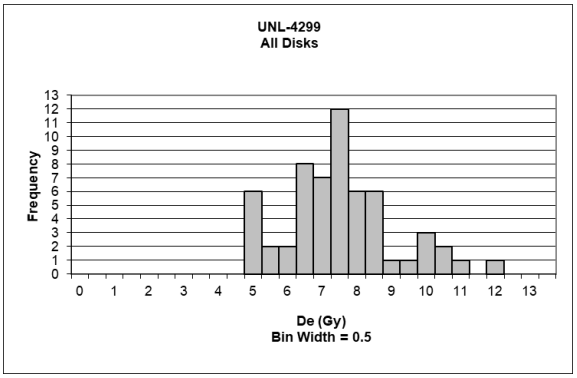

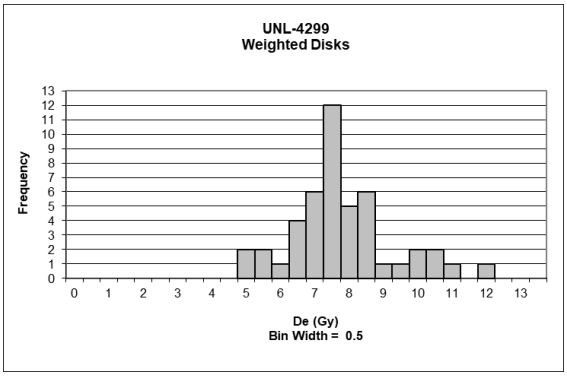

Disc	De	Error	Wt	Age	+/- 1 σ
1	5.579	0.22	1	3.207	1.30
2	9.716	0.16	1	5.584	1.50
3	8.800	0.10	1	5.058	0.88
4	8.027	0.02	1	4.614	0.36
5	7.686	0.09	1	4.418	0.13
6	4.780	0.08	1	2.747	1.84
7	6.409	0.22	1	3.684	0.74
8	6.837	0.31	1	3.930	0.45
9	7.015	0.04	1	4.032	0.33
10	7.201	0.18	1	4.139	0.20
11	9.025	0.01	1	5.187	1.03
12	8.330	0.12	1	4.788	0.56
13	10.074	0.15	1	5.790	1.74
14	7.690	1.41	1	4.420	0.13
15	4.773	0.36	1	2.743	1.84
16	6.530	0.04	1	3.753	0.66
17	6.630	0.18	1	3.811	0.59
18	7.733	0.09	1	4.445	0.16
19	6.226	0.10	1	3.578	0.86
20	6.441	0.01	1	3.702	0.72
21	6.101	0.28	1	3.507	0.95
22	7.250	0.17	1	4.167	0.17
23	7.130	0.09	1	4.098	0.25
24	11.607	0.05	1	6.671	2.78
25	9.605	0.06	1	5.521	1.42
26	7.219	0.09	1	4.149	0.19
27	6.166	0.39	1	3.544	0.90
28	8.186	0.14	1	4.705	0.46
29	7.013	0.17	1	4.031	0.33
30	7.399	0.21	1	4.253	0.07
31	6.945	0.05	1	3.992	0.38
32	6.951	0.18	1	3.995	0.37
33	7.370	0.13	1	4.236	0.09
34	9.866	0.37	1	5.671	1.60
35	7.397	0.01	1	4.251	0.07
36	7.353	0.07	1	4.226	0.10
37	10.803	0.03	1	6.209	2.23
38	4.712	0.11	1	2.708	1.89
39	7.575	0.06	1	4.354	0.05
40	6.719	0.17	1	3.862	0.53
41	4.964	0.21	1	2.853	1.72
42	5.178	0.07	1	2.976	1.57
43	6.556	0.03	1	3.768	0.64
44	8.085	0.01	1	4.647	0.40
45	8.079	0.07	1	4.643	0.39
46	6.143	0.15	1	3.531	0.92
47	4.746	0.16	1	2.728	1.86
48	6.433	0.19	1	3.698	0.72
49	7.507	0.04	1	4.315	0.00
50	4.880	0.51	1	2.805	1.77
51	8.172	0.05	1	4.697	0.45
52	5.752	0.68	1	3.306	1.18
53	6.453	0.47	1	3.709	0.71
54	7.794	0.04	1	4.480	0.20
55	7.467	0.01	1	4.292	0.02
56	7.097	0.41	1	4.079	0.27
57	5.189	0.27	1	2.982	1.56
58	10.266	0.13	1	5.900	1.87

Disc	De	Error	Wt	Age	+/- 1 σ
1	5.579	0.22	1	3.207	1.30
2	9.716	0.16	1	5.584	1.50
3	8.800	0.10	1	5.058	0.88
4	8.027	0.02	1	4.614	0.36
5	7.686	0.09	1	4.418	0.13
6	4.780	0.08	1	2.747	1.84
7	7.015	0.04	1	4.032	0.33
8	7.201	0.18	1	4.139	0.20
9	9.025	0.01	1	5.187	1.03
10	8.330	0.12	1	4.788	0.56
11	10.074	0.15	1	5.790	1.74
12	6.530	0.04	1	3.753	0.66
13	6.630	0.18	1	3.811	0.59
14	7.733	0.09	1	4.445	0.16
15	6.226	0.10	1	3.578	0.86
16	7.250	0.17	1	4.167	0.17
17	7.130	0.09	1	4.098	0.25
18	11.607	0.05	1	6.671	2.78
19	9.605	0.06	1	5.521	1.42
20	7.219	0.09	1	4.149	0.19
21	8.186	0.14	1	4.705	0.46
22	7.013	0.17	1	4.031	0.33
23	7.399	0.21	1	4.253	0.07
24	6.945	0.05	1	3.992	0.38
25	6.951	0.18	1	3.995	0.37
26	7.370	0.13	1	4.236	0.09
27	7.397	0.01	1	4.251	0.07
28	7.353	0.07	1	4.226	0.10
29	10.803	0.03	1	6.209	2.23
30	4.712	0.11	1	2.708	1.89
31	7.575	0.06	1	4.354	0.05
32	6.719	0.17	1	3.862	0.53
33	5.178	0.07	1	2.976	1.57
34	6.556	0.03	1	3.768	0.64
35	8.085	0.01	1	4.647	0.40
36	8.079	0.07	1	4.643	0.39
37	6.143	0.15	1	3.531	0.92
38	6.433	0.19	1	3.698	0.72
39	7.507	0.04	1	4.315	0.00
40	8.172	0.05	1	4.697	0.45
41	6.453	0.47	1	3.709	0.71
42	7.794	0.04	1	4.480	0.20
43	7.467	0.01	1	4.292	0.02
44	7.097	0.41	1	4.079	0.27
45	5.189	0.27	1	2.982	1.56
46	10.266	0.13	1	5.900	1.87
47					
48					
49					
50					
51					
52					
53					
54					

UNL-4300

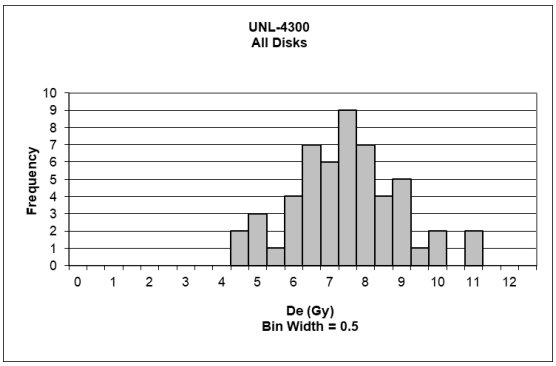

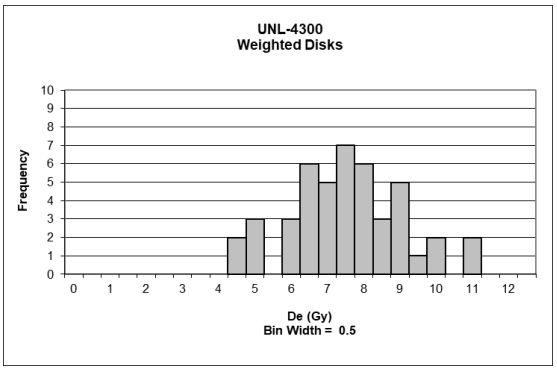

Disc	De	Error	Wt	Age	+/- 1 σ
1	5.188	4.02	1	3.075	1.36
2	8.724	0.23	1	5.171	0.95
3	8.005	0.10	1	4.744	0.48
4	9.116	0.04	1	5.403	1.21
5	7.686	0.40	1	4.555	0.27
6	7.892	0.08	1	4.677	0.41
7	10.876	0.06	1	6.446	2.35
8	8.540	0.16	1	5.061	0.83
9	5.901	0.18	1	3.497	0.89
10	6.811	0.17	1	4.037	0.30
11	7.816	0.09	1	4.633	0.36
12	6.441	0.12	1	3.817	0.54
13	8.878	0.08	1	5.262	1.05
14	4.956	0.15	1	2.937	1.51
15	6.337	0.13	1	3.756	0.61
16	5.897	0.18	1	3.495	0.90
17	6.121	0.03	1	3.628	0.75
18	6.856	0.12	1	4.063	0.27
19	6.230	0.09	1	3.693	0.68
20	9.986	0.11	1	5.919	1.77
21	6.899	0.50	1	4.089	0.24
22	7.130	0.05	1	4.226	0.09
23	4.465	0.08	1	2.646	1.83
24	6.034	0.09	1	3.576	0.81
25	6.712	0.33	1	3.978	0.36
26	7.301	0.11	1	4.327	0.02
27	6.398	0.61	1	3.792	0.57
28	7.174	0.02	1	4.252	0.06
29	8.168	0.12	1	4.841	0.59
30	6.462	0.34	1	3.830	0.53
31	4.775	0.17	1	2.830	1.63
32	6.578	0.06	1	3.899	0.45
33	7.557	0.05	1	4.479	0.19
34	8.887	0.05	1	5.267	1.06
35	7.037	0.14	1	4.171	0.15
36	5.869	0.22	1	3.479	0.92
37	7.238	0.14	1	4.290	0.02
38	7.821	0.08	1	4.635	0.36
39	7.445	0.11	1	4.413	0.11
40	7.087	0.04	1	4.200	0.12
41	6.851	0.14	1	4.061	0.27
42	9.522	0.03	1	5.643	1.47
43	7.249	0.08	1	4.296	0.01
44	10.814	0.07	1	6.409	2.31
45	8.000	0.03	1	4.742	0.48
46	5.691	0.05	1	3.373	1.03
47	7.827	0.10	1	4.639	0.36
48	8.135	0.10	1	4.822	0.56
49	7.145	0.09	1	4.235	0.08
50	4.886	0.08	1	2.896	1.56
51	4.303	0.20	1	2.551	1.94
52	7.691	0.03	1	4.558	0.27
53	8.577	0.04	1	5.084	0.85

Disc	De	Error	Wt	Age	+/- 1 σ
1	8.724	0.23	1	5.171	0.95
2	8.005	0.10	1	4.744	0.48
3	9.116	0.04	1	5.403	1.21
4	7.892	0.08	1	4.677	0.41
5	10.876	0.06	1	6.446	2.35
6	8.540	0.16	1	5.061	0.83
7	5.901	0.18	1	3.497	0.89
8	6.811	0.17	1	4.037	0.30
9	7.816	0.09	1	4.633	0.36
10	6.441	0.12	1	3.817	0.54
11	8.878	0.08	1	5.262	1.05
12	4.956	0.15	1	2.937	1.51
13	6.337	0.13	1	3.756	0.61
14	6.121	0.03	1	3.628	0.75
15	6.856	0.12	1	4.063	0.27
16	6.230	0.09	1	3.693	0.68
17	9.986	0.11	1	5.919	1.77
18	6.899	0.50	1	4.089	0.24
19	7.130	0.05	1	4.226	0.09
20	4.465	0.08	1	2.646	1.83
21	6.034	0.09	1	3.576	0.81
22	7.174	0.02	1	4.252	0.06
23	6.462	0.34	1	3.830	0.53
24	4.775	0.17	1	2.830	1.63
25	6.578	0.06	1	3.899	0.45
26	7.557	0.05	1	4.479	0.19
27	8.887	0.05	1	5.267	1.06
28	7.037	0.14	1	4.171	0.15
29	5.869	0.22	1	3.479	0.92
30	7.238	0.14	1	4.290	0.02
31	7.821	0.08	1	4.635	0.36
32	7.087	0.04	1	4.200	0.12
33	6.851	0.14	1	4.061	0.27
34	9.522	0.03	1	5.643	1.47
35	7.249	0.08	1	4.296	0.01
36	10.814	0.07	1	6.409	2.31
37	8.000	0.03	1	4.742	0.48
38	5.691	0.05	1	3.373	1.03
39	7.827	0.10	1	4.639	0.36
40	8.135	0.10	1	4.822	0.56
41	7.145	0.09	1	4.235	0.08
42	4.886	0.08	1	2.896	1.56
43	4.303	0.20	1	2.551	1.94
44	7.691	0.03	1	4.558	0.27
45	8.577	0.04	1	5.084	0.85
46					
47					
48					
49					
50					
51					
52					
53					

UNL-4301

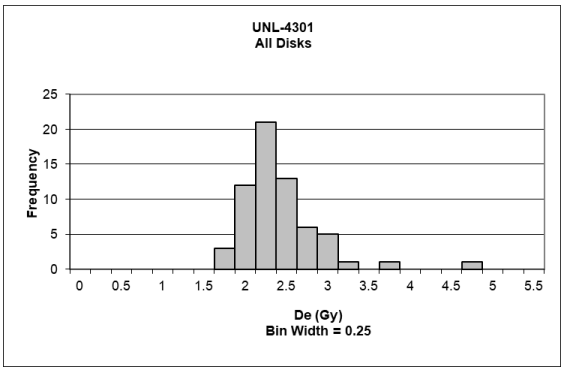

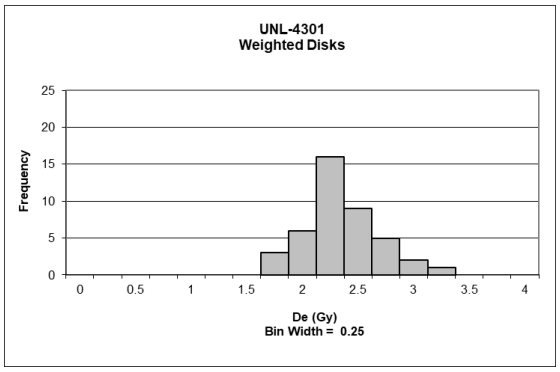

Disc	De	Error	Wt	Age	+/- 1 σ
1	2.528	0.10	1	1.557	0.98
2	4.505	0.09	1	2.775	7.45
3	2.333	0.15	1	1.437	0.34
4	2.780	0.02	1	1.712	1.80
5	1.912	0.06	1	1.178	1.04
6	3.588	0.25	1	2.210	4.45
7	2.096	0.06	1	1.291	0.44
8	2.112	0.10	1	1.301	0.39
9	1.777	0.09	1	1.095	1.48
10	2.213	0.08	1	1.363	0.06
11	2.400	0.08	1	1.478	0.56
12	2.051	0.05	1	1.263	0.59
13	2.217	0.09	1	1.365	0.04
14	2.096	0.09	1	1.291	0.44
15	2.520	0.01	1	1.552	0.95
16	2.111	0.21	1	1.300	0.39
17	2.358	0.08	1	1.453	0.42
18	2.943	0.04	1	1.813	2.34
19	2.213	0.14	1	1.363	0.06
20	2.054	0.05	1	1.265	0.58
21	3.051	0.20	1	1.879	2.69
22	2.531	0.04	1	1.559	0.99
23	2.142	0.09	1	1.319	0.29
24	2.344	0.11	1	1.444	0.37
25	2.321	0.12	1	1.430	0.30
26	1.949	0.15	1	1.201	0.92
27	1.987	0.09	1	1.224	0.80
28	1.699	0.06	1	1.046	1.74
29	1.920	0.03	1	1.182	1.02
30	2.897	0.19	1	1.785	2.19
31	2.102	0.23	1	1.295	0.42
32	2.224	0.01	1	1.370	0.02
33	2.493	0.09	1	1.536	0.86
34	1.736	0.25	1	1.069	1.62
35	2.368	0.18	1	1.458	0.45
36	2.735	0.03	1	1.684	1.65
37	2.389	0.09	1	1.472	0.52
38	2.264	0.03	1	1.395	0.11
39	2.843	0.62	1	1.751	2.01
40	2.887	0.11	1	1.778	2.15
41	1.941	0.24	1	1.196	0.95
42	2.199	0.12	1	1.355	0.10
43	1.873	0.05	1	1.154	1.17
44	2.543	0.15	1	1.566	1.03
45	2.291	0.33	1	1.411	0.20
46	2.151	0.03	1	1.325	0.26
47	2.194	0.14	1	1.352	0.12
48	2.086	0.03	1	1.285	0.47
49	1.762	0.08	1	1.085	1.53
50	1.877	0.09	1	1.156	1.16
51	2.596	0.09	1	1.599	1.20
52	1.958	0.10	1	1.206	0.89
53	2.140	0.22	1	1.318	0.29
54	1.952	0.16	1	1.203	0.91
55	2.327	0.08	1	1.434	0.32
56	2.410	0.23	1	1.484	0.59
57	2.062	0.21	1	1.270	0.55
58	1.920	0.28	1	1.183	1.02
59	2.314	0.10	1	1.426	0.28
60	2.066	0.06	1	1.272	0.54
61	2.054	0.04	1	1.265	0.58
62	2.163	0.11	1	1.332	0.22
63	1.748	0.24	1	1.077	1.58

Disc	De	Error	Wt	Age	+/- 1 σ
1	2.333	0.15	1	1.437	0.34
2	2.780	0.02	1	1.712	1.80
3	2.096	0.06	1	1.291	0.44
4	2.112	0.10	1	1.301	0.39
5	2.400	0.08	1	1.478	0.56
6	2.051	0.05	1	1.263	0.59
7	2.217	0.09	1	1.365	0.04
8	2.096	0.09	1	1.291	0.44
9	2.520	0.01	1	1.552	0.95
10	2.111	0.21	1	1.300	0.39
11	2.213	0.14	1	1.363	0.06
12	3.051	0.20	1	1.879	2.69
13	2.531	0.04	1	1.559	0.99
14	2.142	0.09	1	1.319	0.29
15	2.344	0.11	1	1.444	0.37
16	2.321	0.12	1	1.430	0.30
17	1.987	0.09	1	1.224	0.80
18	1.699	0.06	1	1.046	1.74
19	1.920	0.03	1	1.182	1.02
20	2.102	0.23	1	1.295	0.42
21	2.224	0.01	1	1.370	0.02
22	1.736	0.25	1	1.069	1.62
23	2.368	0.18	1	1.458	0.45
24	2.735	0.03	1	1.684	1.65
25	2.389	0.09	1	1.472	0.52
26	2.887	0.11	1	1.778	2.15
27	2.199	0.12	1	1.355	0.10
28	2.543	0.15	1	1.566	1.03
29	2.151	0.03	1	1.325	0.26
30	2.086	0.03	1	1.285	0.47
31	1.762	0.08	1	1.085	1.53
32	1.877	0.09	1	1.156	1.16
33	2.596	0.09	1	1.599	1.20
34	1.958	0.10	1	1.206	0.89
35	2.140	0.22	1	1.318	0.29
36	1.952	0.16	1	1.203	0.91
37	2.327	0.08	1	1.434	0.32
38	2.410	0.23	1	1.484	0.59
39	2.314	0.10	1	1.426	0.28
40	2.066	0.06	1	1.272	0.54
41	2.163	0.11	1	1.332	0.22
42	1.748	0.24	1	1.077	1.58
43					
44					
45					
46					
47					
48					
49					
50					
51					
52					
53					
54					